AD-A078 613 NATIONAL AERONAUTICS AND SPACE ADMINISTRATION HAMPTO--ETC F/G 1/3
ANALYTICAL INVESTIGATION OF THE LANDING DYNAMICS OF A LARGE AIR--ETC(U)
DEC 79 J R MCGEHEE , H D CARDEN

UNCLASSIFIED NASA-L-13250 NASA-TP-1555 NL

1 OF 1
AD A078613

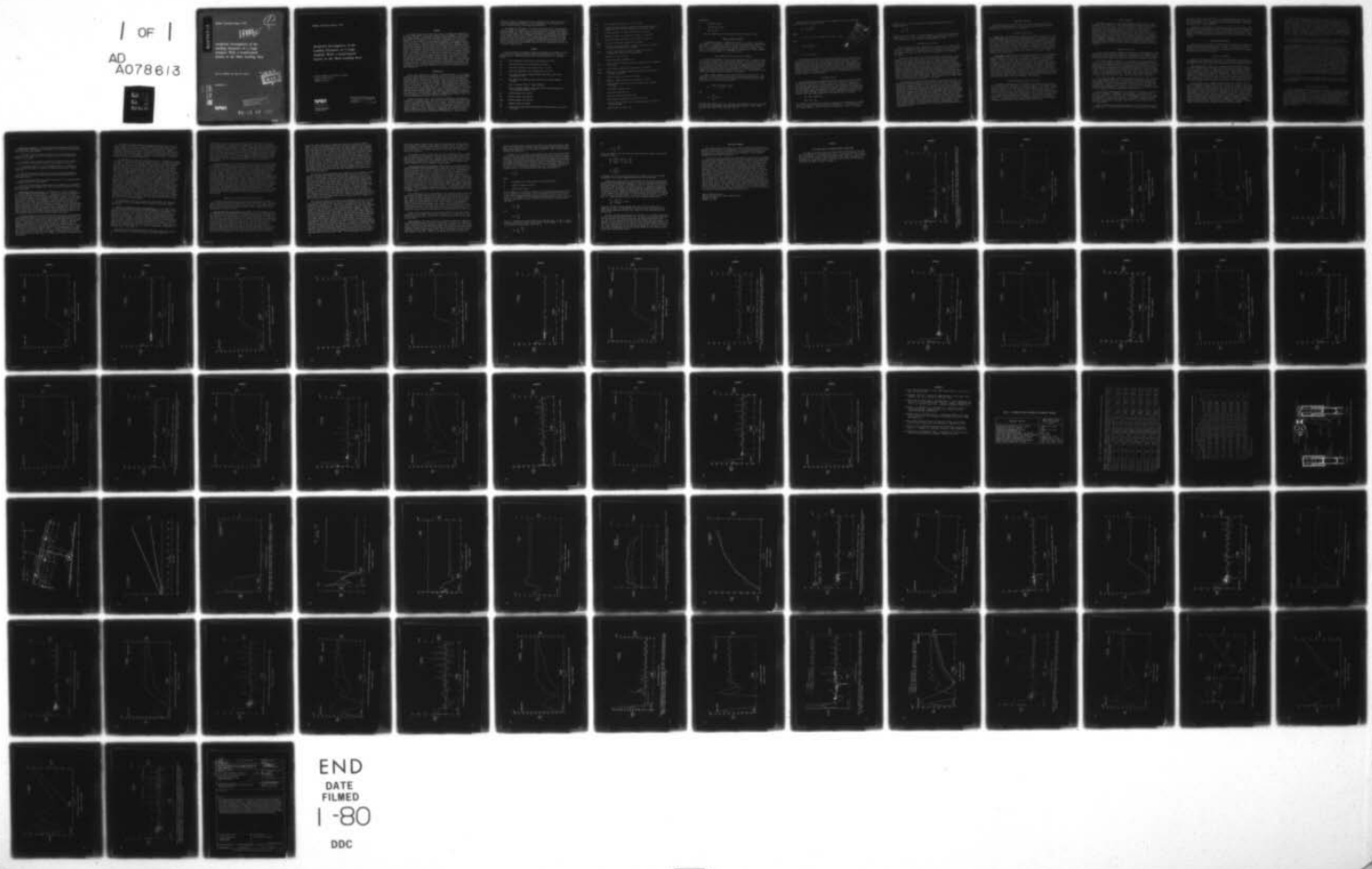

END
DATE FILMED
1-80
DDC

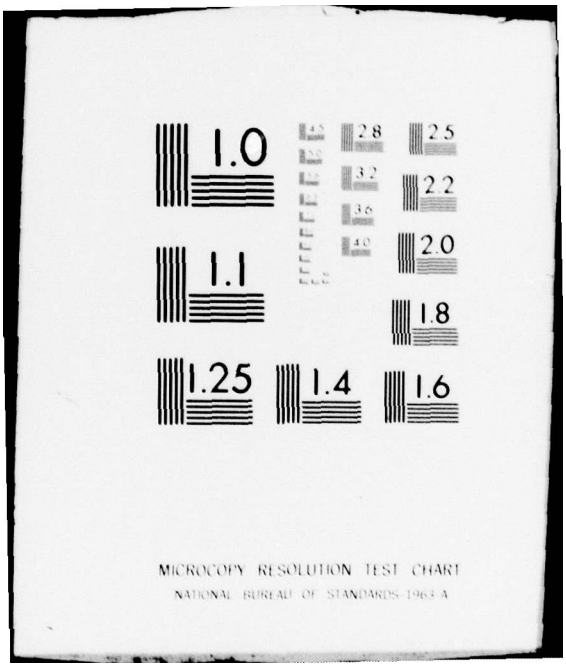
1.0
1.1
1.25
1.4
1.6
2.8
3.2
3.6
4.0
2.5
2.2
2.0
1.8
MICROCOPY RESOLUTION TEST CHART
NATIONAL BUREAU OF STANDARDS-1963-A

NASA Technical Paper 1555

Analytical Investigation of the Landing Dynamics of a Large Airplane With a Load-Control System in the Main Landing Gear

John R. McGehee and Huey D. Carden

DECEMBER 1979

NASA

NASA Technical Paper 1555

Analytical Investigation of the Landing Dynamics of a Large Airplane With a Load-Control System in the Main Landing Gear

John R. McGehee and Huey D. Carden
Langley Research Center
Hampton, Virginia

NASA
National Aeronautics and Space Administration

Scientific and Technical Information Branch

1979

SUMMARY

This paper presents the results of a study to evaluate the capability of an active load-control landing gear computer program (ACOLAG) for predicting the landing dynamics of airplanes with passive and active main gears, and the application of that program in an analytical investigation of the dynamic behavior during landing of a large airplane equipped with both passive and active main gears. Correlations between computed data from ACOLAG, computed data from a flexible aircraft take-off and landing analysis (FATOLA), and preliminary experimental drop-test data for a modified active control main gear from a light airplane indicate that ACOLAG is capable of predicting the landing dynamics of airplanes with both passive and active load-control main landing gears. A parametric study of passive and active main gears indicates that the active gear is more effective in reducing the magnitude of the forces transmitted to the aircraft structure than the passive gear. The effectiveness was most pronounced for those touchdown conditions which would result in large airframe-gear interface forces with the passive gear, that is, large airplane masses, high touchdown sink rates, and uphill runway slopes. The active gear is also effective in reducing airplane motions following initial impact. The reduction of cyclic forces associated with the active gear further indicates the potential for significant reductions in structural fatigue damage during ground operations.

INTRODUCTION

Ground loads imposed on an airplane are important factors in the dynamic loading of the airframe structure and may result in significant fatigue damage. The ground-induced structural vibrations also result in crew and passenger discomfort, and on large flexible airplanes these vibrations can reduce the pilot's capability to control the airplane. These problems of ground-induced vibrations have been encountered with some currently operational transport airplanes, as discussed in references 1 and 2. Such problems will be magnified for supersonic-cruise airplanes because of the increased structural flexibility inherent in their slender-body design, their thin-wing construction, and their high take-off and landing speeds. For example, investigations of the ground ride qualities of one particular design of a supersonic transport conducted in the United States in the sixties indicated extremely high vibration levels in the crew compartment during the take-off roll (ref. 3).

Analytical studies (refs. 3 to 5) have been conducted to determine the feasibility of applying active load controls to the airplane main landing gear to limit the ground loads applied to the airframe. The study reported in reference 4 indicates that a shock strut with a hydraulically controlled actuator in series with the passive elements of the strut provided the most desirable dynamic properties. This study used a linear model as a simplification of an actual airplane shock-strut system but recommended that any future studies should include the nonlinear landing-gear characteristics. Both nonlinear

shock-strut and tire characteristics were included in the study of reference 5, in which a mathematical model of a stiff airplane with a series-hydraulic, active load-control main landing gear was developed.

The purpose of this paper is to present the results from a two-phase program to evaluate the capability of an active load-control landing gear computer program (ACOLAG) for predicting the landing dynamics of airplanes with passive and active main gears, and to apply that program in an analytical investigation of the dynamic behavior during landing of a large airplane equipped with both passive and active main gears. The touchdown parameters varied in the study, for both passive and active main gears, included airplane mass and pitch mass moments of inertia, subsonic aerodynamics, aerodynamic pitch control (elevators), pitch attitude, ground speed, and sink rate, in conjunction with the use of actual runway profiles.

SYMBOLS

The units used for the physical quantities defined in this paper are given first in the International System of Units and parenthetically in the U.S. Customary Units. Measurements and calculations were made in U.S. Customary Units.

A_o area of opening in shock-strut orifice plate, m^2 (ft^2)

A_p cross-sectional area of metering pin, m^2 (ft^2)

A_1 shock-strut hydraulic area (piston area), m^2 (ft^2)

A_2 shock-strut pneumatic area (cylinder area), m^2 (ft^2)

A_3 cross-sectional area of volume between shock-strut piston and cylinder, m^2 (ft^2)

F_e force applied at composite mass center due to elevator moment, N (lbf)

K ratio of elevator moment to applied moment

l distance between composite mass center and elevator hinge axis in body coordinate system, m (ft)

M_a applied moment, N-m (lbf-ft)

M_e elevator moment, N-m (lbf-ft)

$M_{Y,b}$ pitching moment, N-m (lbf-ft)

m_c composite mass, kg (slugs)

m_f one-half of fuselage mass concentrated at fuselage center of gravity, kg (slugs)

m_h	mass assumed concentrated at axle, kg (slugs)
m_w	semispan wing mass assumed concentrated at semispan wing c.g. on spanwise chord containing wing-gear interface, kg (slugs)
p_1	hydraulic pressure in shock-strut piston, Pa (lbf/ft^2)
p_2	pneumatic pressure in shock-strut cylinder, Pa (lbf/ft^2)
Q_o	flow rate through shock-strut orifice, m^3/sec (gal/min)
Q_{pump}	flow rate of hydraulic pump, m^3/sec (gal/min)
Q_{sv1}	flow rate from high-pressure accumulator through servo valve to shock-strut piston, m^3/sec (gal/min)
Q_{sv2}	flow rate from shock-strut piston through servo valve to low-pressure reservoir, m^3/sec (gal/min)
s	shock-strut stroke, m (ft)
t	elapsed time after touchdown, sec
$V_{ac,i}$	initial volume of charging nitrogen in high-pressure accumulator, m^3 (pints)
$V_{ac,t}$	total volume of high-pressure accumulator, m^3 (pints)
V_{cum}	cumulative fluid volume transferred from shock-strut piston to cylinder, m^3 (pints)
V_1	volume of shock-strut piston, m^3 (pints)
V_2	pneumatic volume in shock-strut cylinder, m^3 (pints)
V_3	volume between shock-strut piston and shock-strut cylinder, m^3 (pints)
X	longitudinal coordinate axis
Y	transverse coordinate axis
Z	vertical or normal coordinate axis
β	bulk modulus of hydraulic fluid, N/m^2 (lbf/ft^2)
γ	ratio of specific heat of gas at constant pressure to that at constant volume
η	general slope of runway, deg

Subscripts:

b	body-axis system
g	gravity-axis system
i	initial value

Dots over symbols indicate differentiation with respect to time.

MODIFICATIONS TO ACOLAG

The mathematical model of ACOLAG in reference 5 was used in the present investigation. Subsequent to the publication of that reference, modifications were made to the mathematical model of the series-hydraulic active control gear, to the aerodynamic model of the airplane, and to the main-gear control logic. The equations have been programmed for operation on a digital computer and have a core requirement of 72 000 octal words.

Series-Hydraulic Active Control Gear Model

The mathematical model of the active control gear (ref. 5) assumes instantaneous control response and incompressible hydraulic fluid; however, in reality, delayed response and/or stability problems can arise with an active gear as a consequence of hardware limitations and the compressibility of hydraulic fluid at high operating pressures. Therefore, the mathematical model of the series-hydraulic active control gear was modified to include servo-valve dynamics and compressible-fluid characteristics (ref. 6). These modifications changed the pressure and flow equations of reference 5.

Figure 1 shows schematics of the passive and active shock struts. The conservation of mass of the hydraulic fluid in the shock-strut piston, represented by V_1 in figure 1(a), and consideration of the effect of fluid compressibility lead to equations of the form

$$\dot{p}_1 = \frac{(A_1\dot{s} - Q_o + Q_{sv1} - Q_{sv2})\beta}{V_1}$$

and

$$p_1 = \int_{t=0}^{t} \dot{p}_1 \, dt$$

The servo-valve flow rates Q_{sv1} and Q_{sv2} are functions of servo-valve geometry and spool displacement, instantaneous piston pressure, control supply pressure, and control return pressure (ref. 6).

The pressure-volume relationship for the pneumatic pressure in the shock-strut cylinder (V_2 in fig. 1(a)) is

$$p_2 = p_{2,i}\left(\frac{V_{2,i}}{V_2}\right)^{\gamma}$$

where

$$V_2 = V_{2,i} - (A_2 - A_1 + A_p)s + (V_3 - V_{3,i}) - V_{cum}$$

with

$$V_{cum} = \int_{t=0}^{t} Q_o \, dt$$

and

$$V_3 = V_{3,i} + A_3 s$$

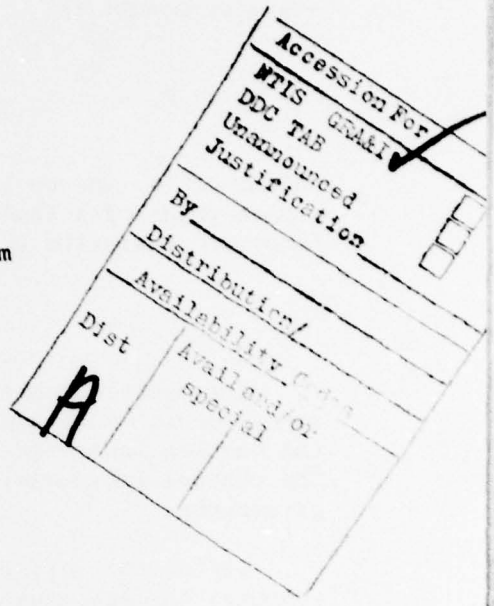

The main-gear shock strut of the simulated airplane has a snubber valve in the orifice plate to restrict flow from the shock-strut cylinder to the piston during strut extension. For a few simulated landings, the piston pressure dropped below the fluid vapor pressure because of the high strut-extension rate coupled with the restricted flow through the snubber valve. Consequently the pressure equations were modified to limit the pressure in the piston to vapor pressure for these conditions. Fluid continues to flow from the cylinder to the piston until the shock-strut pressure returns to charging pressure or until the gear impacts the landing surface.

Aerodynamic Model

The aerodynamic model presented in reference 5 does not include elevators for controlling nose-gear touchdown velocity or the effect of such control on the loading of the main gear. During simulations of airplane landings and roll-out, nose-gear impact velocities and resulting nose-gear forces generated by the simplified nose-gear representation (linear spring with no rebound) were unrealistically large. Consequently, a simplified representation of the elevators was added to ACOLAG. The elevator control (ELCON) was included as a percentage of the other applied moments and of opposite sign, as follows:

$$M_e = KM_a = \text{ELCON} * M_a$$

$$M_{Y,b} = M_a - M_e$$

For example, at touchdown the airplane is assumed to be aerodynamically trimmed with the aerodynamic lift supporting the airplane mass. For this condition the elevator moment is equal in magnitude but opposite in sign to the applied

moment (K = 1.0). The force applied at the composite mass center due to elevator moment is

$$F_e = \frac{M_e}{l}$$

Values of K may be input to simulate changes in elevator control during the impact phase of a landing. During nose-gear impact the elevator moment and force are decreased as the nose-gear force and moment increase.

Main-Gear Control Logic

The operation of the series-hydraulic active control gear is described in reference 5. Subsequent to the publication of reference 5, it was found that the control logic was not conducive to efficient operation of the active gear. The control logic was, therefore, modified as described in the following paragraphs.

During the initial portion of the landing impact, the electronic control computes the airplane kinetic energy in the vertical direction from the measured sink rate and the vehicle mass, which is assumed to remain constant. This energy is apportioned among the main gears and is compared with the remaining work capability of each main-gear shock strut during the stroking process. The work capability of the strut is the product of the instantaneous value of the force at the interface between the gear and the airframe and the remaining shock-strut stroke. When the work capability of the shock strut equals or exceeds the remaining vertical kinetic energy of the aircraft, the control assigns that instantaneous value of the airframe-gear interface force as the limit force and the loading at the interface is controlled about this value during the remainder of the impact. The transition from the impact phase to the roll-out phase is as described in reference 5.

If the gear fully extends and the pressure in the shock-strut piston is less than the charging pressure, then the control adds fluid to the strut until the pressure returns to charging pressure or until the control is required to reduce the airframe-gear force. If the airframe-gear force becomes positive, the gear is stroked, and fluid has been removed, then the control adds fluid to the strut. The rate of addition of fluid is proportional to the difference between the assigned limit force and the instantaneous values of the airframe-gear force. Addition of fluid ceases when control is again required or when the fluid volume in the strut has been returned to the design value. This logic maintains the strut-fluid quantity and pressure at or near passive-gear design values during control inactivity and provides more efficient utilization of the control system. During the roll-out phase of the landing, a control bias returns the gear to the design static stroke in approximately 10 sec. This control bias does not degrade control performance during other phases of operation (ref. 6).

ANALYTICAL MODELING

The passive and active shock struts of the main landing gears and the assumed stiff-airframe geometry of the large airplane were modeled as shown schematically in figures 1 and 2, respectively.

Main-Gear Shock Struts

Passive gear.- The passive-gear shock strut is shown in figure 1(a). The main-landing-gear shock strut of the modeled airplane is an air-over-oil type. The main orifice between the piston and the cylinder is equipped with a snubber valve. The valve remains open during the compression phase of gear operations but reduces the orifice area for flow from the cylinder to the piston during gear extension and thus increases gear damping. The pressure-relief orifices in the orifice tube permit pressure equalization between the orifice tube and the outer portion of the cylinder. Similarly, the orifices in the piston wall permit pressure equalization between the cylinder and the annular volume between piston and cylinder.

Active gear.- Modifications to the passive-gear shock strut to accommodate the series-hydraulic active control are shown in figure 1(b). The control hardware includes a servo valve, a high-pressure accumulator, a low-pressure reservoir, a hydraulic pump, and an electronic control. In addition, the single-wall orifice tube is replaced by an annular tube to permit the control to operate on the fluid in the shock-strut piston. A schematic representation of these modifications is shown by the diagonally lined area in figure 1(b). Control instrumentation consists of an accelerometer to monitor airframe-gear acceleration, a potentiometer to measure strut stroke, and a pressure transducer to measure fluid pressure in the piston. The electronic control utilizes these data in a feedback loop in conjunction with the programmed logic to drive the servo-valve spool and control hydraulic fluid pressure in the shock-strut piston and thus control the force applied to the airframe.

Airplane Geometry and Mass Distribution

A schematic representation of the geometric configuration of the stiff airframe and the mass distribution is shown in figure 2. All geometric dimensions are shown with reference to the airplane composite mass center (airplane center of gravity, c.g.). The geometric locations of all mass centers are assumed to be the same for all mass conditions. Although the geometric location of the hub mass center does change with stroke, its effect on the airplane c.g. is small and is assumed to be negligible. In this study the composite mass center is located at the most allowable aft position of the center of gravity. This location results in the maximum loading (due to mass changes) of the main landing gears during landing impact and roll-out.

Control Hardware

The hardware required for the series-hydraulic control system is shown schematically in figure 1(b). The simulated characteristics of the hardware for this study are the same as those of reference 6. The servo valve is a three-stage, industrial-type valve with a rated flow of 0.0126 m^3/sec (200 gal/min) and a maximum flow rate of 0.0151 m^3/sec (240 gal/min) for a 6.9 MPa (1.0 ksi) pressure drop across the valve. The characteristics of the electronic control as designed in reference 6 are also used for the landing simulations made during this study. The low-pressure reservoir is assumed to be at atmospheric pressure. The hydraulic pump is assumed to supply fluid to the high-pressure accumulator at a flow rate of 0.0006 m^3/sec (9.0 gal/min) and a pressure of 20.7 MPa (3.00 ksi), and the high-pressure accumulator is assumed to supply fluid to the servo valve at a constant pressure of 20.7 MPa (3.00 ksi).

Parameter Variations

In this study touchdown parameters consistent with landing-approach flight operation of the airplane are established. ACOLAG was used to compute the airplane dynamic loads and motions from initial touchdown on the runway through main- and nose-gear impacts followed by a portion of the ground roll-out phase.

For economic computer operation, it is desirable to use the maximum time interval in the integration procedure that satisfies established error tolerances for the integrated variables. An evaluation of the maximum time interval and maximum error tolerances of the integrated variables that could be used without significantly changing the variables was conducted. It was found that a time interval of 0.0001 sec, in conjunction with the error tolerances shown in table I, was the maximum time interval that could be used without noticeable changes in the integrated variables. Therefore, the landing simulations for this study were made using this time interval and these error tolerances.

The touchdown parameter variations include three airplane mass configurations: small, medium, and large. The small mass configuration represents a minimum mass landing condition, and the medium and large mass configurations are selected as 1.4 and 1.8 times greater, respectively, than the small mass configuration. Since the center of gravity is as far aft as allowable, the greater pitch mass moments of inertia for the larger mass configurations impose a greater demand on the main-landing-gear control system.

An analysis of 2385 landings of civil airplanes in reference 7 indicates that only 1 landing in 10 000 had a sink rate equal to or greater than 1.5 m/sec (5.0 ft/sec). Therefore, the maximum design sink rate at touchdown for this study is 1.5 m/sec (5.0 ft/sec). To encompass a range of sink rates at touchdown, 0.3 m/sec (1.0 ft/sec) and 0.9 m/sec (3.0 ft/sec) were also selected. An off-design (emergency) sink rate of 2.4 m/sec (8.0 ft/sec) was also investigated.

Pitch attitudes and ground speeds selected to provide constant-sink-rate touchdowns were 7.5° and 84.4 m/sec (277 ft/sec) for the small mass configura-

tion, 8.7° and 91.4 m/sec (300 ft/sec) for the medium mass configuration, and 10° and 97.8 m/sec (321 ft/sec) for the large mass configuration. The elevator deflection (ELCON = 1.0 for ACOLAG) was initialized at touchdown to maintain the airplane in a trimmed condition.

Landings were simulated for two operational runways with different slopes and unevenness elevation profiles. The elevation profiles of these runways are presented in figure 3 for uphill slopes. For simulated landings on downhill slopes, the unevenness profiles are superposed on the reversed slopes. Touchdown for all landing simulations occurred at the runway threshold (zero runway distance).

RESULTS AND DISCUSSION

The results of this analytical investigation are presented to compare the performance of the airplane with the active control landing gear with the performance with the passive landing gear. Variables in the simulated control system are also presented to illustrate the limitations of the control hardware and logic used in this investigation.

Validation of ACOLAG

Results are presented in figures 4 and 5 to demonstrate the validity of the ACOLAG analysis and computer program for predicting the landing dynamics of airplanes with both passive and active load-control main-landing-gear systems.

Passive-gear mode.- Comparisons of computed data from ACOLAG with data from the validated flexible aircraft take-off and landing analysis (FATOLA, ref. 8) are made in figure 4 to demonstrate the validity of ACOLAG to compute landing dynamics with passive landing-gear systems. Landing dynamics of a large, stiff airplane for a symmetric touchdown on a smooth flat runway were computed with FATOLA and ACOLAG. The sink rate was 1.5 m/sec (5.0 ft/sec), the pitch rate was -0.5 deg/sec nose over, and the c.g. vertical acceleration was zero. Comparisons are shown in figure 4 of control inputs, pitch rates, pitch attitudes, and main-gear strut forces and strokes for the simulated landing.

Elevator deflections in FATOLA and ELCON inputs for simulated elevator control in ACOLAG are shown in figure 4(a). The elevator-control input variations for ACOLAG were defined by trial and error and are denoted by the dashed line in figure 4(a). These elevator-control variations resulted in good agreement with pitch rates, pitch attitudes, and time of nose-gear contact obtained from FATOLA, as shown in figure 4(b). Subsequent to nose-gear contact, some differences in pitch rates result because of differences in nose-gear simulations. In FATOLA, the more realistic nose-gear simulation permits pitch-rate changes as the nose-gear loads and unloads, whereas in ACOLAG the pitch rate is set to 0 deg/sec and the nose-gear force is computed to offset the moment applied by the main gears. The pitch attitude computed in FATOLA is slightly larger than that obtained with ACOLAG following nose-gear contact.

Comparisons of main-gear strut forces are shown in figure 4(c). Strut forces are in good agreement up to nose-gear contact. Differences shown at nose-gear contact result from the elevator and nose-gear simulations used in ACOLAG. Beyond nose-gear contact the forces still agree well; however, strut forces from ACOLAG are greater than those from FATOLA. The differences between the two simulations occur because in FATOLA the angle of attack is slightly greater than the zero-lift angle and in ACOLAG the angle is slightly lower than zero-lift angle. Consequently lift reduces main-gear loads in FATOLA and loads the gear slightly in ACOLAG. Main-gear strokes for the two simulations compare well (fig. 4(d)), until the differences in the aerodynamic lift influence the results, as noted for the shock-strut forces.

The preceding comparisons indicate that the ACOLAG computer program is valid for computing airplane landing loads and motions for symmetric landings of airplanes with stiff airframes and passive main landing gears.

Active-gear mode.- Preliminary validation of the active-gear mode of ACOLAG is accomplished by comparing computed data with experimental results obtained from the test program of reference 6. Comparisons of computed and experimental airframe-gear forces and shock-strut strokes are presented in figure 5 for a gear sink rate of 1.5 m/sec (5.0 ft/sec). As shown in figure 5(a), there was a force imbalance of 2.45 kN (550 lbf) between the experimental data (circular symbols) and the computed results at time of touchdown. The imbalance resulted from differences in the simulated lift force and the inertia force acting at the strut attachment in the experiment. From impulse-momentum considerations, the integral of the force-time curve from the 2.45-kN (550-lbf) level to the time of maximum gear stroke (0.33 sec) dissipates the test mass velocity. Therefore, it is valid to shift the experimental data to reflect a force balance at touchdown as with the computed data. A comparison of the shifted experimental force data (dashed line in fig. 5(a)) with the computed force data indicates good agreement in both magnitude and variations. The good agreement between the computed and experimental strut strokes, shown in figure 5(b), further indicates the validity of shifting the force data for purposes of comparison.

These results indicate that the ACOLAG computer program is valid for predicting the dynamics of light airplanes with active gears during the impact phase of landings.

Operational Considerations

Data are presented to show the operation of an active load-control system in the main landing gear of a large airplane. The data are presented as time-history plots of airframe-gear forces, shock-strut strokes, and fuselage mass-center displacements along the Z_g axis for airplane landing simulations with both passive and active gears. For the active-gear simulations, hydraulic-fluid flow rates and volume of fluid transferred are also presented to illustrate the operational compatibility of the simulated control hardware and the modified landing-gear shock strut. All landing simulations with the active gear were computed with a constant pressure of 20.7 MPa (3.00 ksi) in the high-pressure accumulator.

Formulated constraints.- To assure meaningful performance of the active load-control main landing gears investigated in this study the following operational constraints were imposed:

1. The control must never remove a quantity of fluid from the strut greater than the volume of fluid in the piston of the fully extended strut (0.010 m^3 (21.8 pints)).

2. The control must never add a quantity of fluid to the strut equal to or greater than the instantaneous value of the gas volume in the strut.

3. The maximum shock-strut stroke encountered during any landing simulation should never equal or exceed the allowable design stroke (0.508 m (20.0 in.)).

4. The control-hardware characteristics for an optimum design should supply hydraulic fluid at the flow rates required by the dynamic behavior of the shock strut.

5. All the aforementioned constraints must be met for the range of design touchdown parameters of the airplane.

6. The active load-control landing gear must be adaptable for accommodating greater than design touchdown sink rates which may be encountered in emergency situations.

Performance within constraints.- To show operation within the imposed constraints, typical data are presented in figure 6 for landing simulations of all the airplane mass configurations at a touchdown sink rate of 0.9 m/sec (3.0 ft/sec) on runway A with both uphill and downhill slopes. Data for these mass configurations for other touchdown sink rates, runway slopes, and runway unevenness are presented in the appendix. Tabulated results are shown in table II for all airplane landing simulations on runway A with active load-control main gears. The data are presented as follows: percent airframe-gear-force reductions of the active gear relative to the passive gear during initial impact and main-gear response to nose-gear impact; maximum flow rate of fluid from and into the strut; maximum volume of fluid removed from or added to the strut; maximum shock-strut stroke encountered during landing simulations; and the allowable volume of fluid that could be added to the strut.

The maximum volume of the fluid removed from the strut during the landing simulations was 0.0081 m^3 (17.20 pints), which is approximately 79 percent of the allowable volume, and occurred for the medium mass configuration at a sink rate of 1.5 m/sec (5.0 ft/sec) on the uphill slope of runway A. The maximum volume of fluid added to the strut was 0.0072 m^3 (15.10 pints), which is approximately 56 percent of the allowable volume and occurred during the landing simulation of the large mass configuration at a sink rate of 1.5 m/sec (5.0 ft/sec) on the uphill slope of runway A. The maximum shock-strut stroke used by the active gear was 0.480 m (18.9 in.), which is 95 percent of allowable stroke and occurred during initial impact of the landing for the large mass configuration at a sink rate of 1.5 m/sec (5.0 ft/sec) on the uphill slope of runway A.

The servo valve became saturated (maximum displacement of servo-valve spool, ±0.0025 m (±0.10 in.)) during the removal of fluid from the strut at initial impact for all landing simulations, indicating that the control-hardware characteristics used were not for an optimum design. However, this nonoptimum design was sufficient to substantially reduce the forces with the active gear during initial impact. Therefore, the performance of the active load-control gear has been demonstrated over the design range of touchdown parameters within the imposed constraints.

The adaptability of the active load-control gear to accommodate off-design sink rates is illustrated by data presented in figure 7. Airframe-gear forces are shown in figure 7(a) for landing simulations of the large mass configuration with both passive and active gears. Landings were made on the uphill slope of runway A with a sink rate of 2.4 m/sec (8.0 ft/sec). The control logic was the same as that used with design sink rates. Following initial impact the airplane rebounded from the runway and sustained second impacts at sink rates of approximately 1.2 m/sec (3.9 ft/sec) and 1.4 m/sec (4.7 ft/sec) for the passive and active gears, respectively. After initial impact the active-gear control had transitioned from the impact limit force to a roll-out limit force of zero. The designed force limits of ±8.896 kN (±2000 lbf) were too low and the allowable shock-strut stroke was exceeded during the second impact for this simulated emergency condition. Consequently, the present control logic requires modifications which will either increase the roll-out force limits if the touchdown sink rate is greater than the maximum sink rate for which the control was designed, or reset the control to the impact mode following rebound. For this study the roll-out force limits were increased from ±8.896 kN (±2000 lbf) to ±133.45 kN (±30 000 lbf). As a result of these large roll-out force limits, the control was not required after the second impact and the maximum stroke capability of the shock strut was not exceeded, as shown in figure 7(b). The force reductions after nose-gear impact result from changes in shock-strut pressure and fluid volume effected by the control during the initial and second impacts.

The performance of the active load-control main landing gear simulated in this study has thus been demonstrated for operation within the imposed constraints.

Effect of accumulator pressure and pump capacity.- The airplane landing simulations with active load-control gears were made with the assumption of a constant 20.7 MPa (3.00 ksi) pressure in the high-pressure accumulator. To maintain this pressure with the large flow rates encountered would require a more massive accumulator or a hydraulic pump with a large pumping capacity requiring excessive power. A limited study was conducted to determine the effect of varying accumulator pressure and pump capacity on the performance of the active gear. Results of the study are presented in figure 8 for airplane landing simulations of the large mass configuration on the uphill slope of runway A at a touchdown sink rate of 1.5 m/sec (5.0 ft/sec). These conditions required the largest transfer of fluid from the high-pressure accumulator to the shock strut. (See table II.)

Two accumulator-volume and pump-capacity combinations were investigated: an accumulator volume of 0.038 m^3 (10.0 gal) and a pump capacity of

0.0006 m^3/sec (9 gal/min); and an accumulator volume of 0.019 m^3 (5.0 gal) and a pump capacity of 0.0032 m^3/sec (50 gal/min). As shown in figure 8(a), neither combination of accumulator volume and pump capacity had any appreciable effect on the airframe-gear force. However, figure 8(b) shows that the shock-strut extension is less for these two combinations compared with the extension for the constant accumulator pressure during the high-pressure phase of operation. The shock-strut extension for the 5-gal accumulator and the 50-gal/min pump is less than that for the 10-gal accumulator and 9-gal/min pump. These data indicate that the results of the parametric study at a constant accumulator pressure during the high-pressure phase of control operation are conservative.

Effect of braking.- An investigation of the effects of the combined operation of the active load-control gear and a simplified antiskid braking system was conducted for the large mass configuration with a sink rate of 0.9 m/sec (3.0 ft/sec) on the uphill slope of runway A. Airframe-gear-force and shock-strut-stroke time histories are shown in figure 9 for brake application after nose-gear impact. Comparison of figures 9(a) and 9(b) with figures 6(i) and 6(j), respectively, illustrates the effect of braking on the airplane landing simulations with passive and active gears. Following brake application with passive gears, the magnitudes of the airframe-gear forces and shock-strut strokes increase. The active gear, however, controls the airframe-gear forces effectively during braking, but at a higher frequency of operation. Shock-strut strokes for the active gear (fig. 9(b)) indicate that the stroke returns to the designed static stroke more rapidly with braking than without braking (fig. 6(j)). No detrimental effects on the performance of the active gear coupled with the simplified antiskid braking were encountered. Indeed, it is possible that improved braking performance could be realized, since the active gear maintains a more constant force at the tire-runway interface than the passive gear.

Comparison of Passive and Active Gear Results

The typical data presented in figure 6 and the tabulated data shown in tables II and III are used to compare the results obtained for the active load-control gear with those obtained for the passive gear. These comparisons are made for airframe-gear forces and shock-strut strokes, fuselage mass-center displacements, and cyclic forces.

Airframe-gear forces and shock-strut strokes.- The airframe-gear forces and shock-strut strokes computed for typical airplane landing simulations with both passive and active main gears are compared in figure 6 for the same landing conditions. The various phases of the landing simulations are shown in figure 6(a) for both types of main gears. The initial impact and rebound phase for the airplane with the passive gear differs from that with the active gear, since the active gear reduces the shock-strut force (at the expense of increased shock-strut stroke, fig. 6(b)). The reduced shock-strut force results in smaller airframe-gear and ground forces. Nose-gear contact occurred at approximately the same time for the landing simulations with both passive and active gears, indicating that the rotational impulse applied to the airplane was approximately the same with both passive and active gears

during the impact phase and the rebound and rotation to nose-gear contact phase. Since the airframe-gear and ground forces were smaller with the active gear than they were with the passive gear, the moment applied to the airplane during the impact and rebound phase had to be sustained for a longer period of time. This was the case, as shown by the longer period of decelerating (negative) airframe-gear force (fig. 6(a)) and also by the greater period of ground-force application as indicated by the sustained shock-strut stroke for the active gear (fig. 6(b)). During nose-gear impact, the airframe-gear force for the airplane landing simulation with the active gear was less than that with the passive gear. The shock-strut stroke was only slightly greater than that of the passive gear for the small mass configuration (fig. 6(b)), but was sustained at a greater stroke for a longer period of time. Subsequent to nose-gear impact (during the roll-out phase), the airframe-gear force for the landing simulation with the active gear was generally smaller than that of the passive gear and the shock-strut strokes were approximately the same for the small mass configuration.

The results of the airframe-gear-force comparisons for the landing simulations of the medium and large mass configurations (figs. 6(e), 6(g), 6(i), and 6(k)) are the same as those for the small mass configuration (figs. 6(a) and 6(c)). The results of the shock-strut-stroke comparisons for the larger mass configurations are the same as those of the small mass configuration during the initial impact and rebound phase. However, during the rotation to nose-gear contact, the shock-strut strokes for the larger mass configurations show that the main gear does not extend as much as it did with the small mass configuration. This shortened stroke is indicative of reduced airplane motions. In addition, during the nose-gear impact and roll-out phases, the shock-strut strokes for the active gear were less than those of the passive gear because of the control logic employed. However, as the time during roll-out increased, the shock-strut stroke of the active gear approached that of the passive gear, which had attained the value of stroke required to support the static mass of the airplane.

The tabulated percent force-reduction data presented in table II are used to illustrate the effectiveness of the active load-control gear and to aid in discussion of the effects of airplane mass, touchdown sink rate, and runway slope on airframe-gear forces. The active load-control gear was most effective in reducing the airframe-gear forces during main-gear response to nose-gear impact, as shown by the large values of percent force reduction in table II. Significant reductions were also achieved during the initial-impact phase for all the landing simulations investigated. The airframe-gear-force reductions generally increased for the larger mass configurations for landing simulations at the same touchdown sink rate and on the same runway slope during both initial impact and main-gear response to nose-gear impact. For the same mass configuration and runway slope, the airframe-gear-force reductions generally increased for the larger touchdown sink rates. The effect of runway slope was primarily discernible during initial impact, for which the airframe-gear-force reduction was generally greater for the landing simulations on the uphill runway slope at constant mass and touchdown sink rate. This result is to be expected, since the airframe-gear forces for the passive-gear landing simulation are greater because of the added component of sink rate due to airplane horizontal motion into the uphill slope. The airframe-gear forces for the

active-gear landing simulation were essentially the same for landing simulations on uphill or downhill runway slopes. A similar effect of runway slope on airframe-gear-force reduction occurred during the roll-out phase and is most pronounced for the landing simulations of the large mass configuration (figs. 6(i) and 6(k)).

The foregoing results indicate that the active load-control gear is effective in reducing the airframe-gear force relative to that occurring with the passive gear during all phases of a landing. The effectiveness of the active gear was most pronounced for those touchdown conditions which result in large airframe-gear forces with the passive gear; that is, large airplane masses, higher touchdown sink rates, and uphill runway slopes.

Fuselage mass-center displacements.- Comparisons of airplane motions for landing simulations with both passive and active main gears are made with the typical data shown in figure 10. Gravity vertical axis Z_g displacements of the fuselage mass center, which is located 3.05 m (10.0 ft) forward of the airplane composite mass center (airplane c.g.), are shown, relative to its displacement at touchdown, as a function of time. The data presented are for simulations of the medium mass configuration on the uphill slope of runway A at each of the touchdown sink rates investigated. The various phases of the landing simulations which affect the airplane motion are indicated in figure 10(a). Since very little rotation occurs during initial impact, the shock-strut stroke is primarily responsible for the fuselage mass-center displacement. Subsequent to initial impact and prior to nose-gear contact, the fuselage mass-center displacement is due to airplane rebound and rotation. Following nose-gear contact and impact, the displacement results from the change in runway elevation due to the uphill slope.

The fuselage mass-center displacements for the landing simulation with the active gear are greater during initial impact than those occurring with the passive gear because of the greater shock-strut stroke required by the active gear. However, during rebound from initial impact and rotation through nose-gear impact, the displacements are significantly reduced by the active gear compared with those of the passive gear. This reduction in displacement results from the reduced rebound of the airplane with the active gear due to controlled variations of the shock-strut stroke. The magnitude of the secondary motions, which occur with the passive gear during the roll-out phase, is reduced by the active gear through control of the shock-strut force and stroke.

These results are typical of those obtained during the airplane landing simulations for the small and large mass configurations. These results indicate that the active gear is effective in reducing airplane motions following initial impact.

Cyclic forces.- The cyclic forces on an airplane structure are important since the fatigue damage sustained by the structure is primarily a function of cyclic loadings due to the ground-air-ground loads, maneuver loads, gust loads, acoustic loads, and ground operational loads. For most parts of a conventional transport airplane structure, the fatigue damage sustained from cyclic ground operational loads is small compared with the fatigue damage sustained during other phases of operation. However, the application of active controls to

reduce aerodynamic maneuver and/or gust loads or increased operation of supersonic cruise airplanes at altitudes where the number of gusts encountered are considerably smaller will cause the ground operational loads to become proportionately more important.

A comparison of the typical airframe-gear-force time histories presented in figure 6 for the simulated airplane landings with passive and active gears shows that the magnitude of the cyclic forces with the active gear was substantially less than that with the passive gear during all phases of the landings. An in-depth structural-fatigue analysis is not considered appropriate for the analytical data presented in this paper; however, to obtain an indication of the effect of the reduction in cyclic forces on fatigue damage, obtained with the active gear, the following procedure was used. The fatigue life of a structure (ref. 4), for fully reversed stress, may be expressed by

$$N = \frac{A}{\sigma^5}$$

where

A a constant for a given material and loading pattern

N number of cycles to failure

σ peak-to-peak stress

and the exponent 5 is a typical value used in structural-fatigue analysis and is the value used in this study. Since the airplane structure in this study is the same for landing simulations with the passive and active gears, the term A is a constant and force reductions are equivalent to stress reductions. Therefore, the number of cycles to failure for the airplane structure can be expressed as

$$N_p = \frac{A}{F_p^5}$$

and

$$N_a = \frac{A}{F_a^5}$$

where F represents the peak-to-peak forces and subscripts p and a represent passive and active gears, respectively. Fatigue damage D can be defined as the inverse of the fatigue life, that is,

$$D_p = \frac{1}{N_p} = \frac{F_p^5}{A}$$

and

$$D_a = \frac{1}{N_a} = \frac{F_a{}^5}{A}$$

Hence, the damage to the structure with the active gear relative to that with the passive gear is

$$\frac{D_a}{D_p} = \frac{F_a{}^5/A}{F_p{}^5/A} = \frac{F_a{}^5}{A}\frac{A}{F_p{}^5} = \frac{F_a{}^5}{F_p{}^5}$$

or

$$D_a = \left(\frac{F_a}{F_p}\right)^5 D_p$$

The damage occurring with the passive gear is assumed to be unity to permit evaluation of the relative damage occurring with the active gear.

Results of the application of this procedure to the cyclic airframe-gear forces obtained from landing simulations of the large mass configuration with passive and active gears at a touchdown sink rate of 0.9 m/sec (3.0 ft/sec) on the uphill slope of runway A are shown in figure 11. Negative and positive force bounds for the passive and active gears were obtained by averaging the rms values of the peak negative and peak positive forces measured during the landing simulations. Summing the absolute values of the force bounds results in the average of the rms values of all peak-to-peak forces equal to 59.920 kN (13 471 lbf) for the passive gear F_p and 14.13 kN (3177 lbf) for the active gear F_a. Applying these forces in the relative damage equation gives

$$\frac{D_a}{D_p} = \left(\frac{14.13}{59.920}\right)^5 = 0.0007$$

Since the structural-fatigue damage which occurs with the passive gear is assumed to be unity, the damage which occurred with the active gear for the same landing conditions was less than 1 percent of that resulting with the passive gear.

The data obtained from applying this procedure to all landing simulations of this study are presented in table III. The data are presented as peak negative and positive rms average forces and rms average peak-to-peak forces (F_p and F_a) for landing simulations with both passive and active gears. The potential of the active gear to reduce structural fatigue damage (relative to that of the passive gear) is also shown for each landing simulation made during the study. The average value of this fatigue damage is 0.14; that is, structural fatigue damage with the active gear was 86 percent less than that which would occur with the passive gear.

CONCLUDING REMARKS

This paper presents the results of a study to evaluate the capability of ACOLAG for predicting the landing dynamics of airplanes with passive and active main gears, and results of the application of that program to an analytical investigation of the dynamic behavior during landing of a large airplane equipped with both types of main gears.

Correlations between computed data from ACOLAG, computed data from FATOLA, and preliminary experimental drop-test data (for a modified active control main gear from a light airplane) indicate that ACOLAG is valid for predicting the landing dynamics of airplanes with both passive and active load-control main landing gears. Results from the analytical parameter study show that the active load-control gear performs within formulated operational constraints. The operation of a simplified antiskid braking system was shown to have no detrimental effects on the performance of the active gear, and it is possible that improved braking performance could be obtained with the active gear. A comparison of the passive- and active-gear results indicates that the active gear is more effective in reducing airframe-gear forces than the passive gear for all parameters investigated and during all phases of a landing. The effectiveness of the active gear was most pronounced for those touchdown conditions which would result in developing large airframe-gear forces with the passive gear, that is, large airplane masses, higher touchdown sink rates, and uphill runway slopes. The active gear is also effective in reducing airplane motions following initial impact. The reduction in cyclic forces resulting from use of the active gear indicates the potential for significant reductions in structural fatigue damage during ground operations.

Langley Research Center
National Aeronautics and Space Administration
Hampton, VA 23665
October 16, 1979

APPENDIX

ADDITIONAL DATA FOR AIRPLANE LANDING SIMULATIONS

This appendix presents data for airplane landing simulations of the small mass configuration at a touchdown sink rate of 1.5 m/sec (5.0 ft/sec) on the uphill and downhill slopes of the more uneven runway (runway B). Data are also presented for the airplane landing simulations of all mass configurations at touchdown sink rates of 0.3 m/sec (1.0 ft/sec) and 1.5 m/sec (5.0 ft/sec) on the uphill and downhill slopes of runway A.

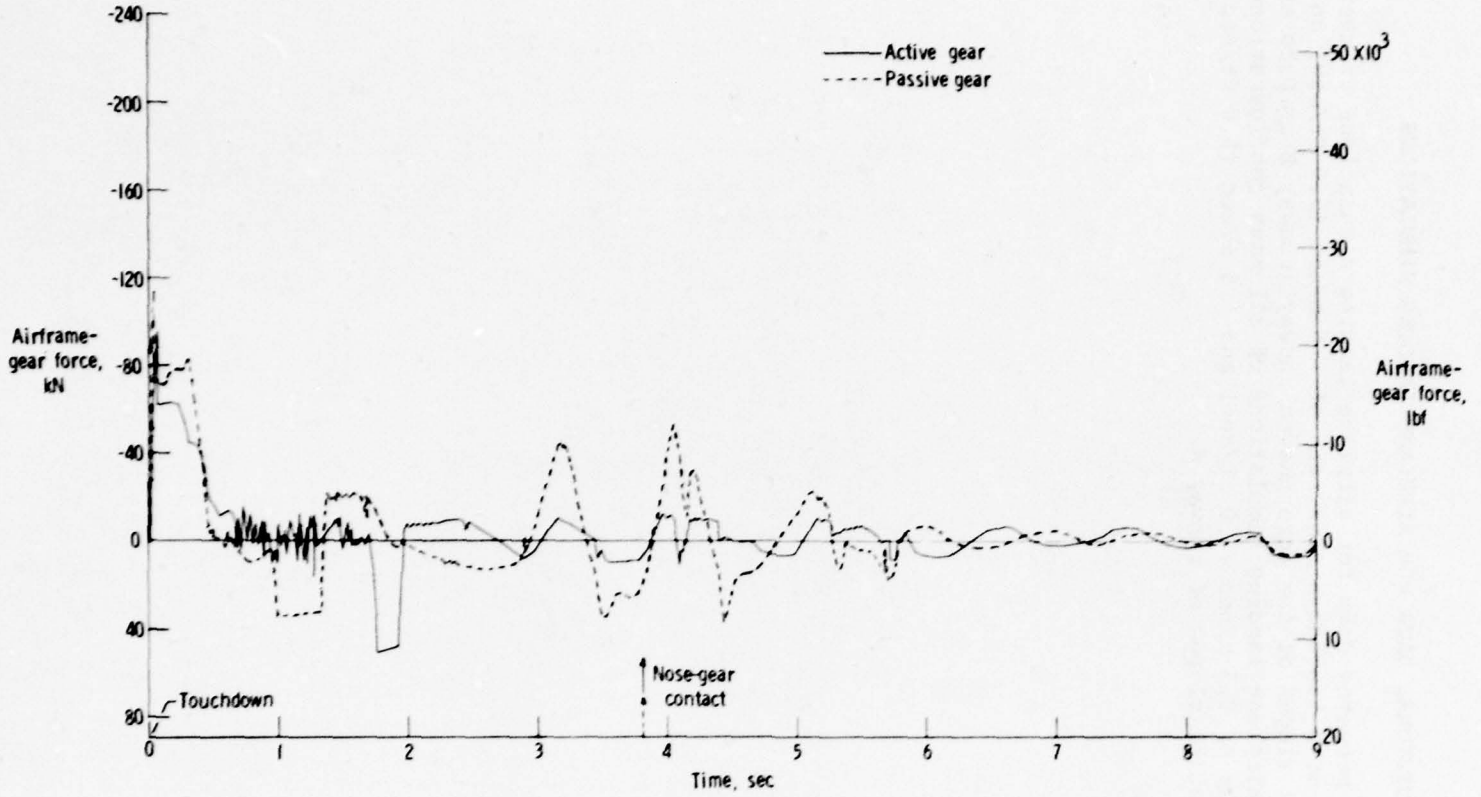

(a) Airframe-gear forces; uphill runway.

Figure A1.- Airframe-gear force and shock-strut-stroke time histories for landing simulations of airplane with passive and active main gears. Small mass configuration; runway B; sink rate, 1.5 m/sec (5.0 ft/sec).

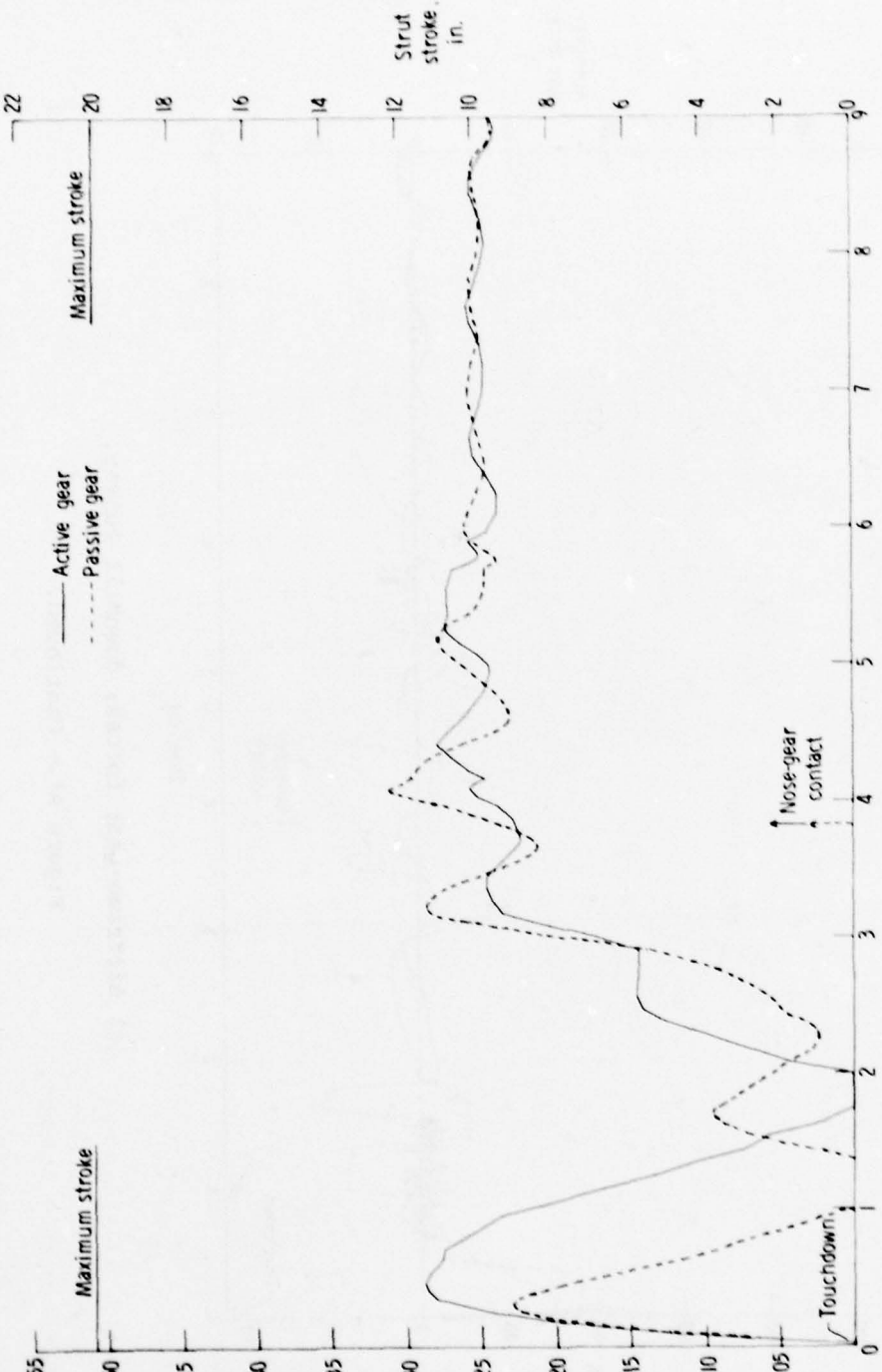

(b) Shock-strut strokes; uphill runway.

Figure A1.- Continued.

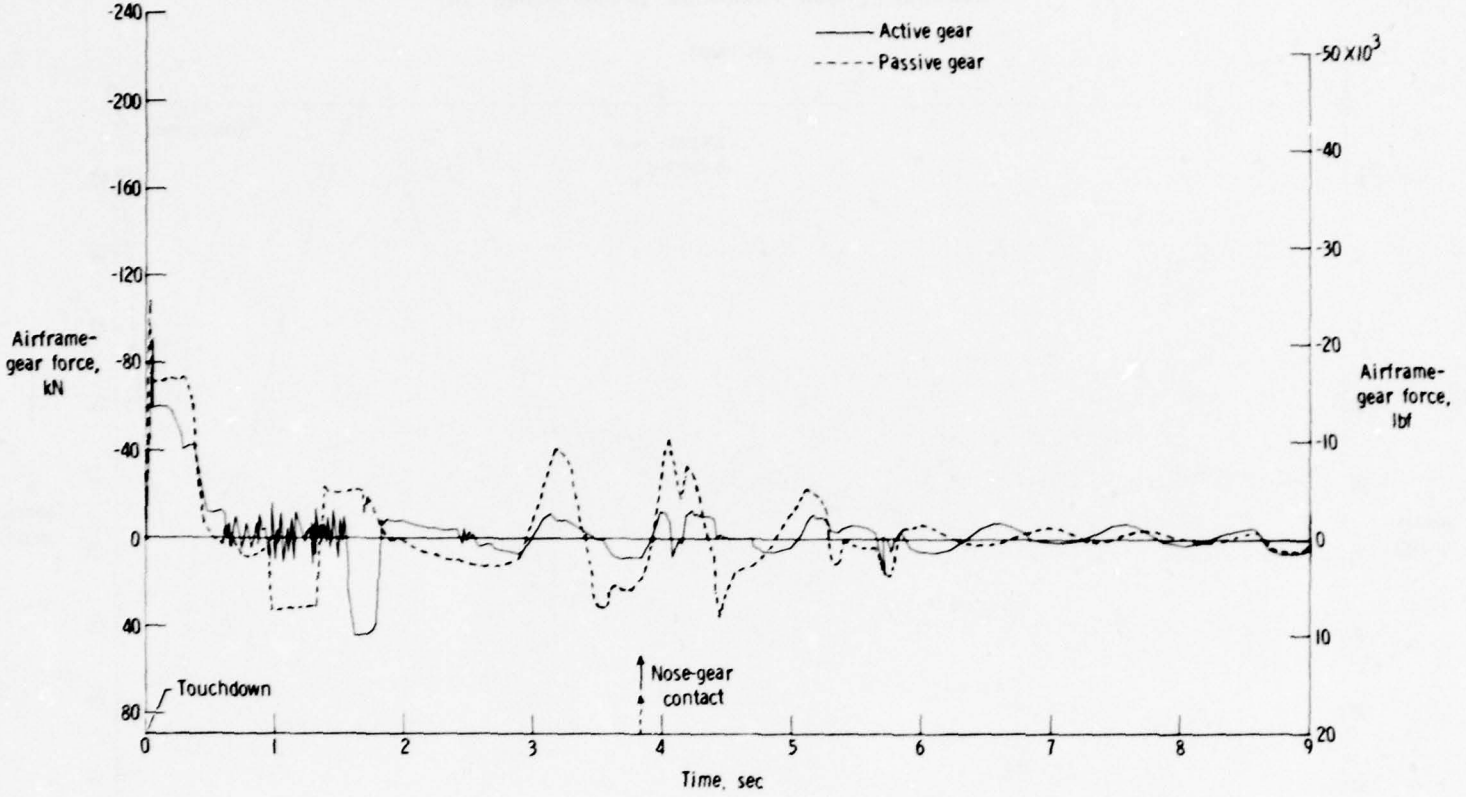

(c) Airframe-gear forces; downhill runway.

Figure A1.- Continued.

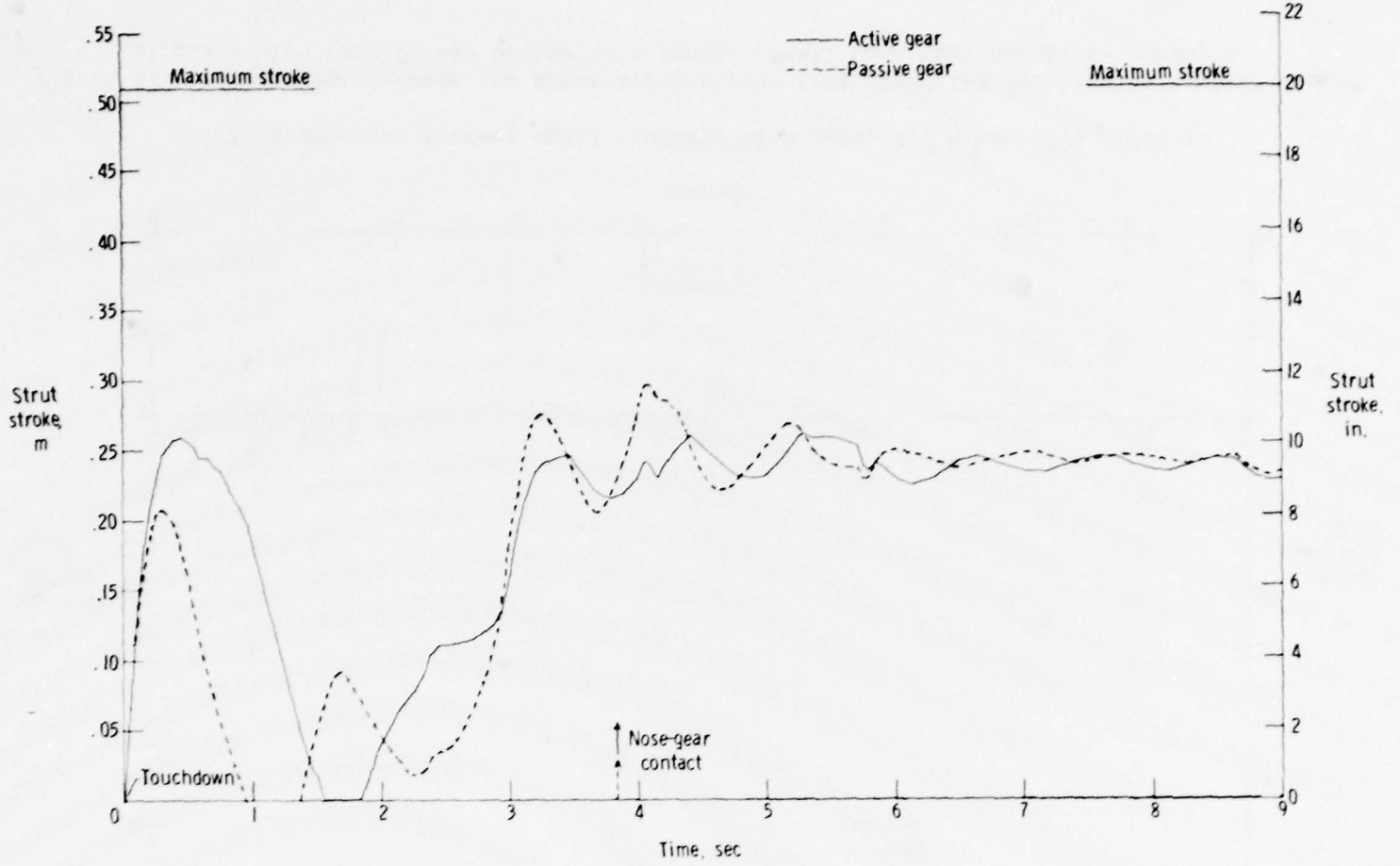

(d) Shock-strut strokes; downhill runway.

Figure A1.- Concluded.

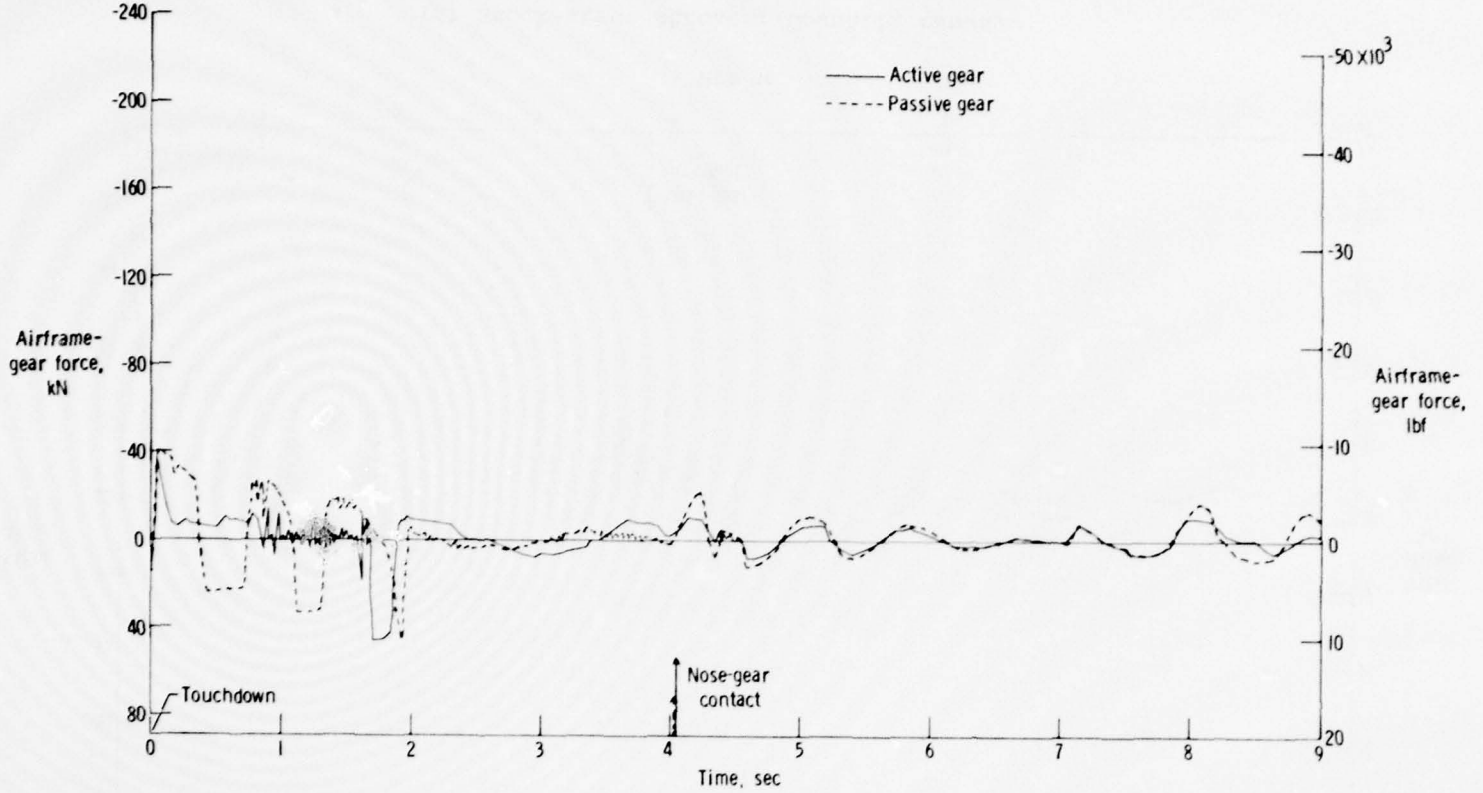

(a) Airframe-gear forces; uphill runway; sink rate, 0.3 m/sec (1.0 ft/sec).

Figure A2.- Airframe-gear-force and shock-strut-stroke time histories for landing simulations of airplane with passive and active main gears. Small mass configuration; runway A.

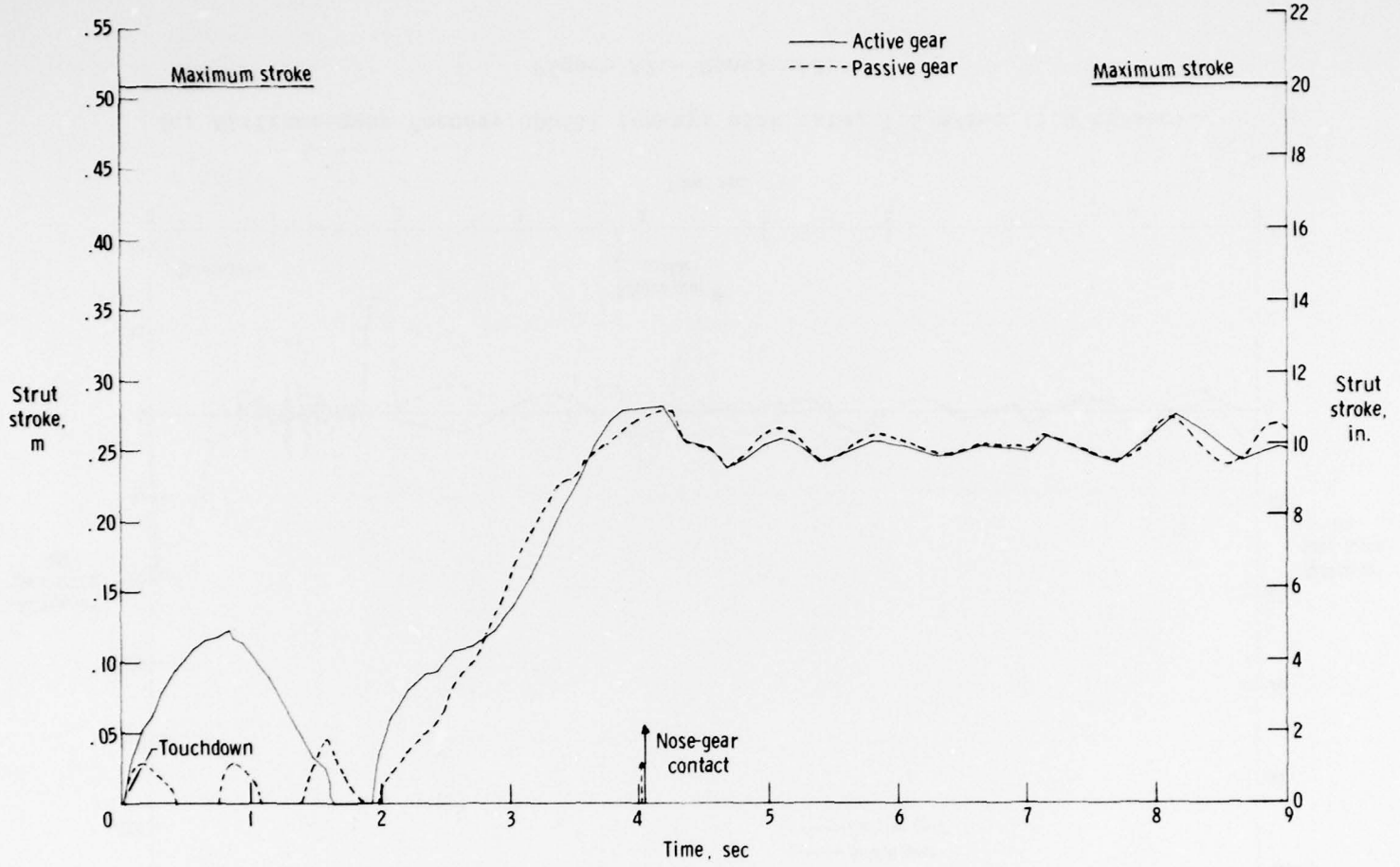

(b) Shock-strut strokes; uphill runway; sink rate, 0.3 m/sec (1.0 ft/sec).

Figure A2.- Continued.

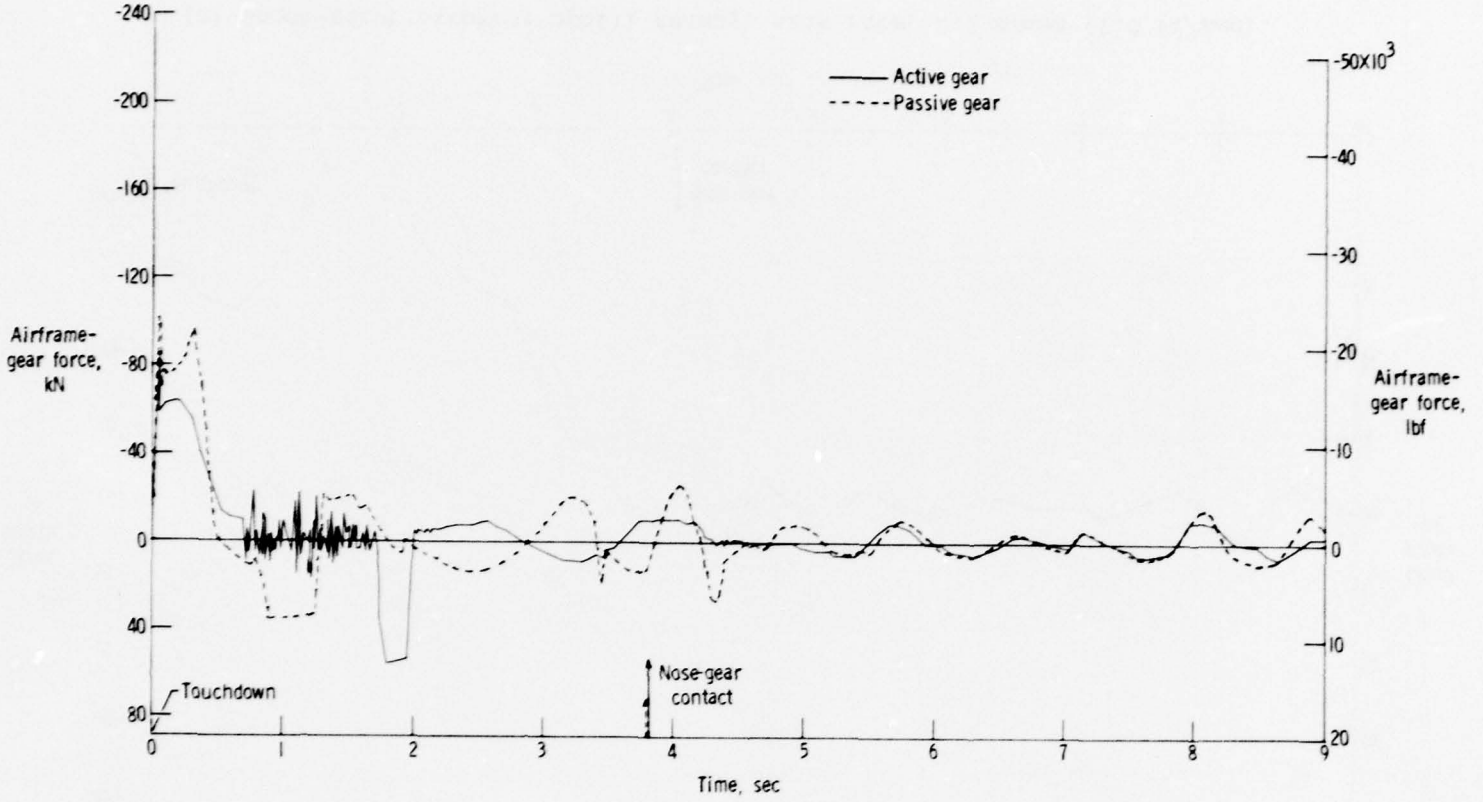

(c) Airframe-gear forces; uphill runway; sink rate, 1.5 m/sec (5.0 ft/sec).

Figure A2.- Continued.

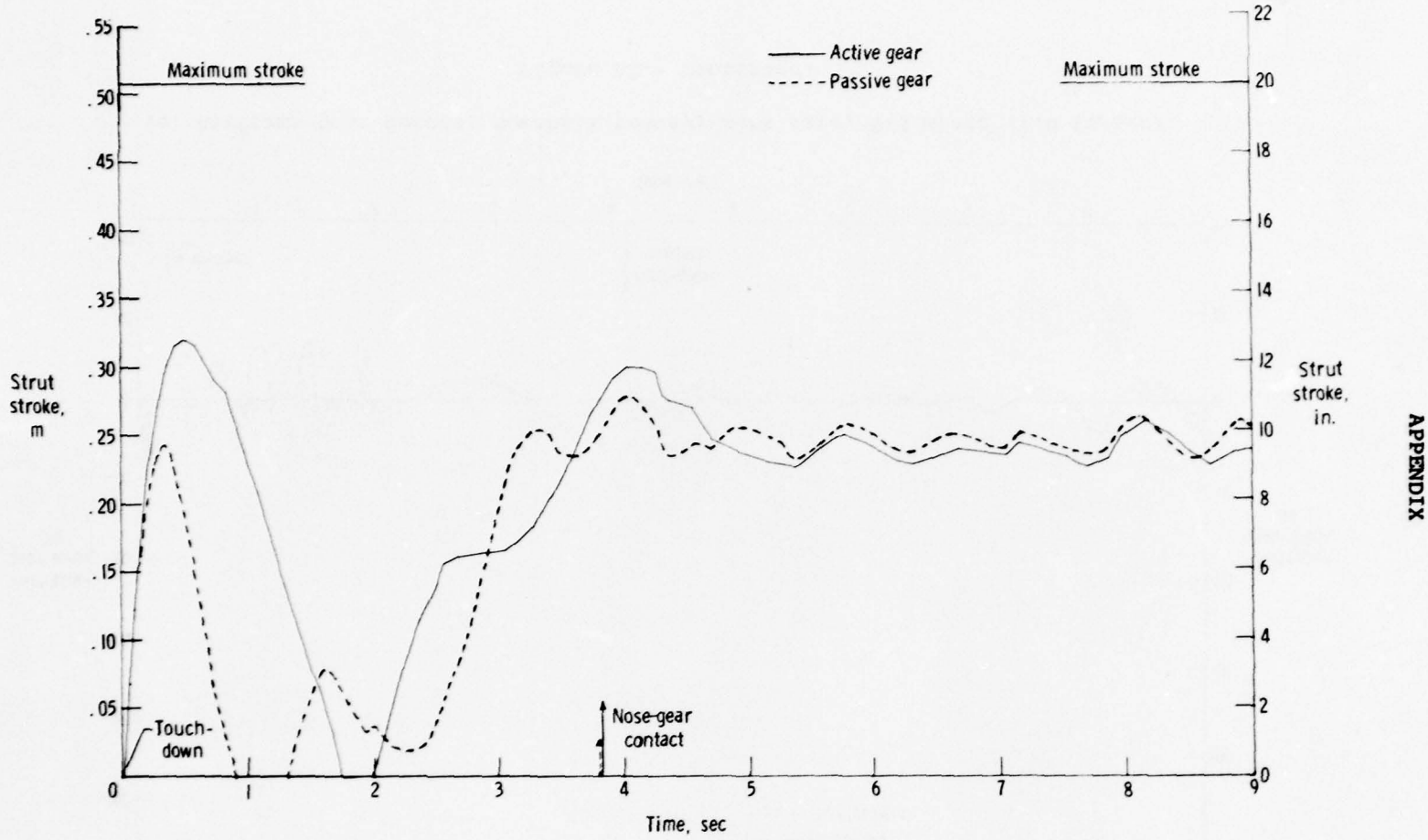

(d) Shock-strut strokes; uphill runway; sink rate, 1.5 m/sec (5.0 ft/sec).

Figure A2.- Continued.

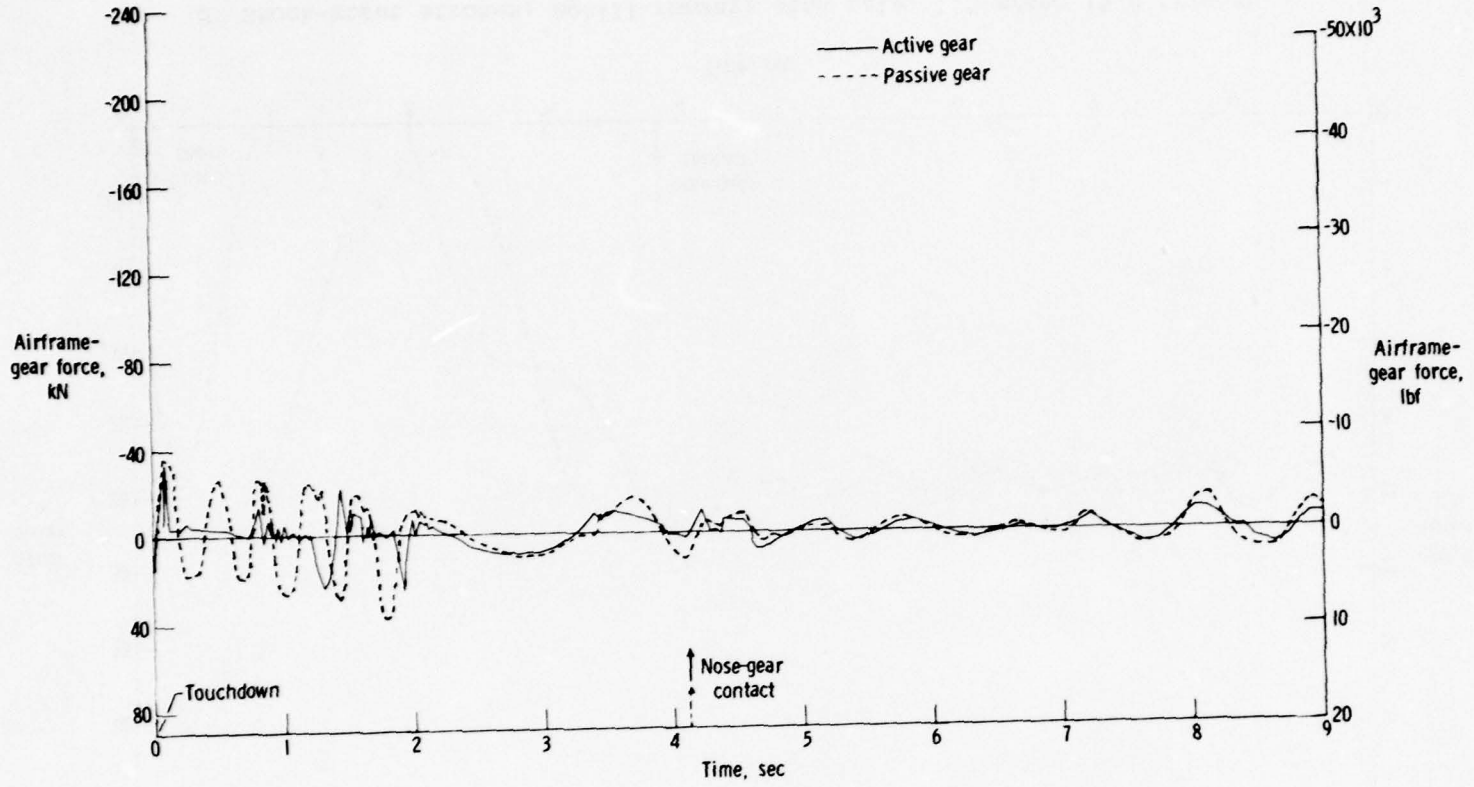

(e) Airframe-gear forces; downhill runway; sink rate, 0.3 m/sec (1.0 ft/sec).

Figure A2.- Continued.

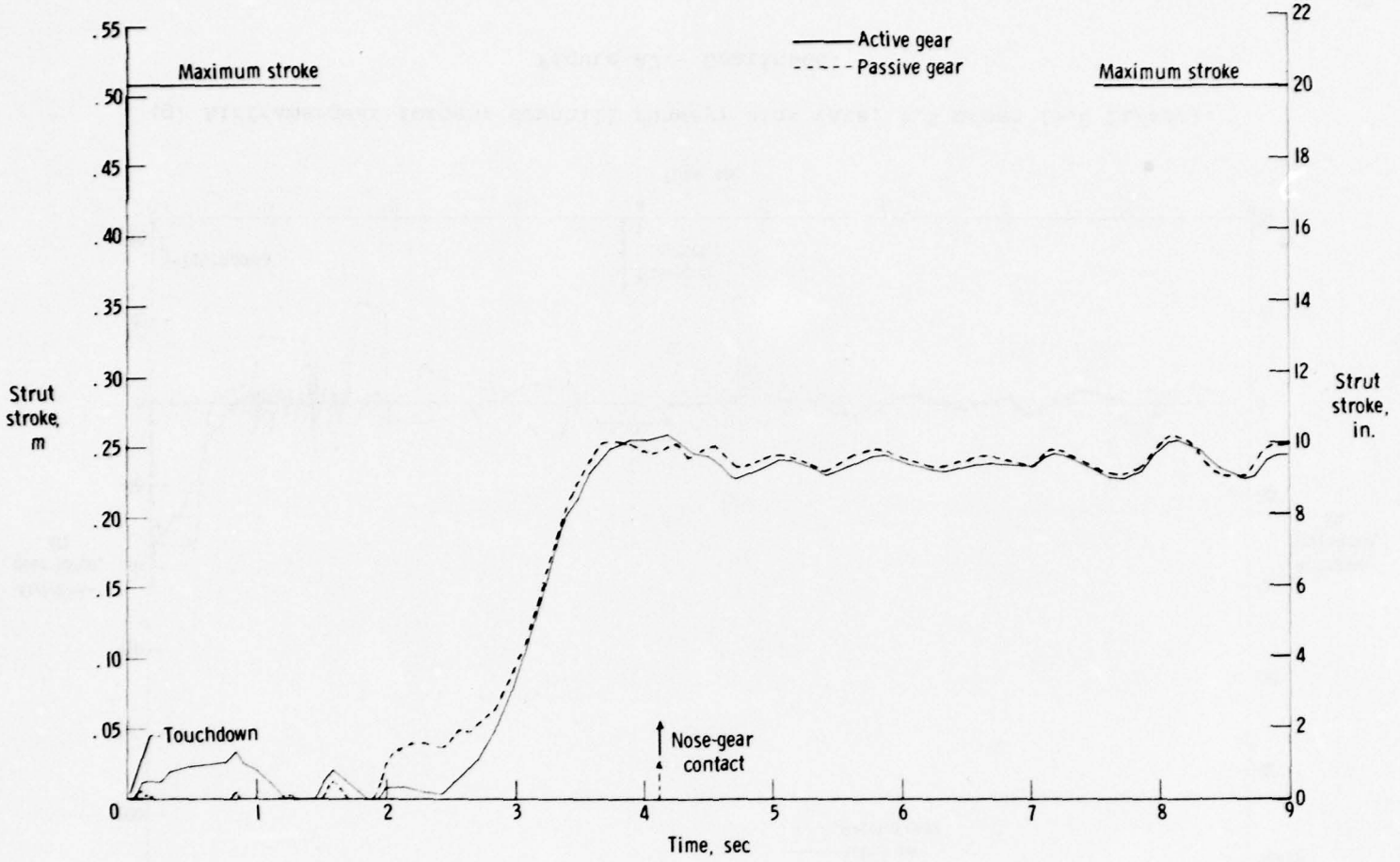

(f) Shock-strut strokes; downhill runway; sink rate, 0.3 m/sec (1.0 ft/sec).

Figure A2.- Continued.

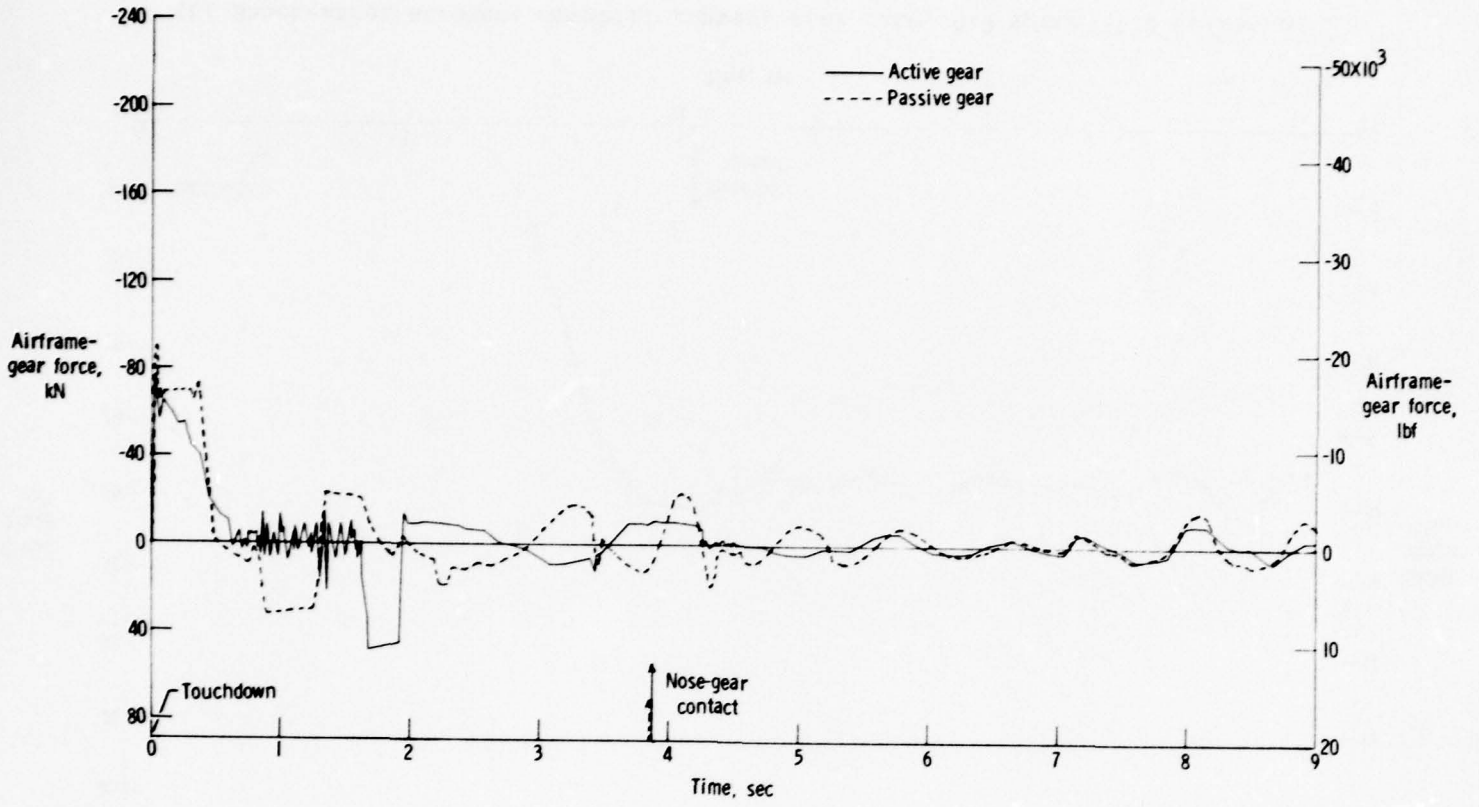

(g) Airframe-gear forces; downhill runway; sink rate, 1.5 m/sec (5.0 ft/sec).

Figure A2.- Continued.

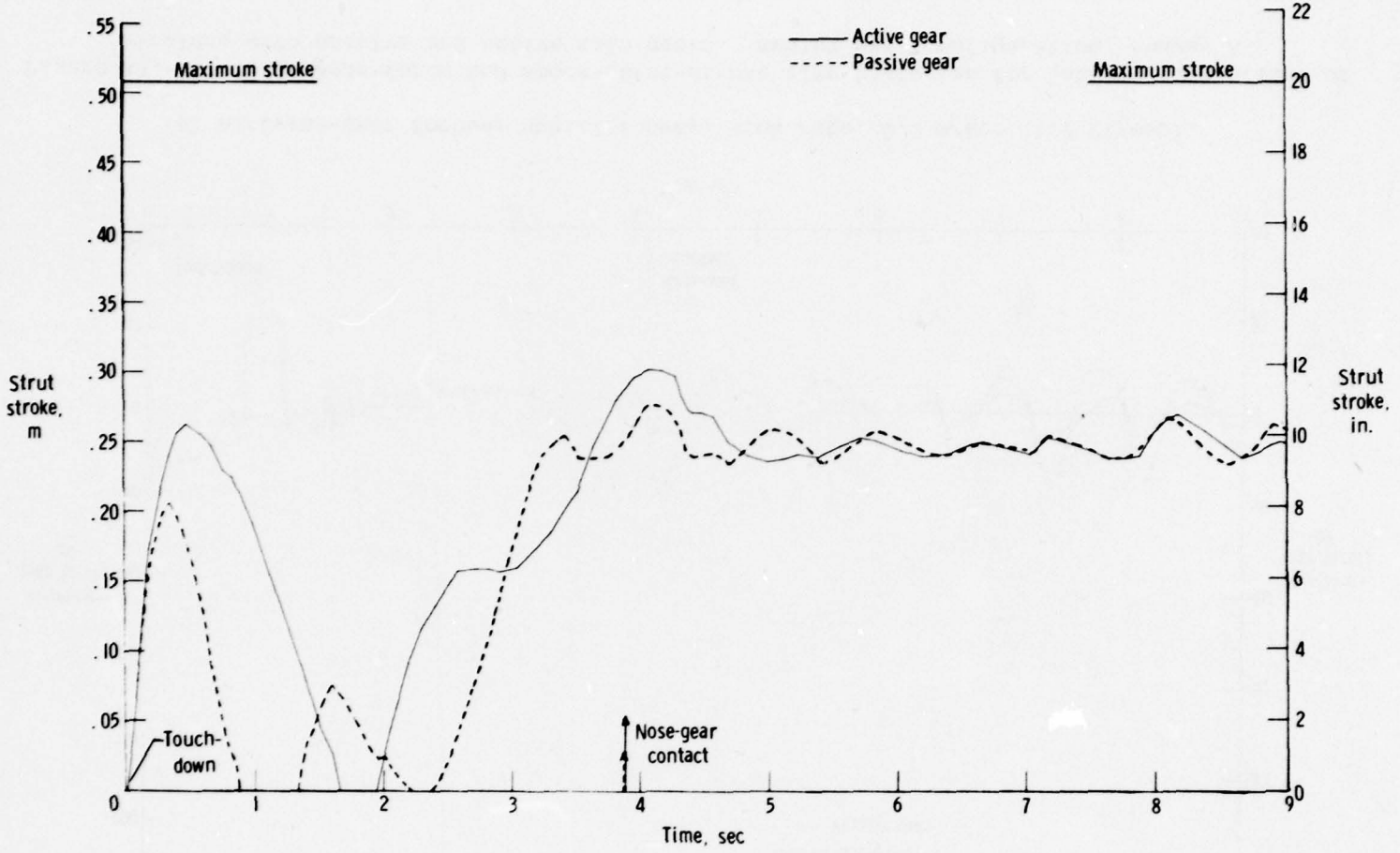

(h) Shock-strut strokes; downhill runway; sink rate, 1.5 m/sec (5.0 ft/sec).

Figure A2.- Concluded.

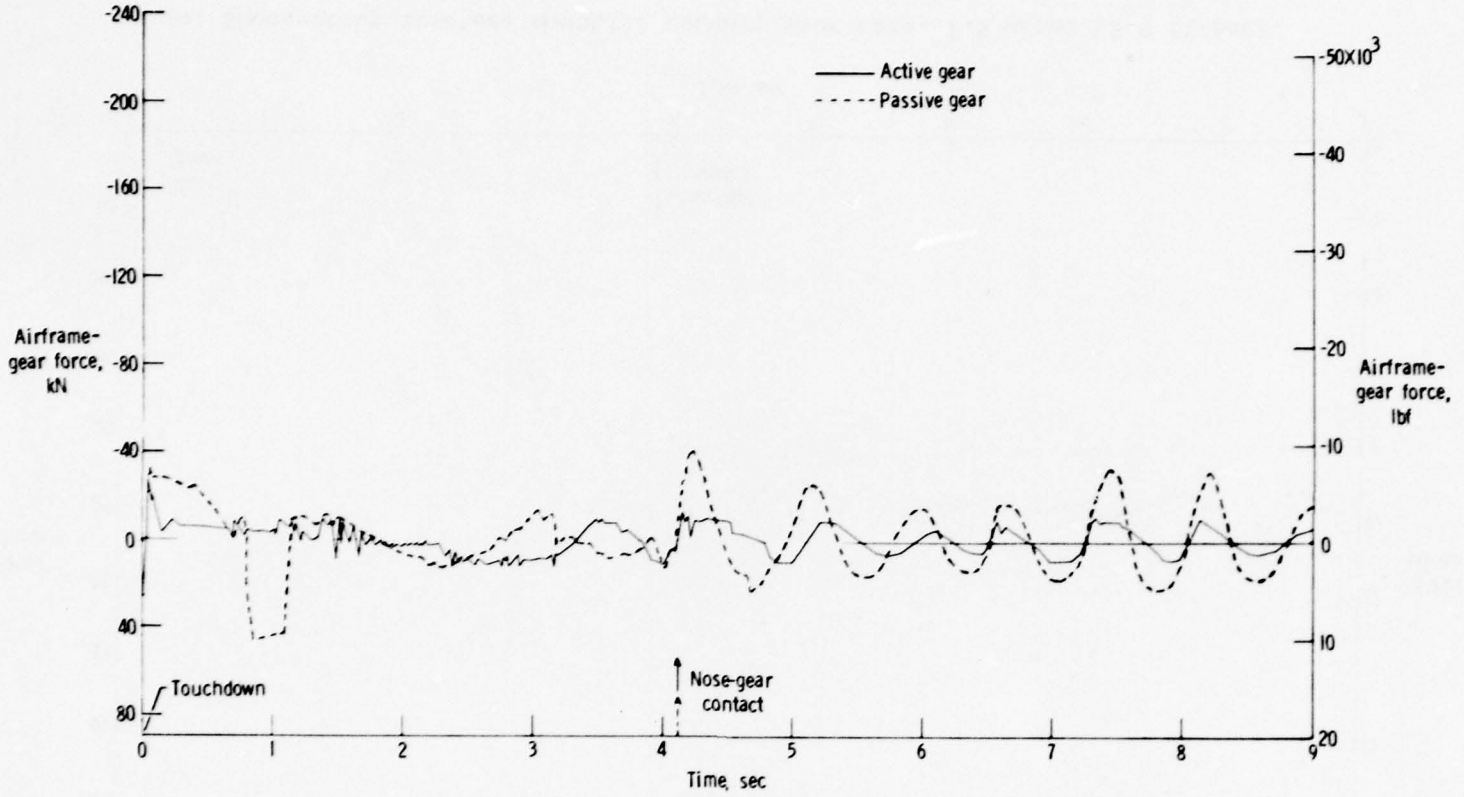

(a) Airframe-gear forces; uphill runway; sink rate, 0.3 m/sec (1.0 ft/sec).

Figure A3.- Airframe-gear-force and shock-strut-stroke time histories for landing simulations of airplane with passive and active main gears. Medium mass configuration; runway A.

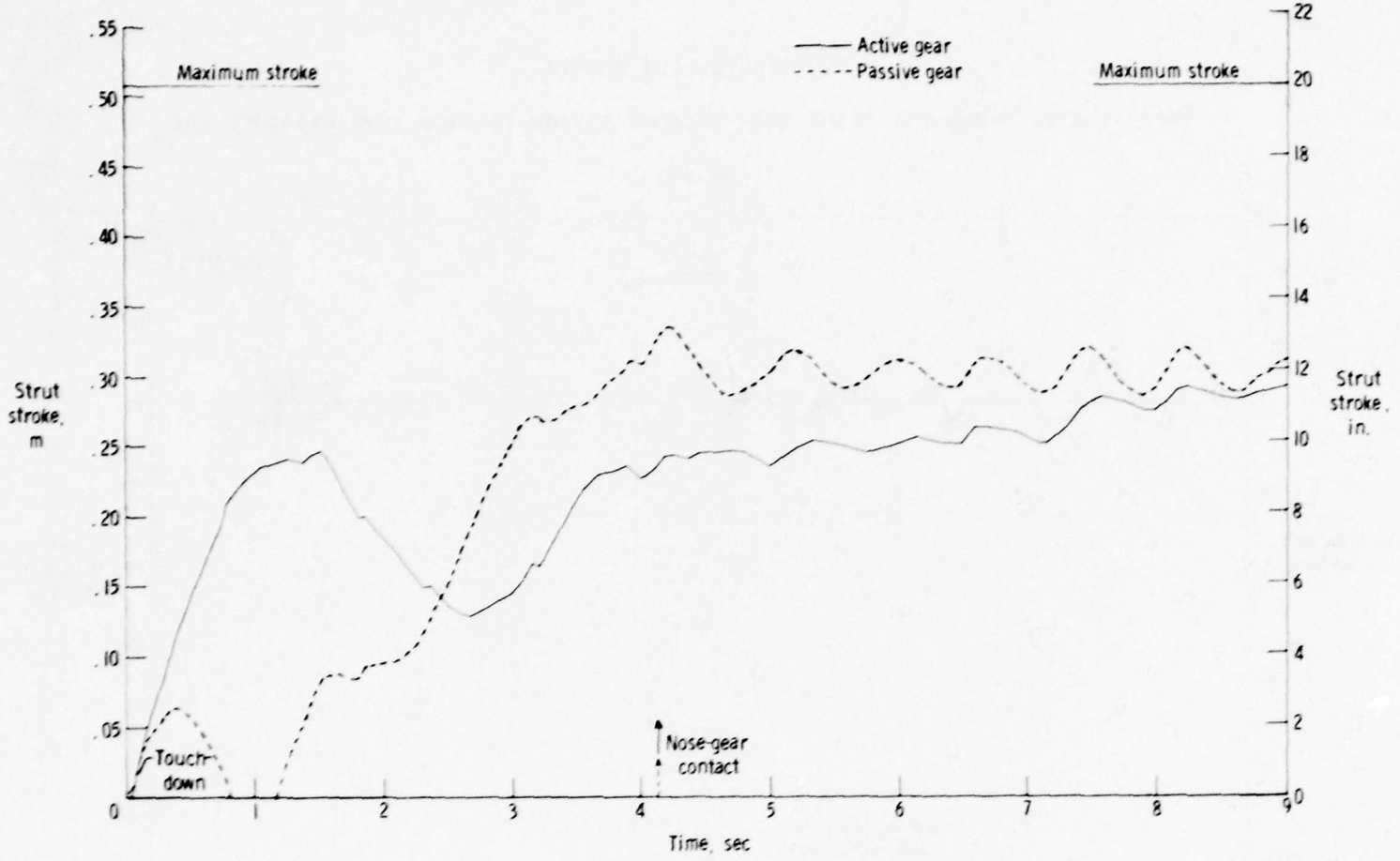

(b) Shock-strut strokes; uphill runway; sink rate, 0.3 m/sec (1.0 ft/sec).

Figure A3.- Continued.

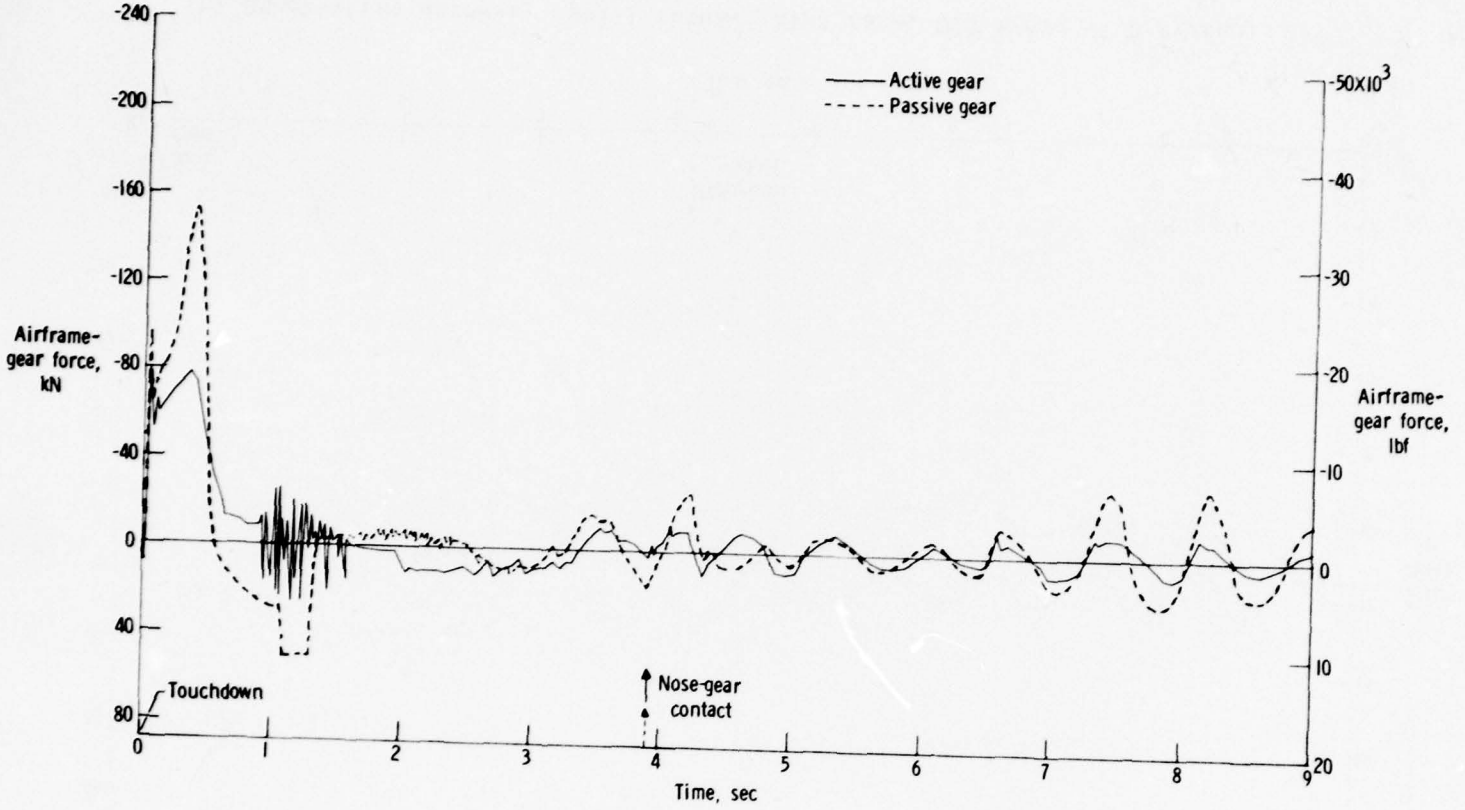

(c) Airframe-gear forces; uphill runway; sink rate, 1.5 m/sec (5.0 ft/sec).

Figure A3.- Continued.

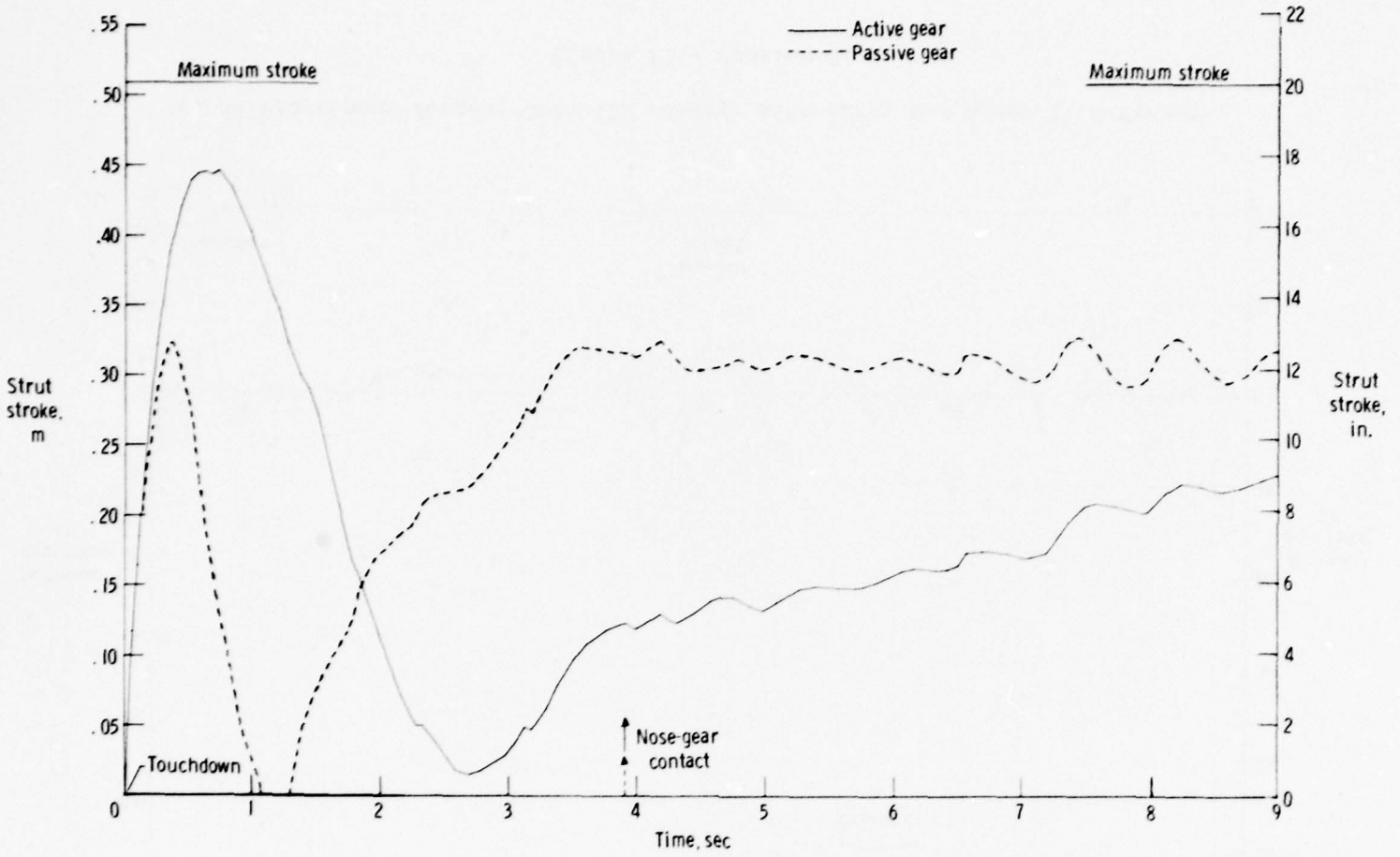

(d) Shock-strut strokes; uphill runway; sink rate, 1.5 m/sec (5.0 ft/sec).

Figure A3.- Continued.

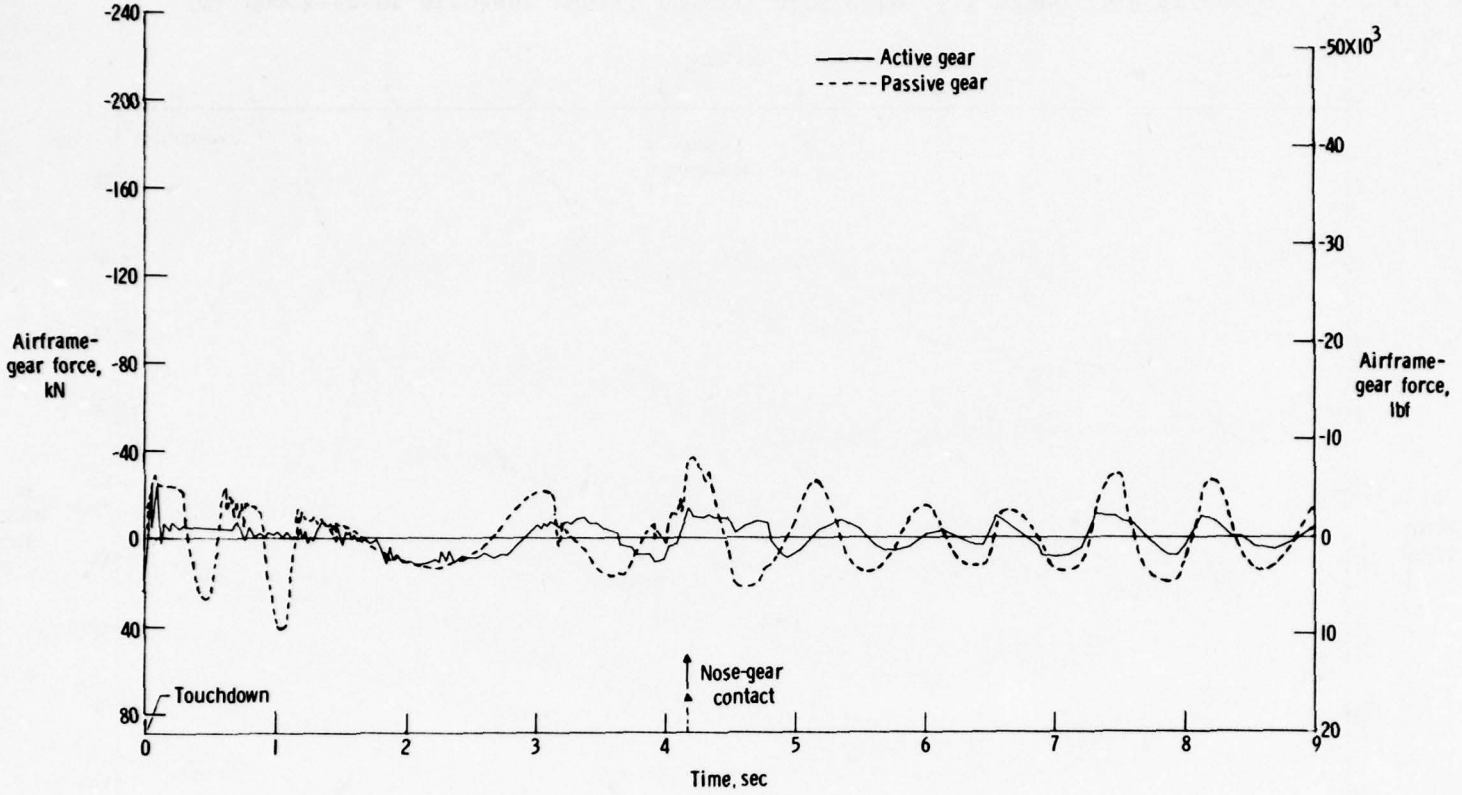

(e) Airframe-gear forces; downhill runway; sink rate, 0.3 m/sec (1.0 ft/sec).

Figure A3.- Continued.

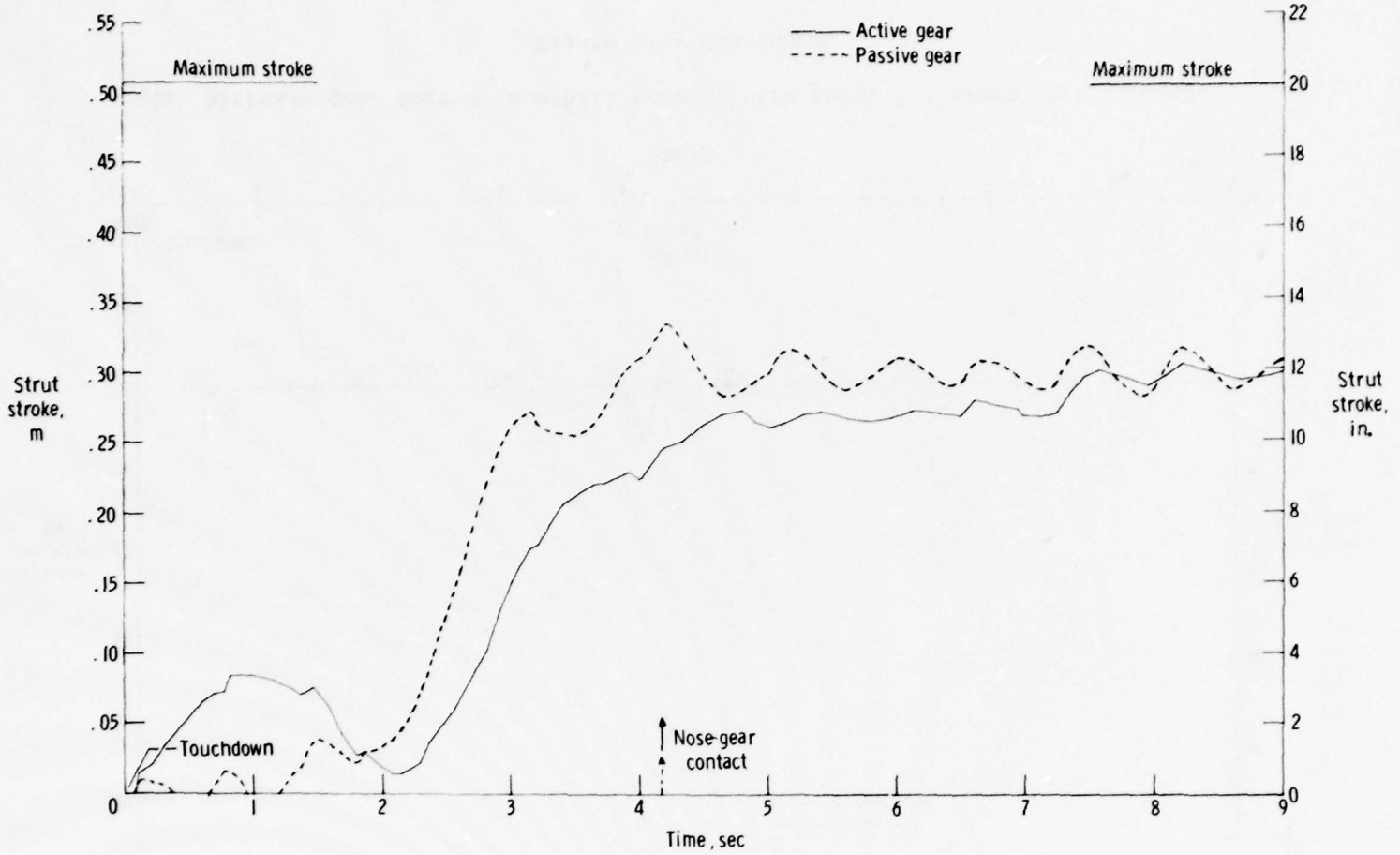

(f) Shock-strut strokes; downhill runway; sink rate, 0.3 m/sec (1.0 ft/sec).

Figure A3.- Continued.

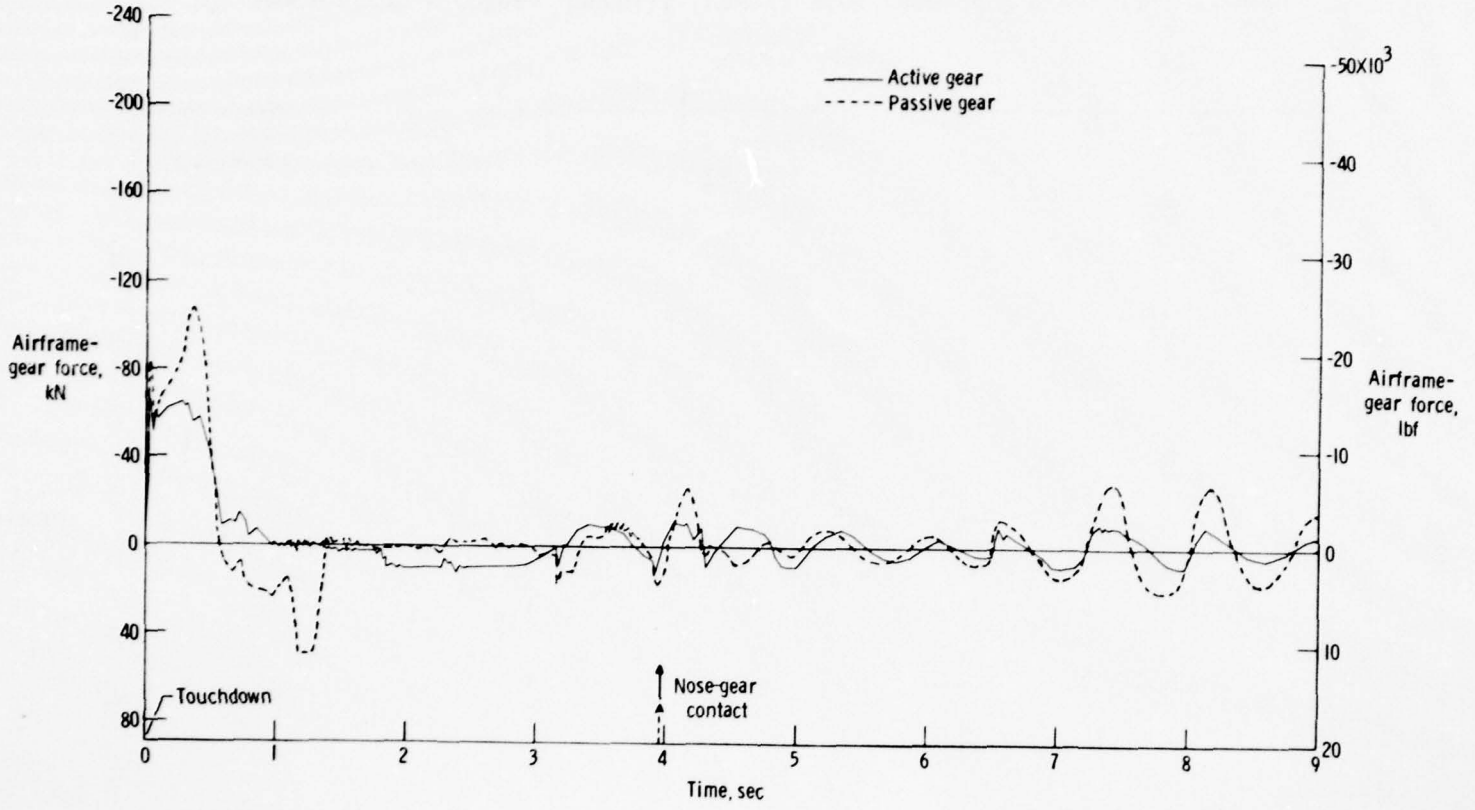

(g) Airframe-gear forces; downhill runway; sink rate, 1.5 m/sec (5.0 ft/sec).

Figure A3.- Continued.

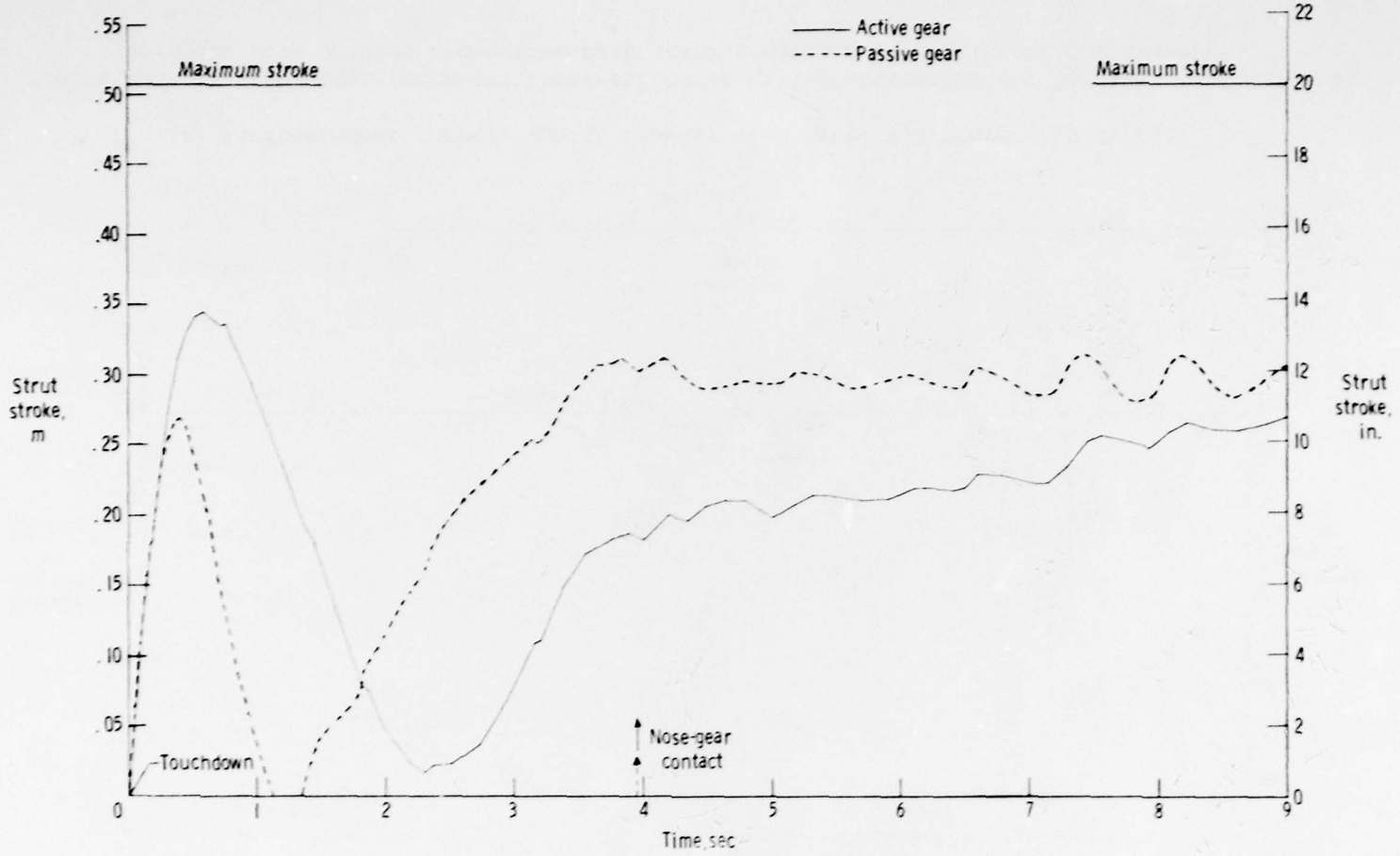

(h) Shock-strut strokes; downhill runway; sink rate, 1.5 m/sec (5.0 ft/sec).

Figure A3.- Concluded.

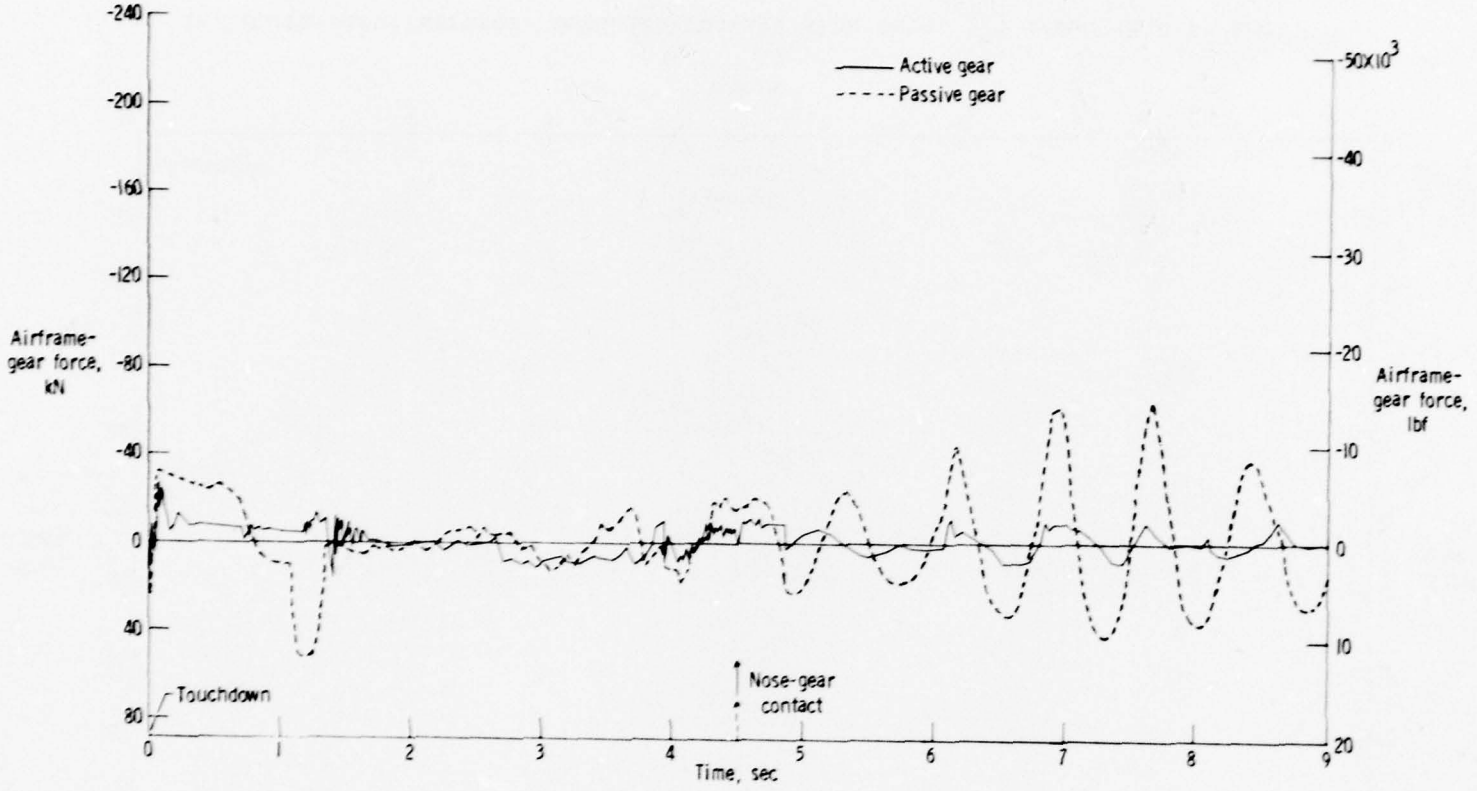

(a) Airframe-gear forces; uphill runway; sink rate, 0.3 m/sec (1.0 ft/sec).

Figure A4.- Airframe-gear-force and shock-strut-stroke time histories for landing simulations of airplane with passive and active main gears. Large mass configuration; runway A.

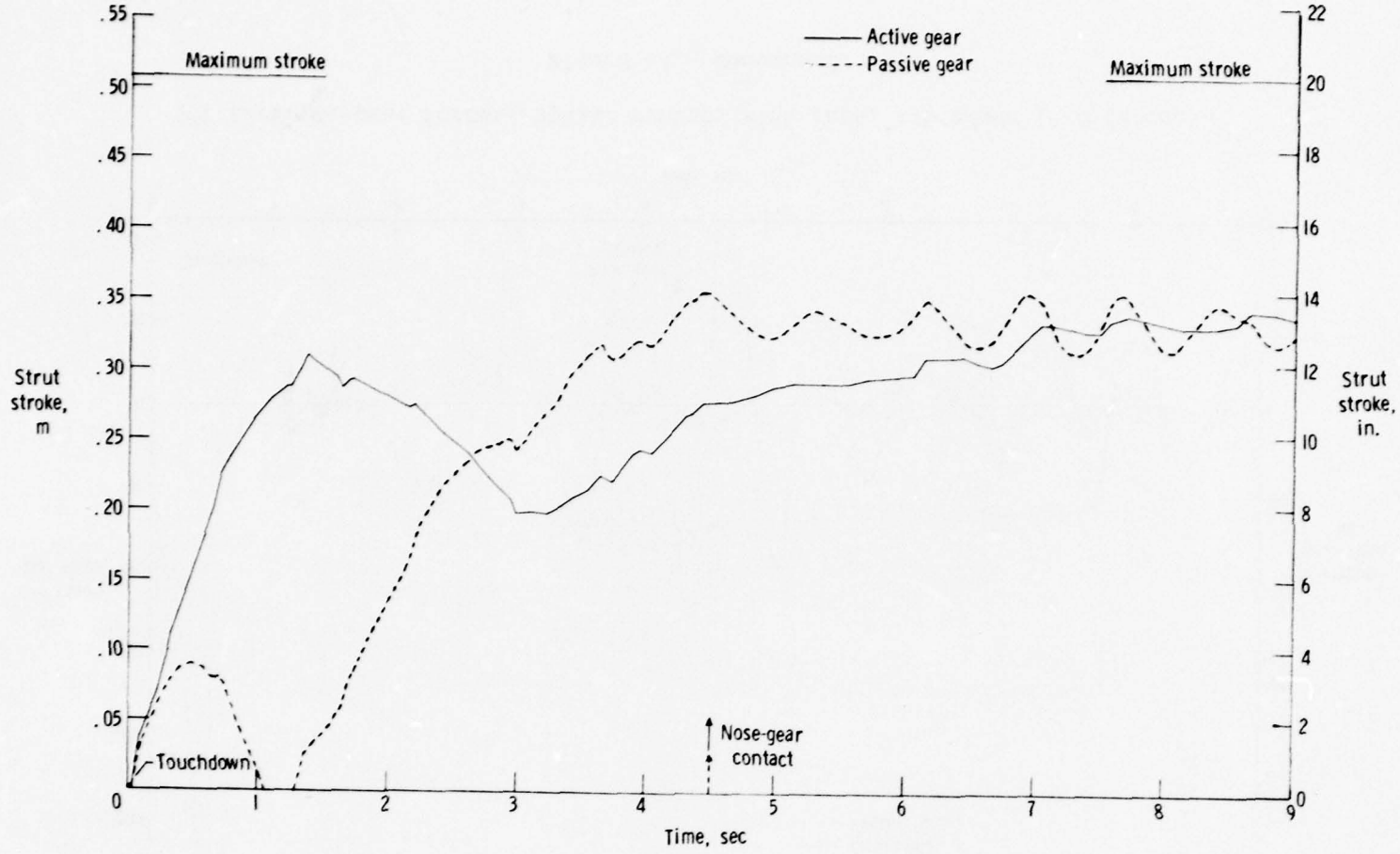

(b) Shock-strut strokes; uphill runway; sink rate, 0.3 m/sec (1.0 ft/sec).

Figure A4.- Continued.

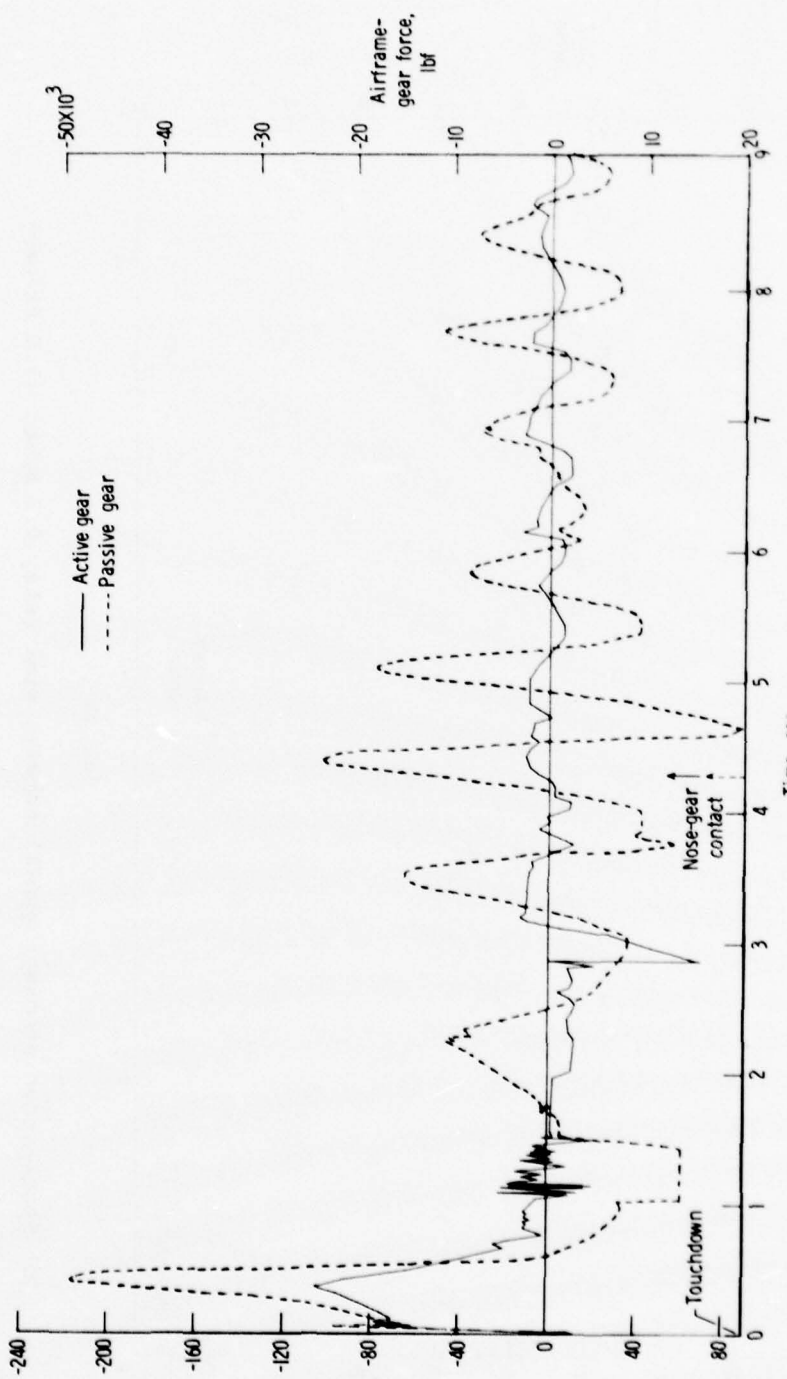

(c) Airframe-gear forces; uphill runway; sink rate, 1.5 m/sec (5.0 ft/sec).

Figure A4.- Continued.

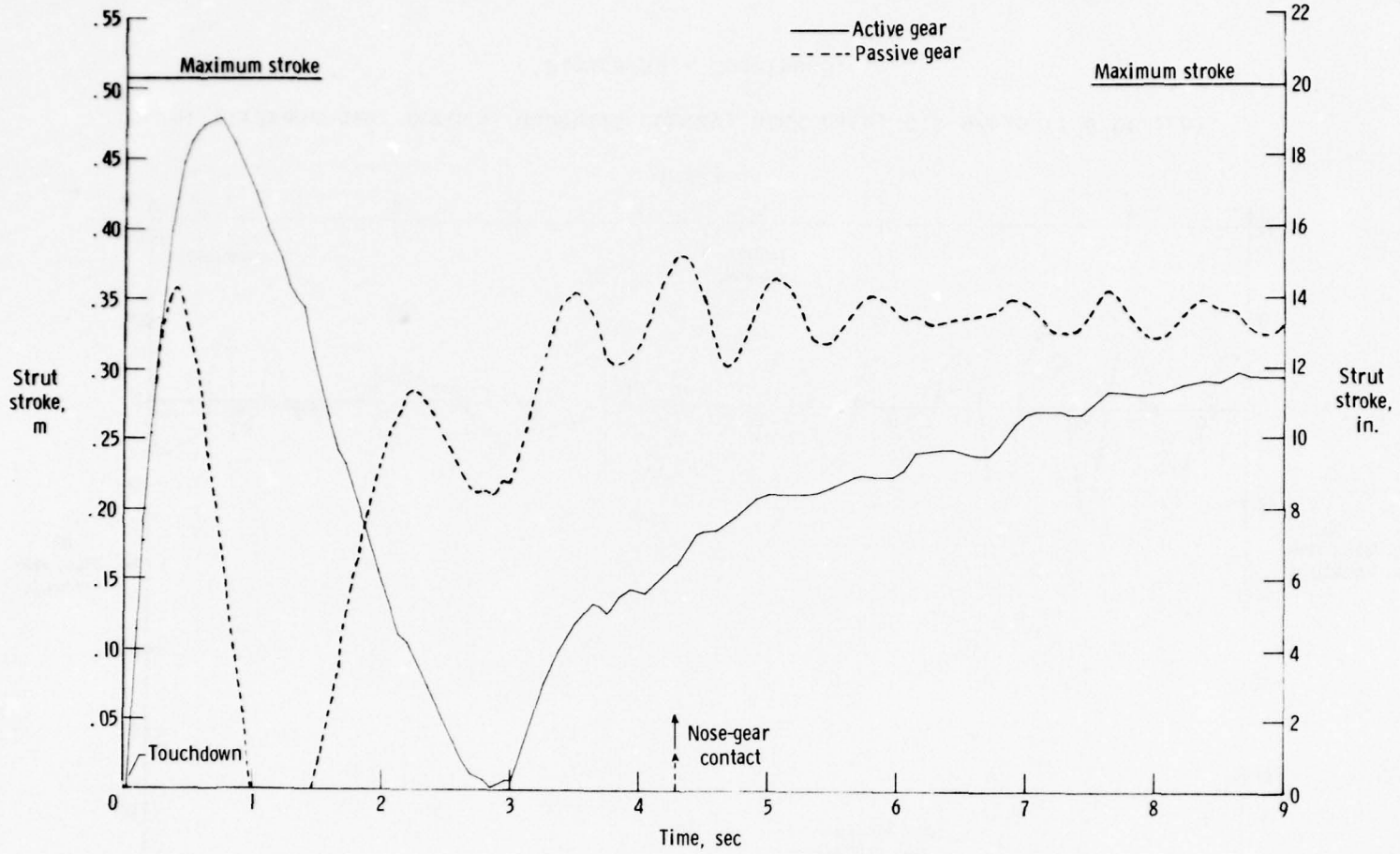

(d) Shock-strut strokes; uphill runway; sink rate, 1.5 m/sec (5.0 ft/sec).

Figure A4.- Continued.

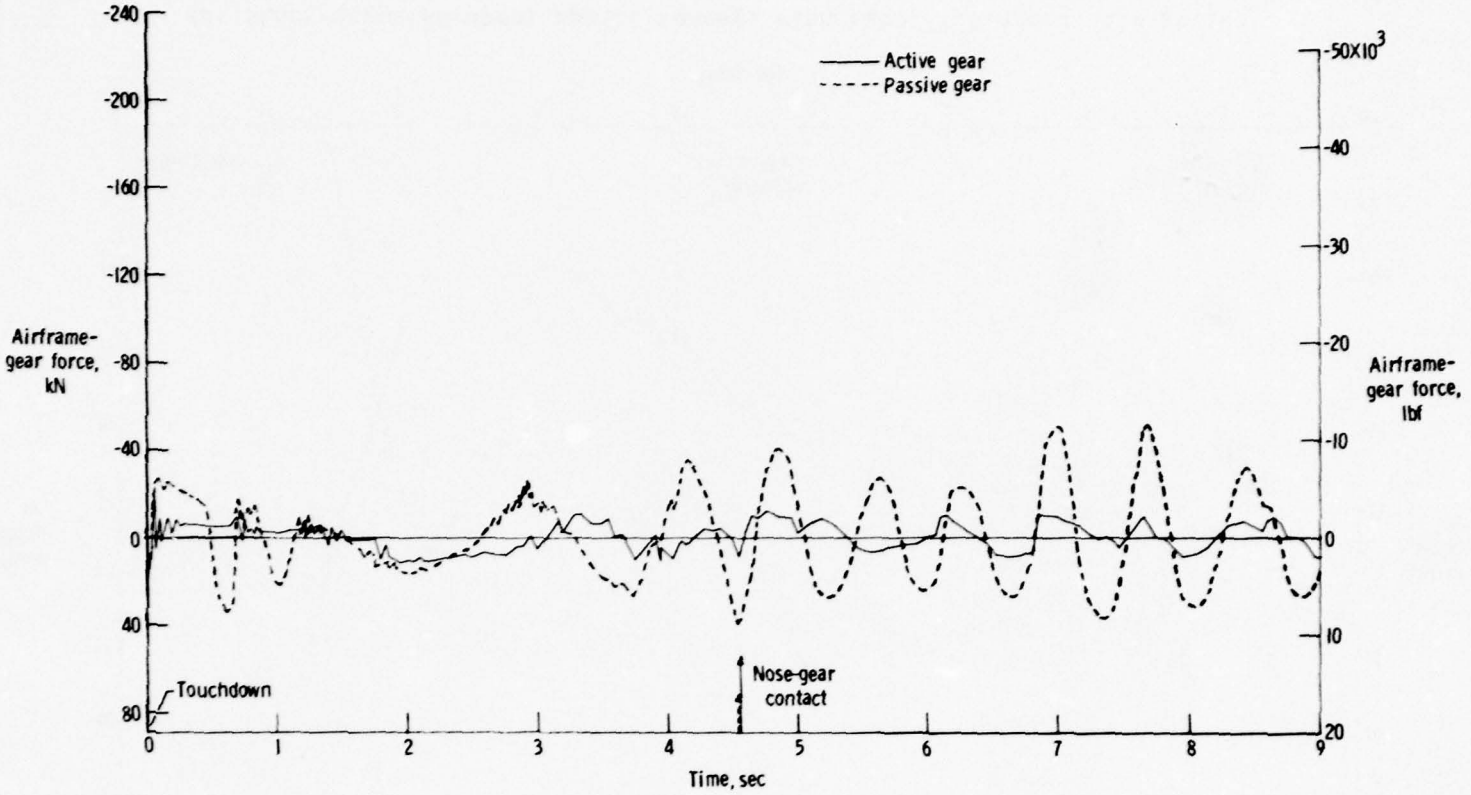

(e) Airframe-gear forces; downhill runway; sink rate, 0.3 m/sec (1.0 ft/sec).

Figure A4.- Continued.

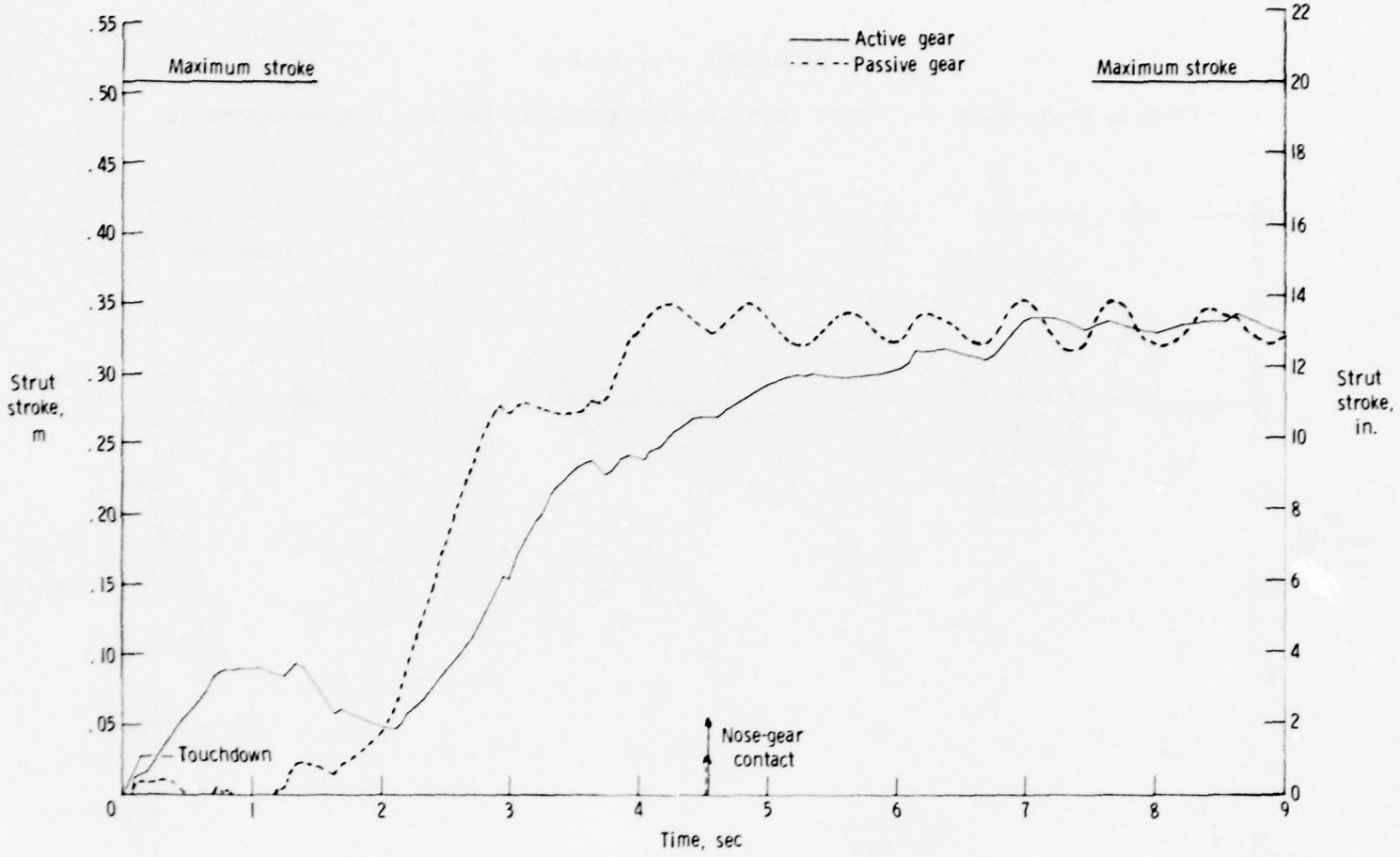

(f) Shock-strut strokes; downhill runway; sink rate, 0.3 m/sec (1.0 ft/sec).

Figure A4.- Continued.

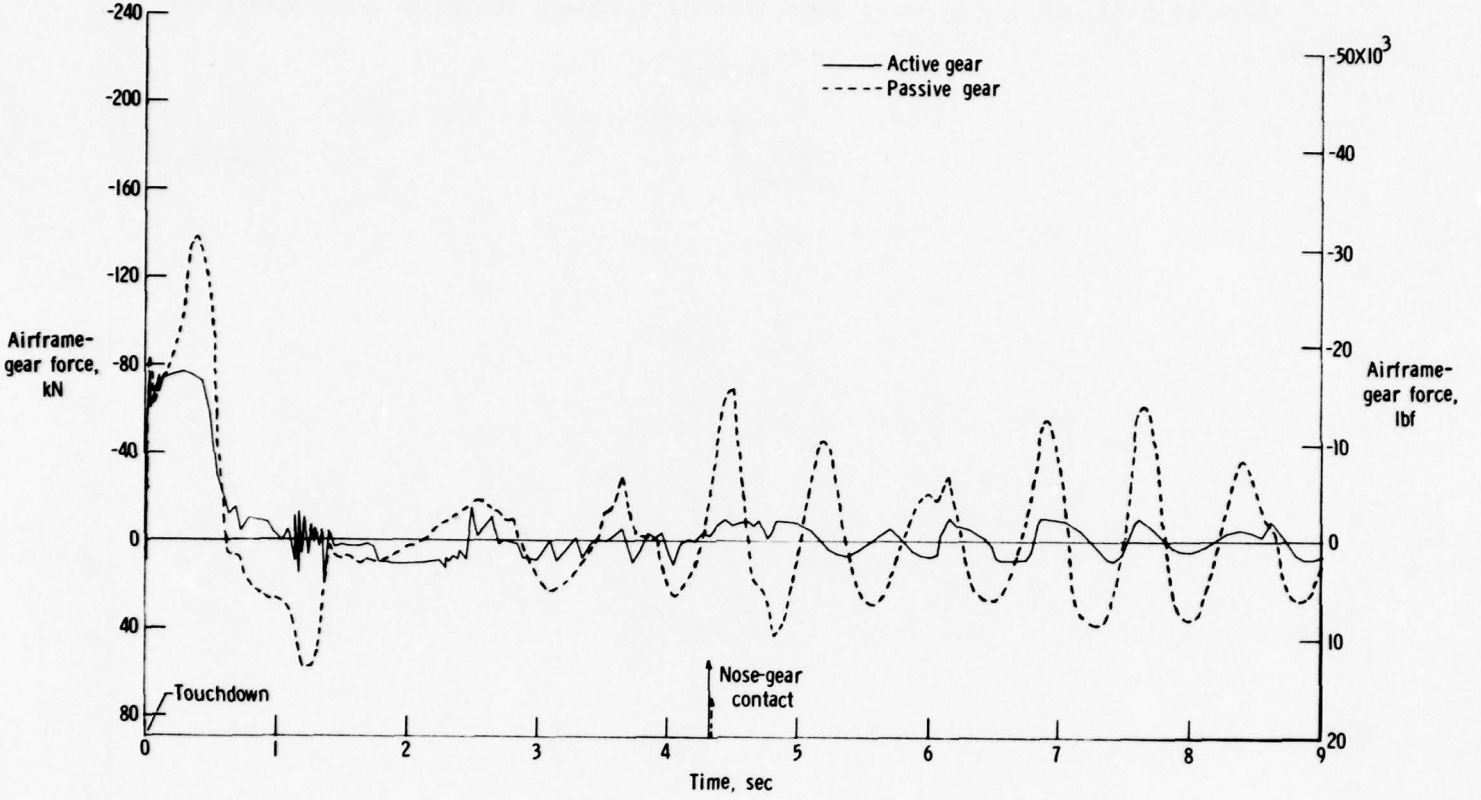

(g) Airframe-gear forces; downhill runway; sink rate, 1.5 m/sec (5.0 ft/sec).

Figure A4.- Continued.

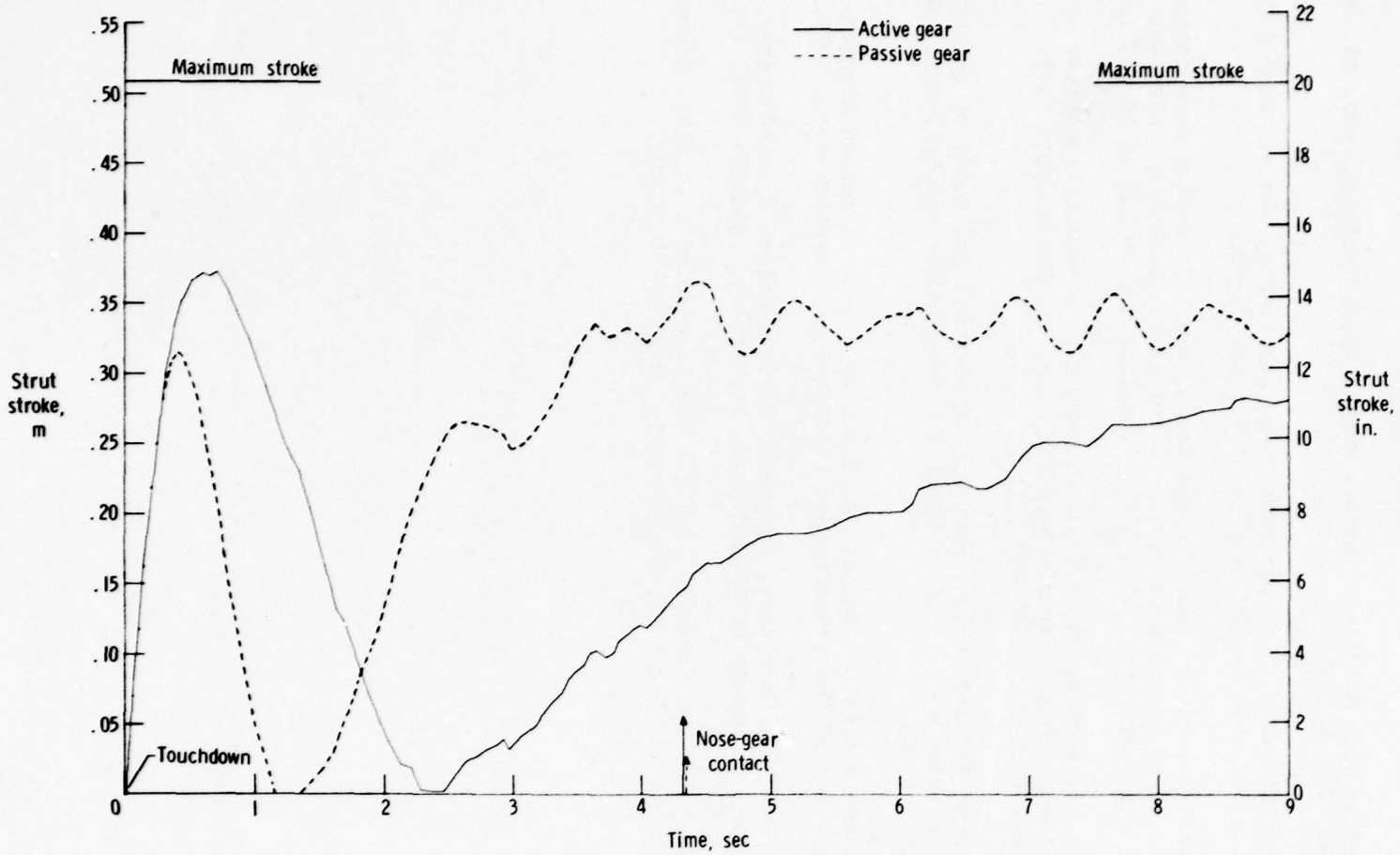

(h) Shock-strut strokes; downhill runway; sink rate, 1.5 m/sec (5.0 ft/sec).

Figure A4.- Concluded.

REFERENCES

1. DC-10 Landing Gear Modified. Aviat. Week & Space Technol., vol. 98, no. 12, Mar. 19, 1973, p. 181.

2. Ropelewski, Robert R.: Airbus Test Tempo Quickening. Aviat. Week & Space Technol., vol. 98, no. 10, Mar. 5, 1973, pp. 32-35.

3. Wignot, Jack E.; Durup, Paul C.; and Gamon, Max A.: Design Formulation and Analysis of an Active Landing Gear. Volume I. Analysis. AFFDL-TR-71-80, Vol. 1, U.S. Air Force, Aug. 1971. (Available from DDC as AD 887 127L.)

4. Bender, E. K.; Berkman, E. F.; and Bieber, M.: A Feasibility Study of Active Landing Gear. AFFDL-TR-70-126, U.S. Air Force, July 1971. (Available from DDC as AD 887 451L.)

5. McGehee, John R.; and Carden, Huey D.: A Mathematical Model of an Active Control Landing Gear for Load Control During Impact and Roll-Out. NASA TN D-8080, 1976.

6. Ross, Irving; and Edson, Ralph: An Electronic Control for an Electro-hydraulic Active Control Aircraft Landing Gear. NASA CR-3113, 1979.

7. Westfall, John R.; Milwitzky, Benjamin; Silsby, Norman S.; and Dreher, Robert C.: A Summary of Ground-Loads Statistics. NASA TN 4008, 1957.

8. Carden, Huey D.; and McGehee, John R.: Validation of a Flexible Aircraft Take-Off and Landing Analysis (FATOLA). NASA TP-1025, 1977.

TABLE I.- INTEGRATION ERROR TOLERANCES FOR DEPENDENT VARIABLES

Dependent variable	Upper bound of local relative truncation error
Translational velocities, m/sec (ft/sec)	0.0003 (1.0×10^{-3})
Rotational velocities, rad/sec	0.01
Translational displacements, m(ft)	0.0003 (1.0×10^{-3})
Rotational displacements, rad	0.01
Shock-strut hydraulic pressure, Pa (lbf/ft^2)	48.3 (1.01)
Servo-valve spool acceleration, cm/sec^2 (in/sec^2)	2.54 (1.00)
Servo-valve spool velocity, cm/sec (in/sec)	0.0254 (1.00×10^{-2})
Servo-valve spool displacement, cm (in.)	0.000254 (1.00×10^{-4})
Hydraulic fluid flow rates, m^3/sec (gal/min)	1.64×10^{-9} (2.60×10^{-5})
Fluid volume transferred, m^3 (pints)	2.83×10^{-5} (5.98×10^{-2})

TABLE II.- RESULTS OF PARAMETER STUDY FOR LANDING SIMULATIONS ON RUNWAY A WITH ACTIVE LOAD-CONTROL GEAR

Touchdown sink rate		Percent force reduction, $100*(1 - P_a/F_p)$		Maximum flow rate from strut		Maximum fluid removed[a]		Maximum flow rate into strut		Maximum fluid added		Maximum strut stroke		Allowable added fluid[b]	
m/sec	ft/sec	Initial impact	Main-gear response to nose-gear impact	m^3/sec	gal/min	m^3	pints	m^3/sec	gal/min	m^3	pints	m	in.	m^3	pints
Small mass configuration, uphill slope															
0.3	1.0	7	51	0.010	151	0.0024	5.0	0.016	254	0.0001	0.2	0.279	11.0	0.0108	22.9
.9	3.0	15	57	.010	166	.0040	8.4	.013	199	.0002	.4	.287	11.3	.0114	24.1
1.5	5.0	24	48	.013	213	.0059	12.5	.015	242	.0002	.4	.325	12.8	.0133	28.2
Small mass configuration, downhill slope															
0.3	1.0	8	-13	0.009	142	0.0007	1.5	0.011	172	0.0004	0.8	0.264	10.4	0.0118	25.0
.9	3.0	19	48	.010	157	.0028	6.0	.014	229	.0003	.6	.277	10.9	.0132	28.0
1.5	5.0	16	54	.012	197	.0049	10.4	.019	302	.0004	.9	.302	11.9	.0133	28.2
Medium mass configuration, uphill slope															
0.3	1.0	15	67	0.010	156	0.0049	10.3	0.010	163	0.0025	5.2	0.302	11.9	0.0088	18.5
.9	3.0	24	48	.011	173	.0060	12.7	.013	205	.0032	6.8	.330	13.0	.0104	22.0
1.5	5.0	48	55	.014	224	.0081	17.2	.018	290	.0066	14.0	.445	17.5	.0126	26.6
Medium mass configuration, downhill slope															
0.3	1.0	17	60	0.009	141	0.0017	3.6	0.010	152	0.0026	5.6	0.312	12.3	0.0119	25.2
.9	3.0	21	69	.010	160	.0044	9.2	.013	203	.0044	9.2	.274	10.8	.0131	27.7
1.5	5.0	34	57	.012	195	.0064	13.6	.016	258	.0045	9.5	.325	12.8	.0115	24.3
Large mass configuration, uphill slope															
0.3	1.0	14	43	0.010	151	0.0062	13.0	0.011	170	0.0026	5.4	0.351	13.8	0.0095	20.0
.9	3.0	47	84	.011	170	.0077	16.3	.013	209	.0043	9.0	.401	15.8	.0111	23.5
1.5	5.0	51	89	.015	240	.0079	16.8	.017	284	.0071	15.1	.480	18.9	.0127	26.8
Large mass configuration, downhill slope															
0.3	1.0	16	70	0.009	141	0.0018	3.8	0.012	189	0.0027	5.7	0.345	13.6	0.0120	25.4
.9	3.0	21	78	.010	163	.0052	11.0	.012	187	.0051	10.7	.315	12.4	.0116	24.5
1.5	5.0	40	87	.014	222	.0058	12.2	.016	253	.0071	15.0	.373	14.7	.0132	27.9

[a]Shock-strut piston contains 0.0103 m^3 (21.80 pints) of hydraulic fluid for fully extended strut.
[b]Allowable added fluid to shock strut at time of maximum fluid added.

TABLE III.- POTENTIAL FOR REDUCTION OF FATIGUE DAMAGE WITH ACTIVE LOAD-CONTROL MAIN LANDING GEAR

Sink rate		Peak rms average forces								F_p		F_a		$D_a/D_p = (F_a/F_p)^5$
		Passive gear				Active gear								
		Negative		Positive		Negative		Positive						
m/sec	ft/sec	kN	lbf	kN	lbf	kN	lbf	kN	lbf	kN	lbf	kN	lbf	(a)
Small mass configuration, uphill slope														
0.3	1.0	19.16	4 307	8.98	2018	13.69	3078	14.75	3317	28.14	6 326	28.44	6394	1.05
.9	3.0	11.74	2 640	9.08	2221	7.92	1781	4.48	1006	20.82	4 681	12.40	2788	.07
1.5	5.0	16.01	3 599	11.26	2531	12.67	2849	8.37	1881	27.27	6 131	21.04	4729	.27
Small mass configuration, downhill slope														
0.3	1.0	10.56	2 374	9.59	2156	7.43	1670	5.45	1224	20.15	4 530	12.87	2894	0.11
.9	3.0	10.21	2 295	8.88	1996	7.42	1667	5.93	1332	19.09	4 292	13.34	2999	.17
1.5	5.0	14.75	3 316	8.49	1909	11.08	2490	9.27	2083	23.24	5 225	20.35	4574	.51
Medium mass configuration, uphill slope														
0.3	1.0	15.44	3 471	12.72	2860	8.37	1881	5.47	1230	28.17	6 332	13.84	3111	0.03
.9	3.0	14.60	3 282	12.42	2793	8.81	1980	7.21	1621	27.02	6 074	16.02	3601	.07
1.5	5.0	20.04	4 506	11.15	2507	11.72	2635	6.78	1523	31.19	7 012	18.50	4159	.07
Medium mass configuration, downhill slope														
0.3	1.0	15.78	3 548	13.70	3079	7.00	1573	5.06	1138	29.48	6 627	12.06	2711	[b]0.01
.9	3.0	14.65	3 294	11.91	2677	8.81	1980	6.99	1572	26.56	5 971	15.80	3552	.07
1.5	5.0	15.47	3 477	10.27	2308	9.52	2140	5.69	1279	25.74	5 787	15.21	3419	.07
Large mass configuration, uphill slope														
0.3	1.0	23.90	5 373	20.76	4666	7.00	1574	4.34	976	44.66	10 039	11.34	2550	[b]0.01
.9	3.0	36.45	8 194	23.47	5277	7.57	1701	6.57	1476	59.92	13 471	14.13	3177	[b].01
1.5	5.0	51.65	11 611	30.02	6748	11.61	2611	10.21	2296	81.67	18 359	21.82	4907	[b].01
Large mass configuration, downhill slope														
0.3	1.0	22.04	4 955	20.13	4525	6.63	1490	5.69	1279	42.17	9 480	12.32	2769	[b]0.01
.9	3.0	24.48	5 503	19.02	4275	6.94	1560	5.47	1229	43.50	9 779	12.41	2790	[b].01
1.5	5.0	30.09	8 562	20.36	4576	7.95	1788	6.29	1414	53.95	12 128	14.24	3202	[b].01
Average														0.14

[a]Calculated for $D_p = 1.0$.
[b]0.01 established as lower limit.

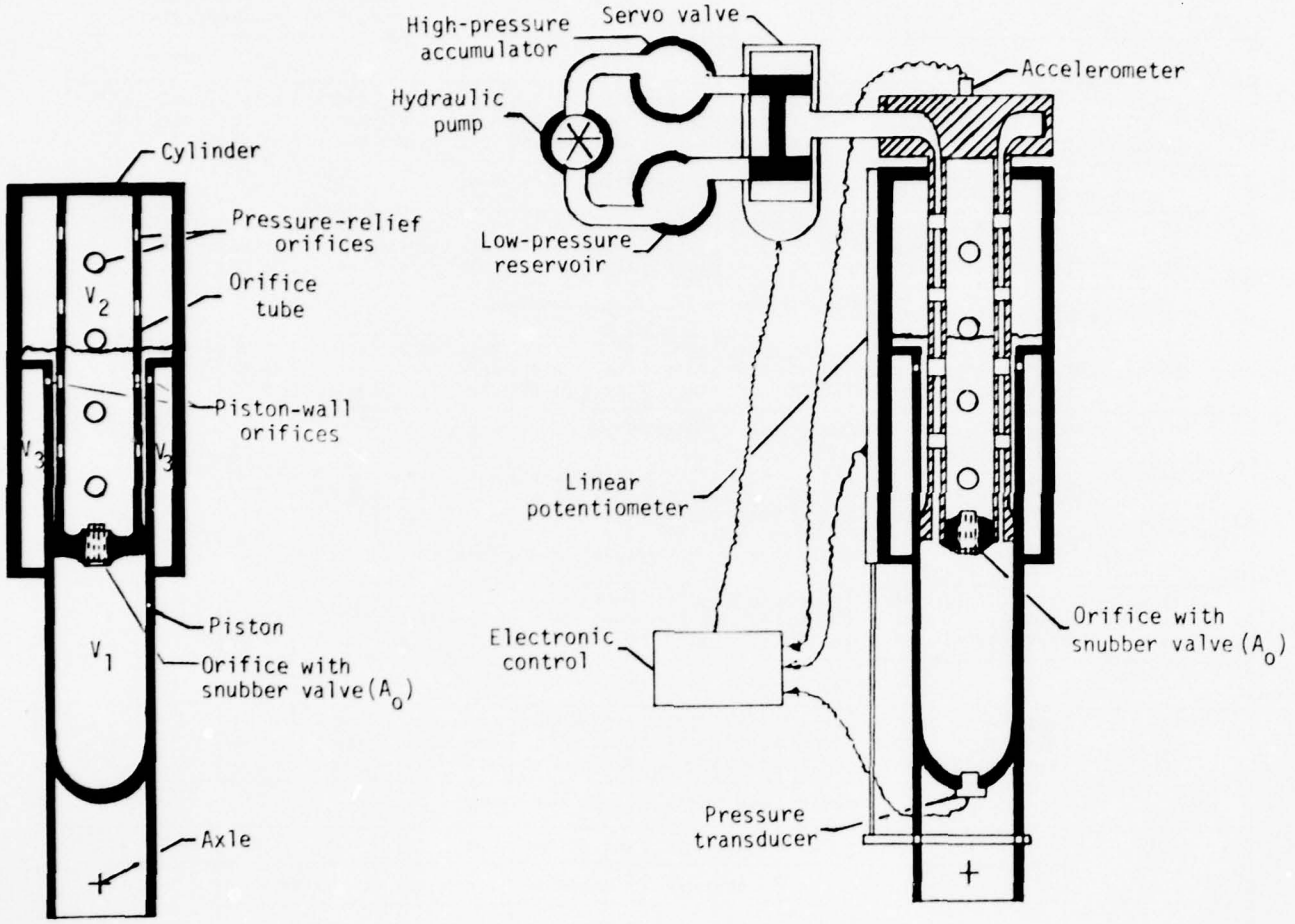

Figure 1.- Cross-sectional schematics of passive and active shock struts.

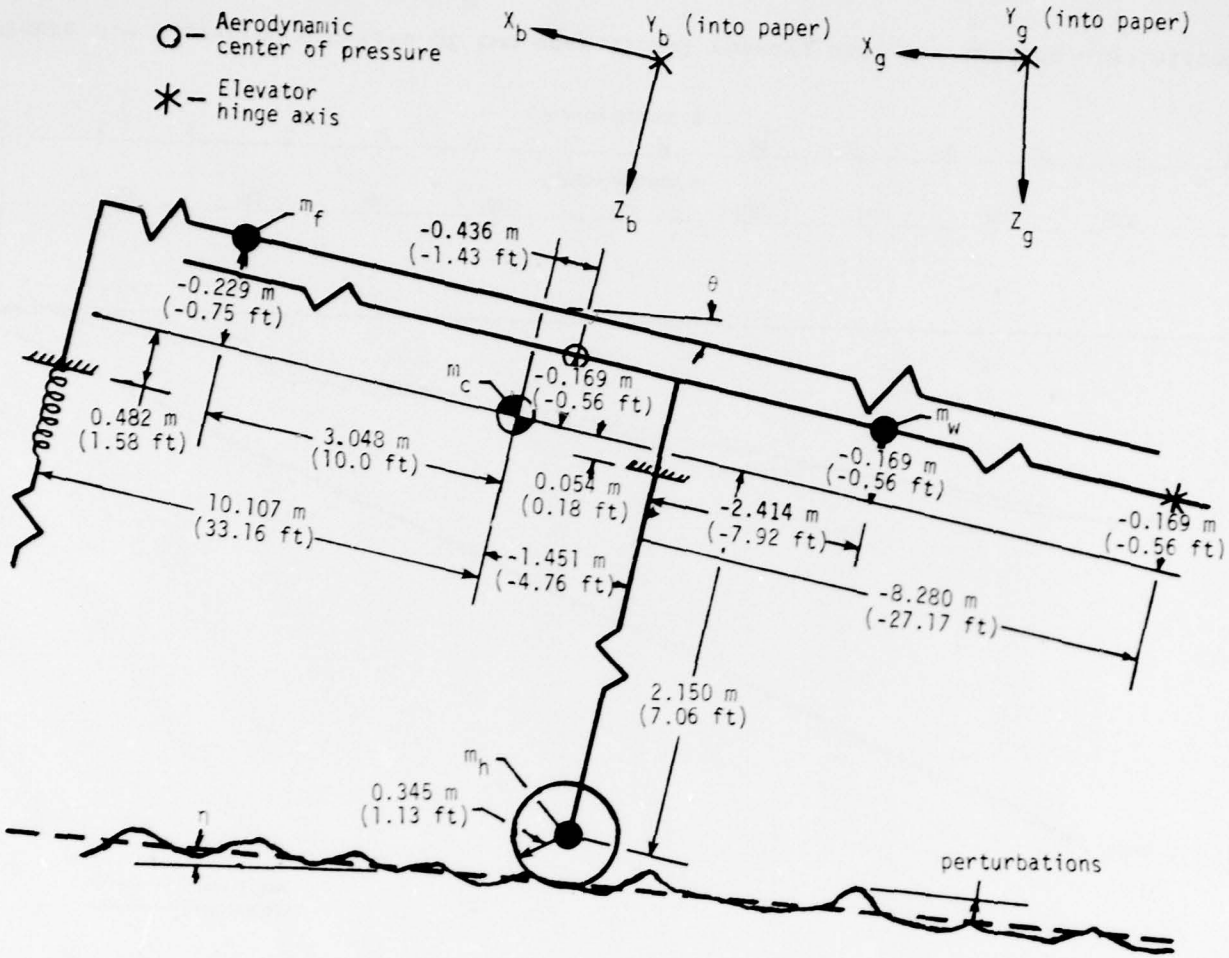

Figure 2.- Schematic of rigid-airframe configuration used for study. (Dimensions are not to scale.)

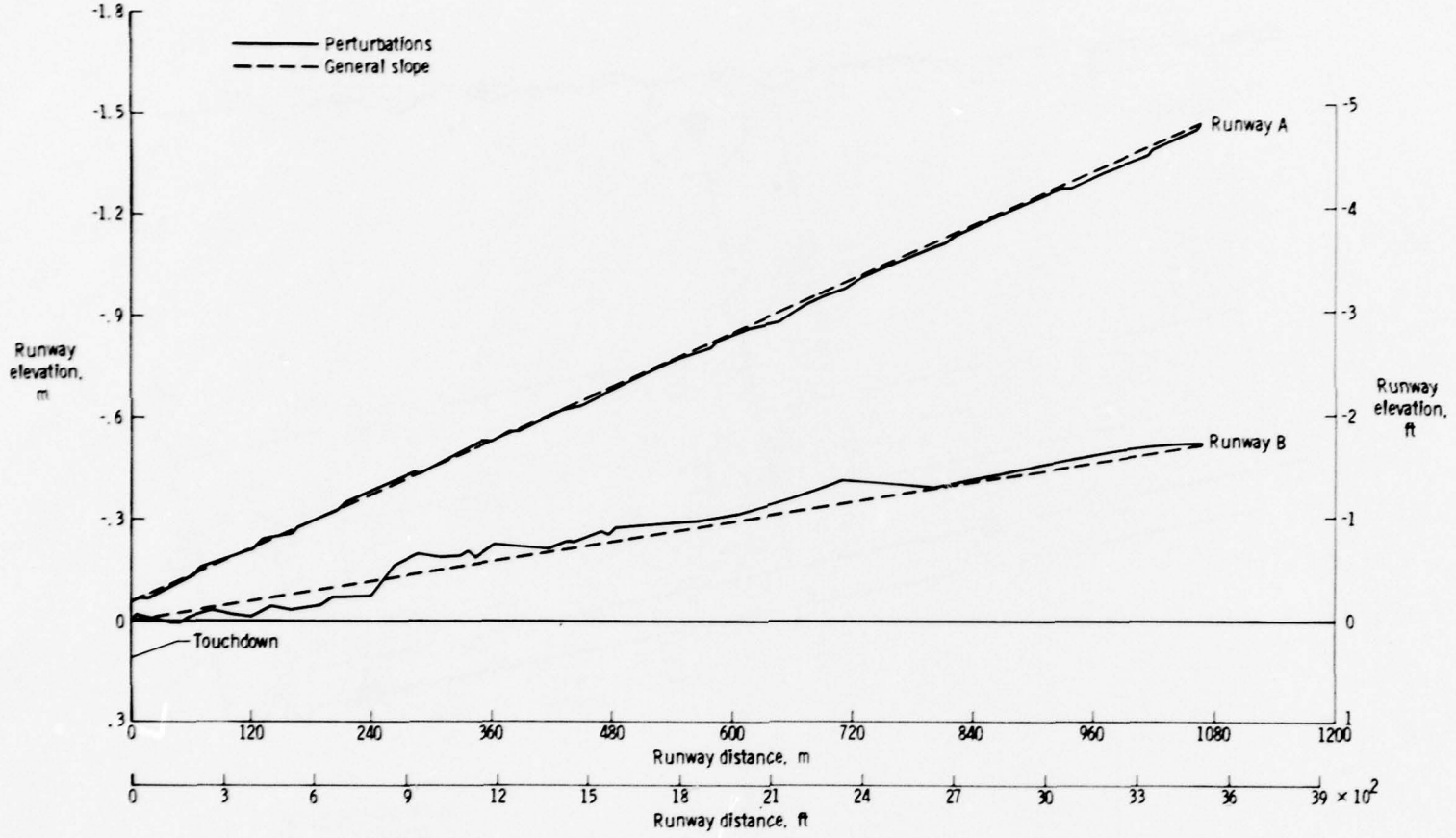

Figure 3.- Elevation profiles of two operational runways used for landing simulations.

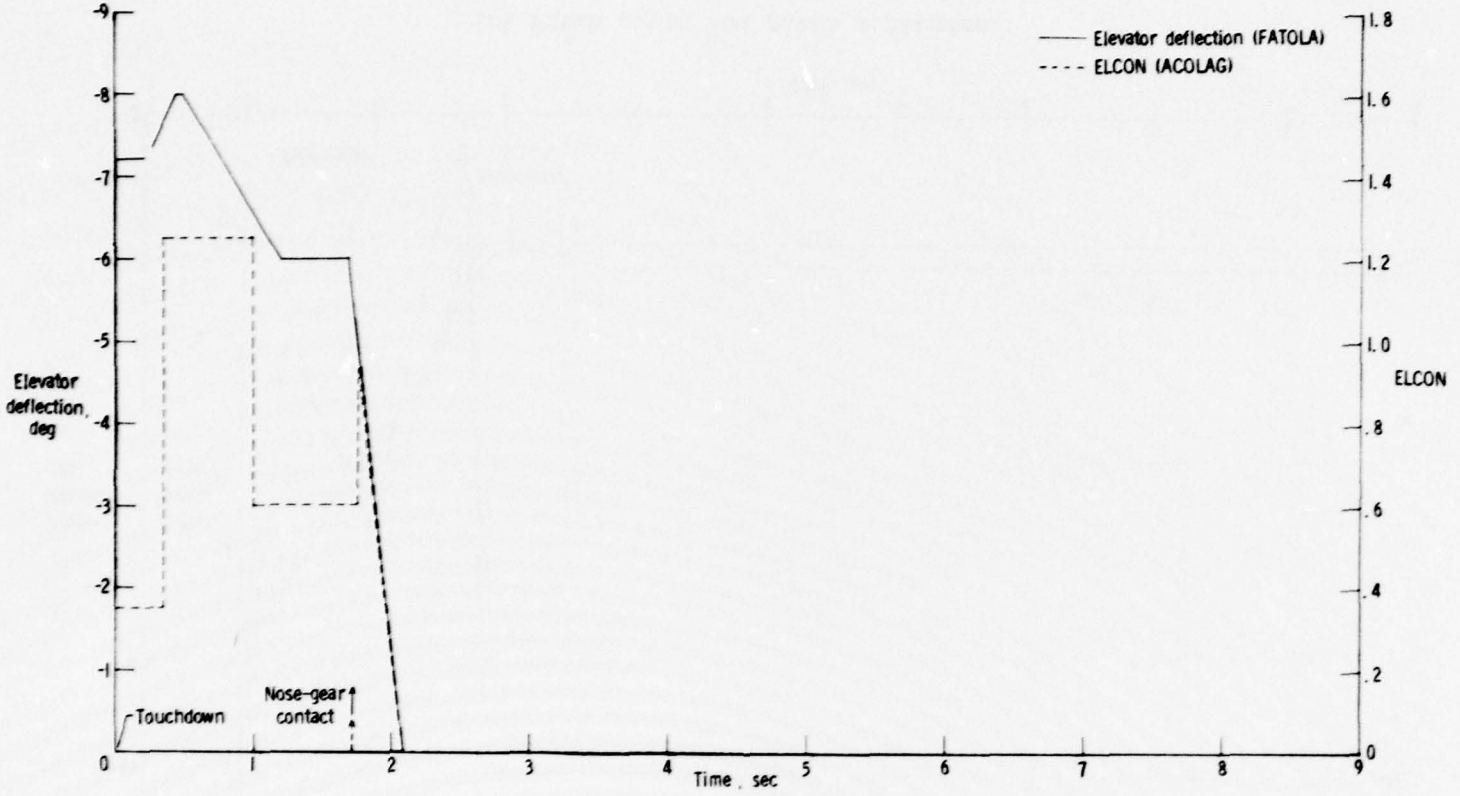

(a) Elevator-control inputs.

Figure 4.- Comparison of data time histories obtained from FATOLA and ACOLAG for a symmetrical landing with a passive gear on a flat smooth runway. Sink rate, 1.5 m/sec (5.0 ft/sec).

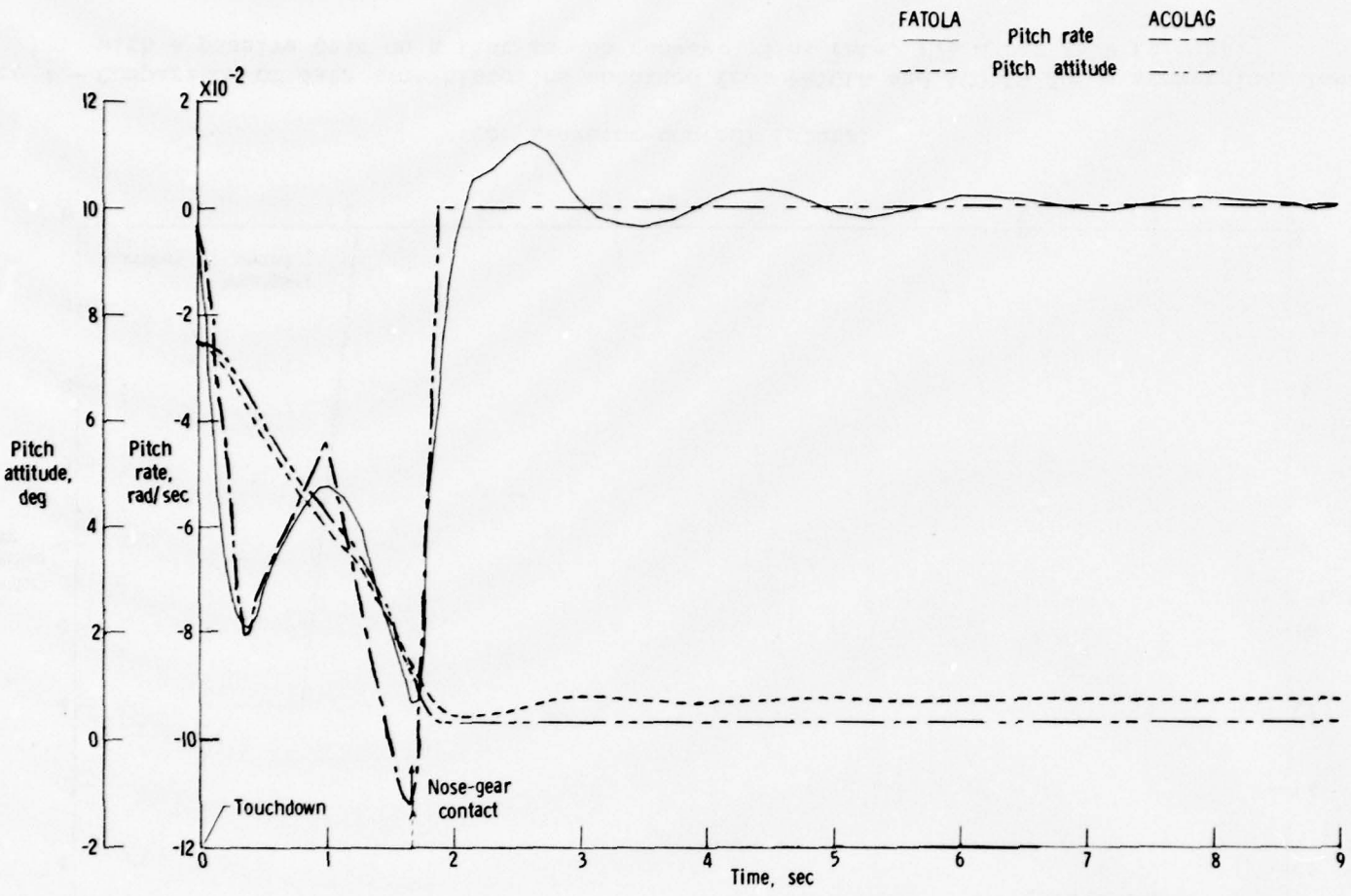

(b) Pitch rates and pitch attitudes.

Figure 4.- Continued.

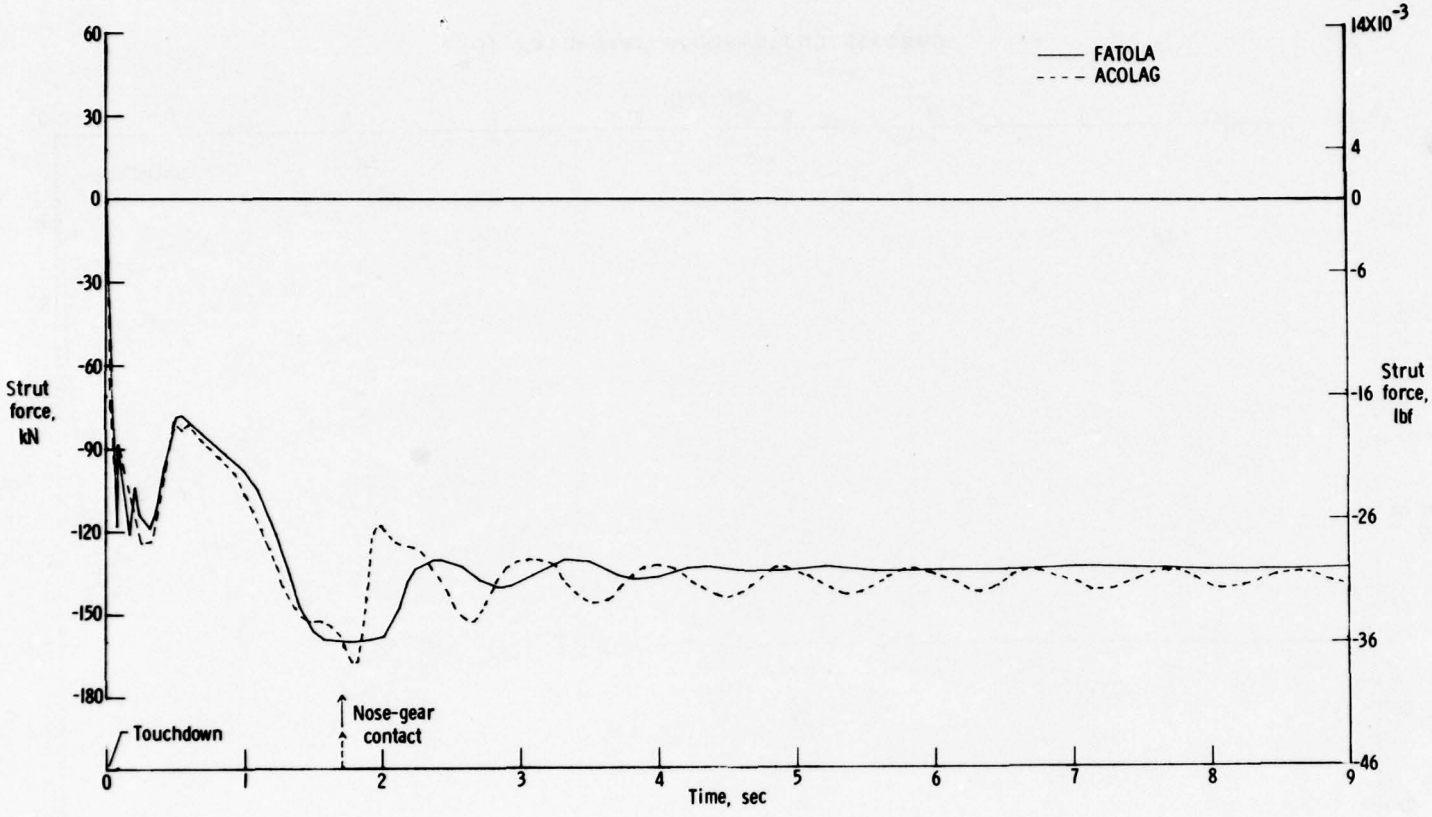

(c) Main-gear shock-strut forces.

Figure 4.- Continued.

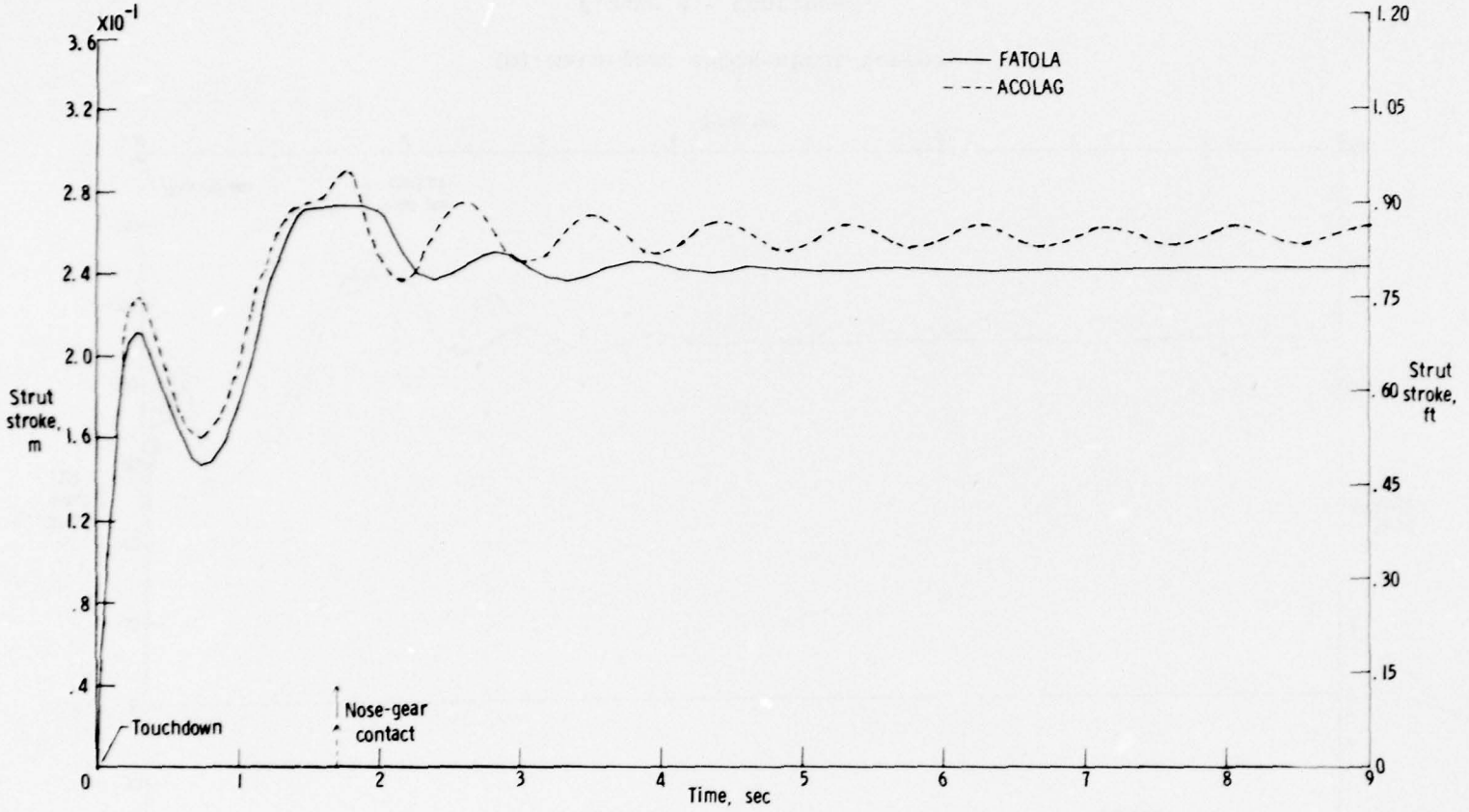

(d) Main-gear shock-strut strokes.

Figure 4.- Concluded.

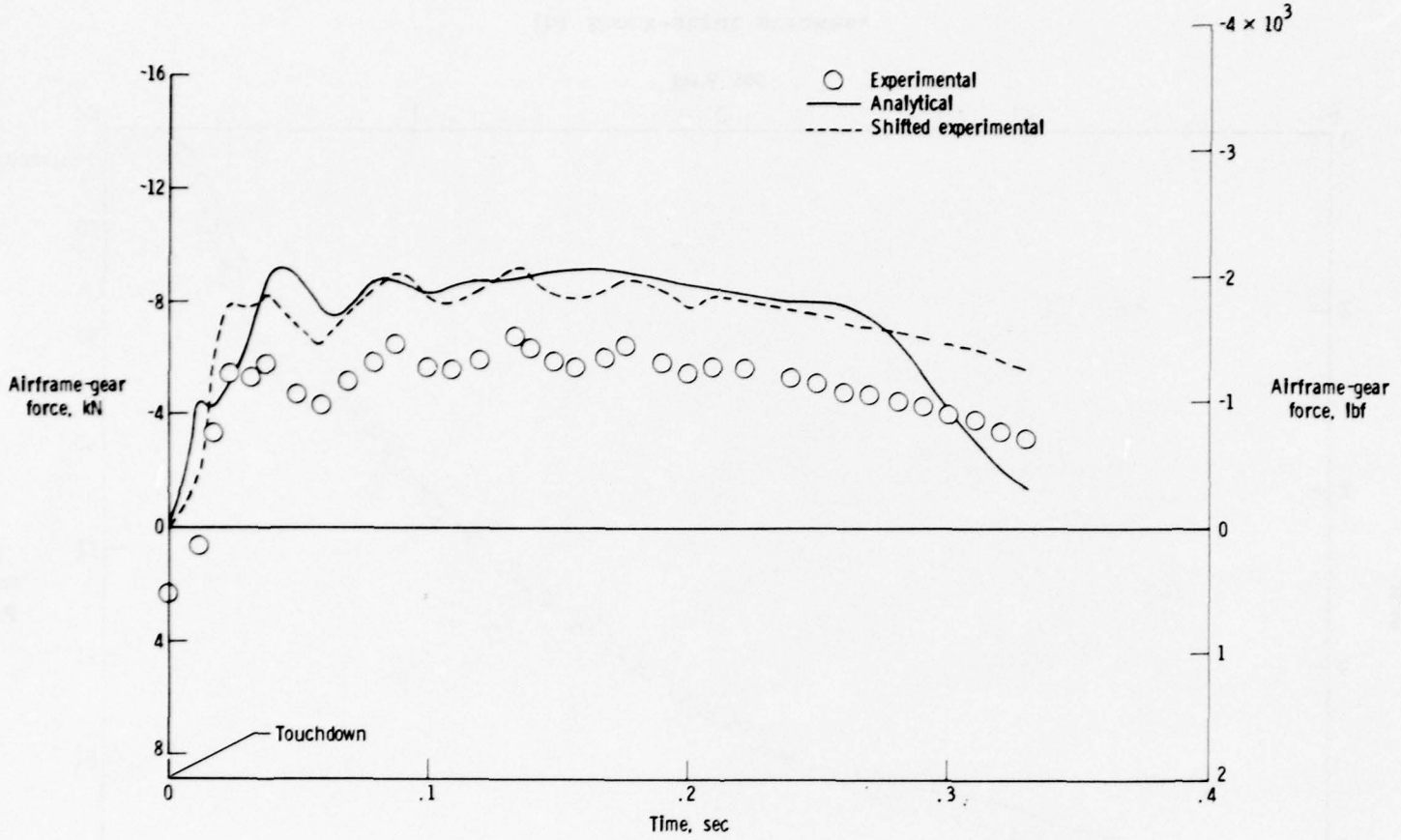

(a) Airframe-gear forces.

Figure 5.- Comparison of experimental data with data computed from ACOLAG for drop test of active control main gear from light aircraft. Sink rate, 1.5 m/sec (5.0 ft/sec).

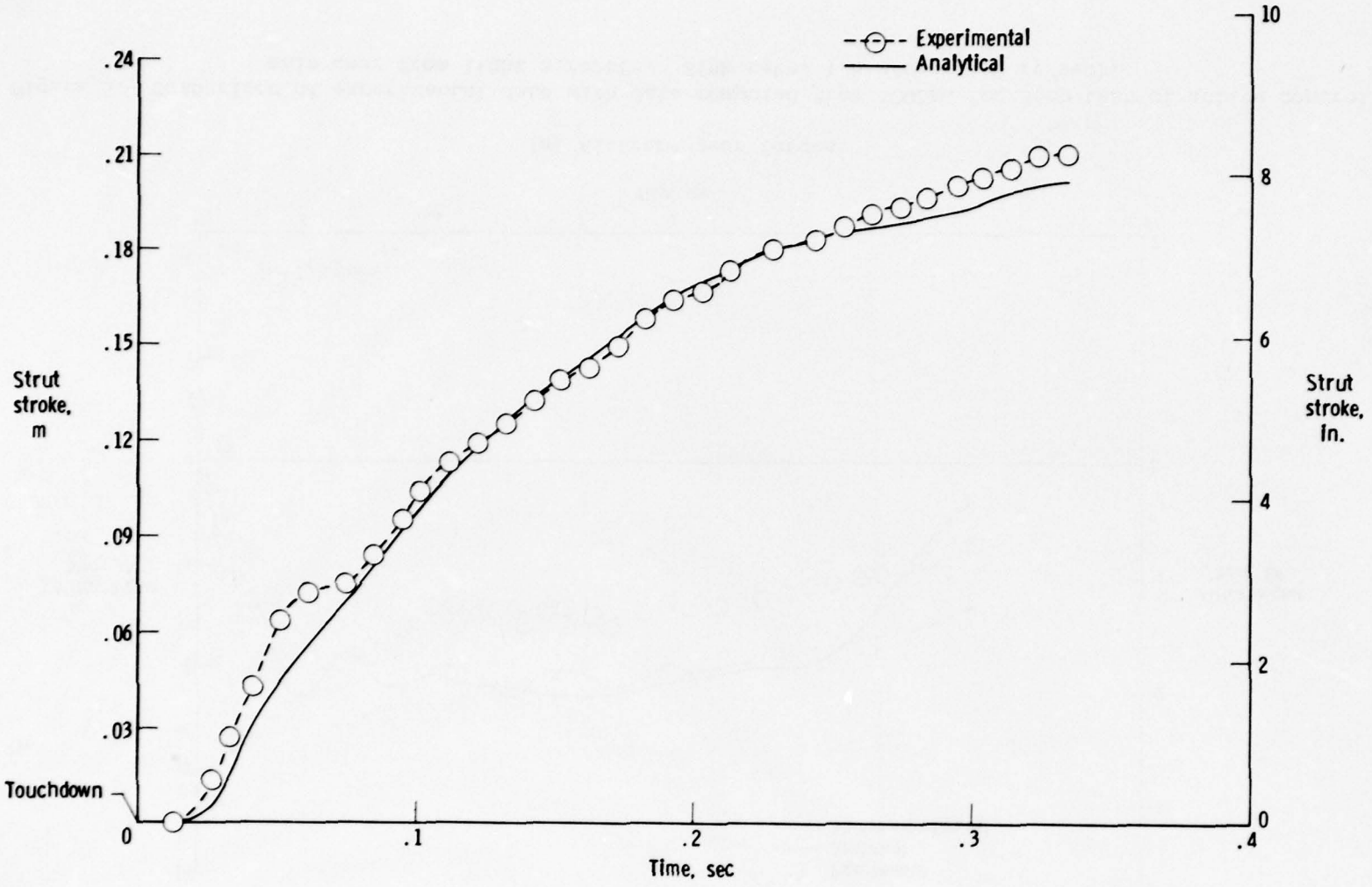

(b) Shock-strut strokes.

Figure 5.- Concluded.

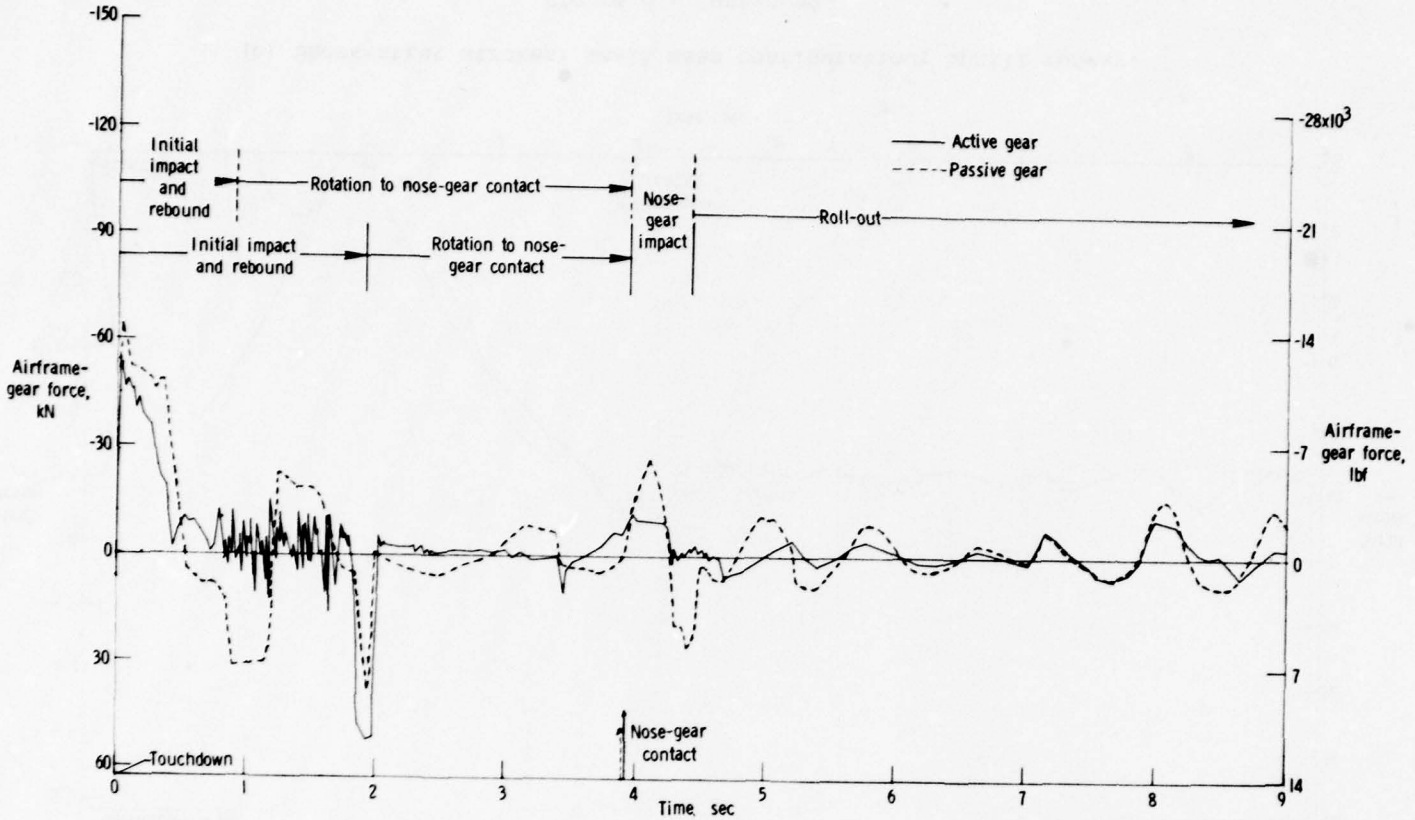

(a) Airframe-gear forces; small mass configuration; uphill runway.

Figure 6.- Airframe-gear-force and shock-strut-stroke time histories for typical landing simulations of airplane with passive and active main gears. Runway A; sink rate, 0.9 m/sec (3 ft/sec).

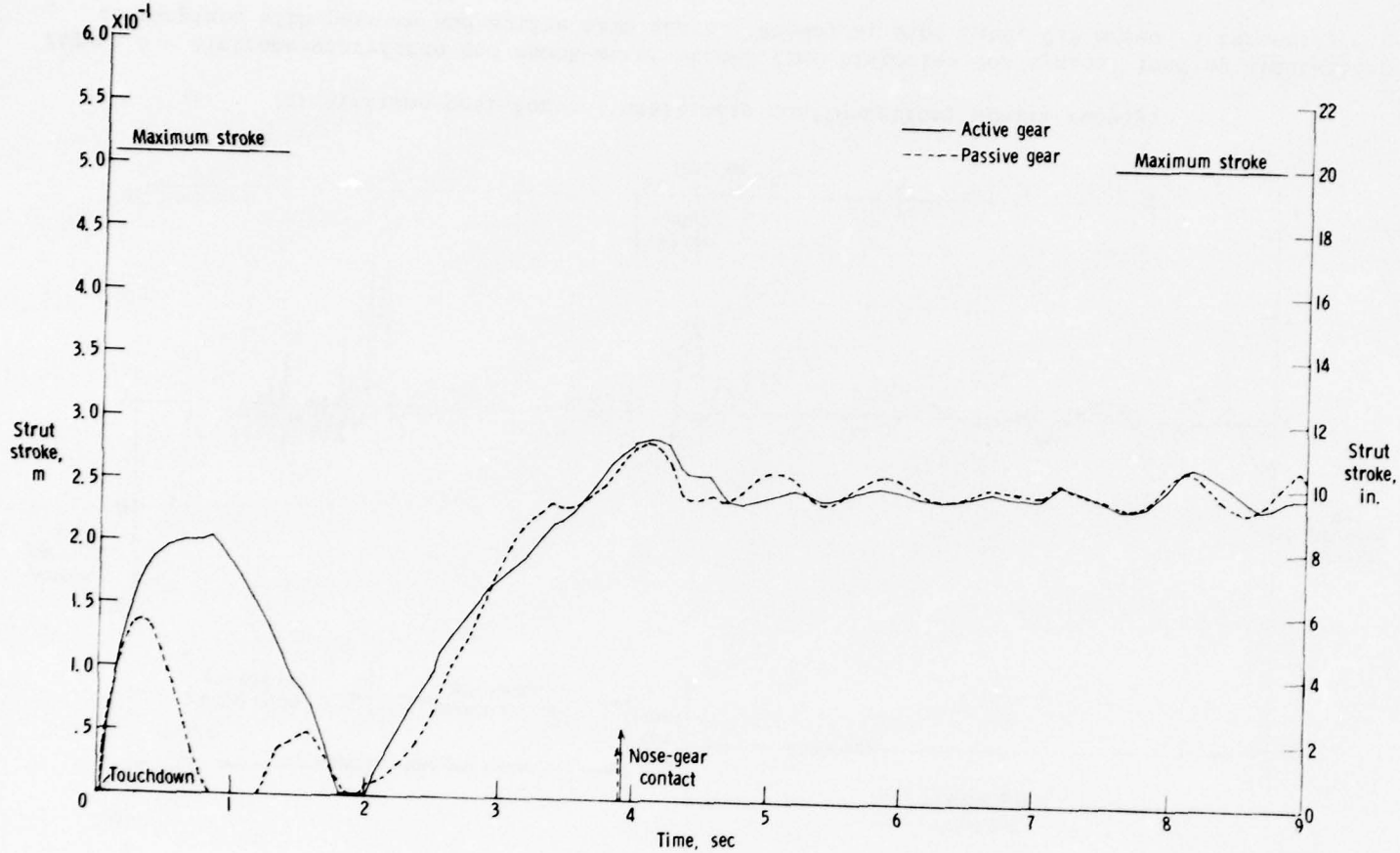

(b) Shock-strut strokes; small mass configuration; uphill runway.

Figure 6.- Continued.

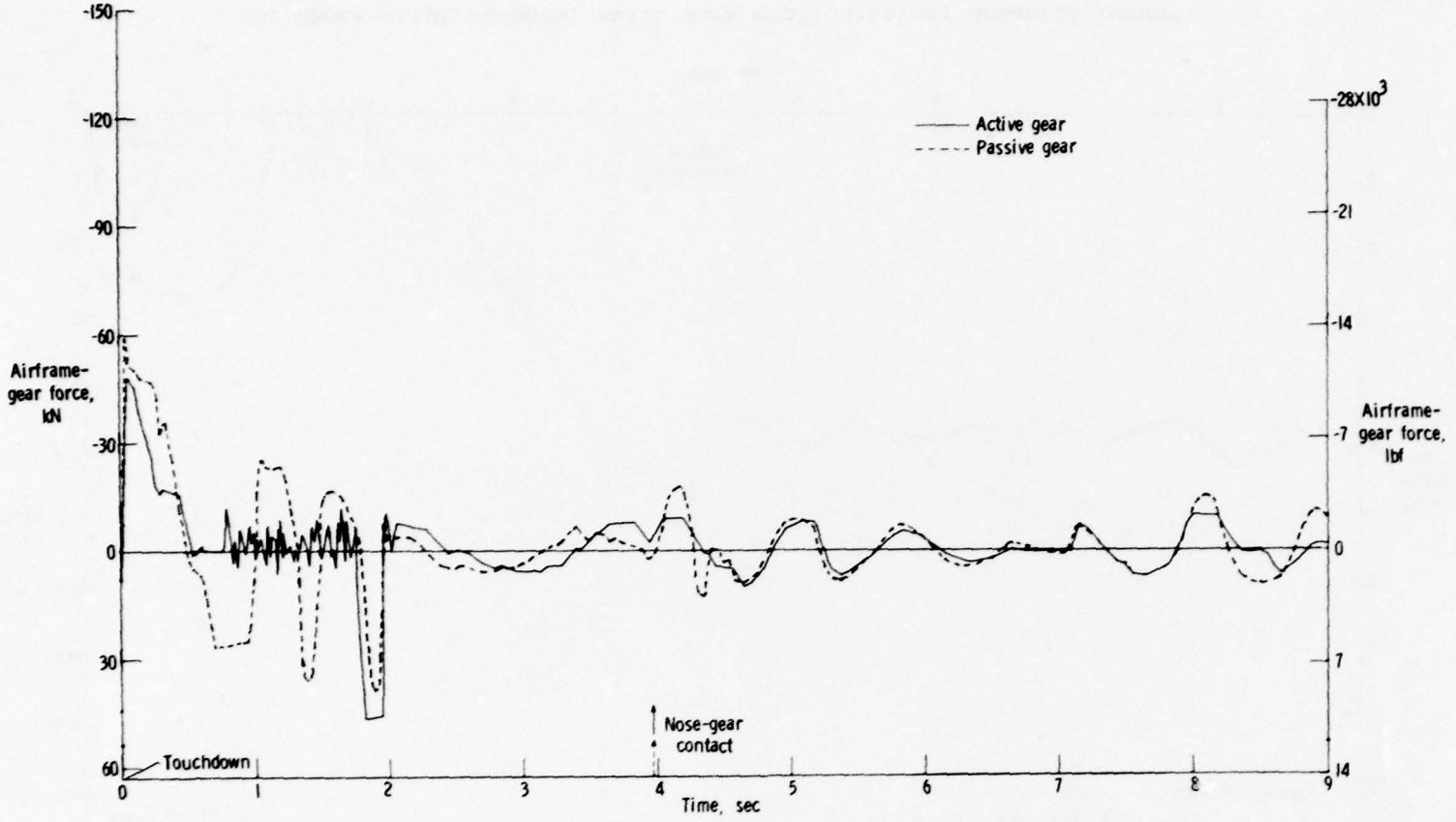

(c) Airframe-gear forces; small mass configuration; downhill runway.

Figure 6.- Continued.

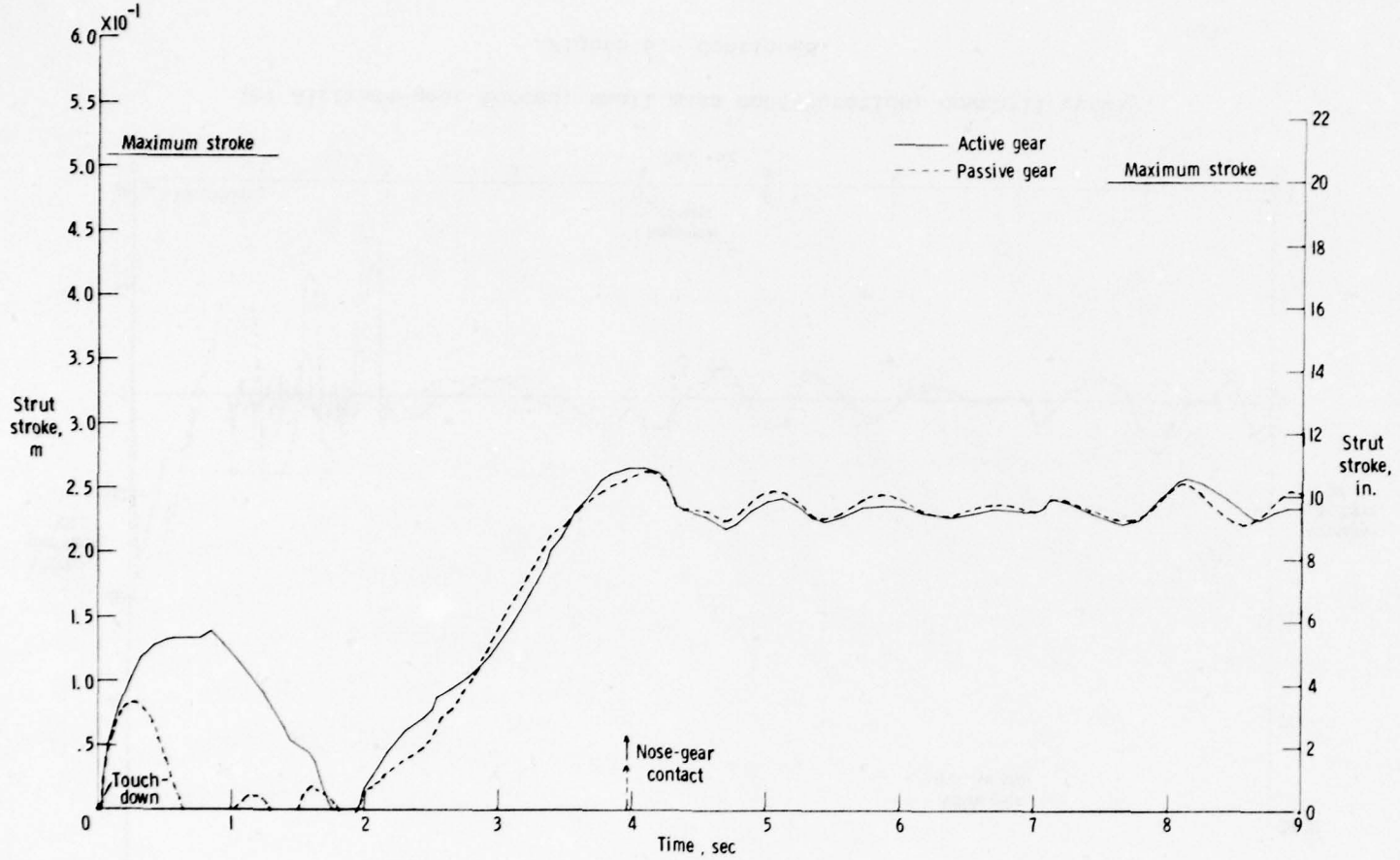

(d) Shock-strut strokes; small mass configuration; downhill runway.

Figure 6.- Continued.

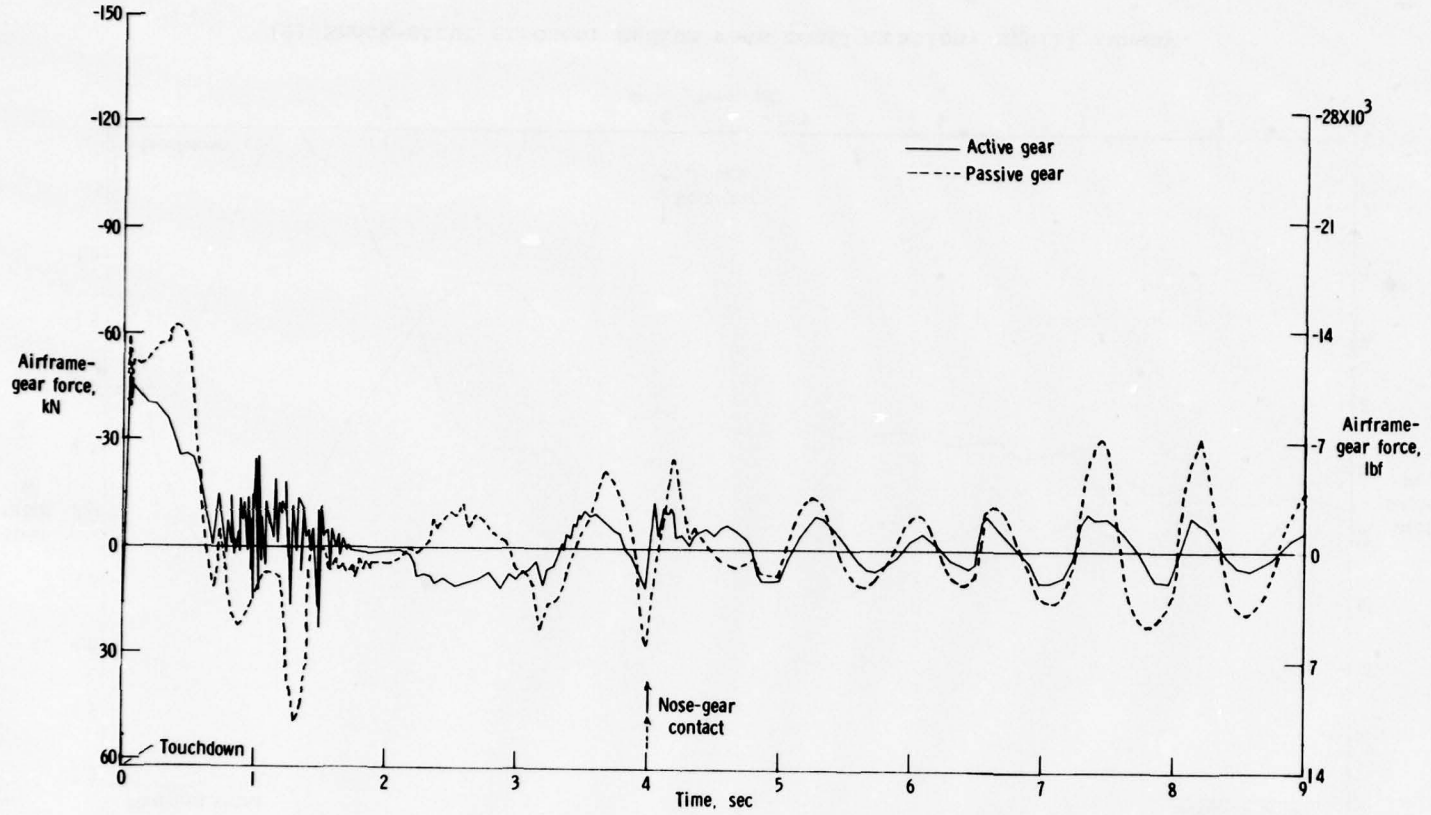

(e) Airframe-gear forces; medium mass configuration; uphill runway.

Figure 6.- Continued.

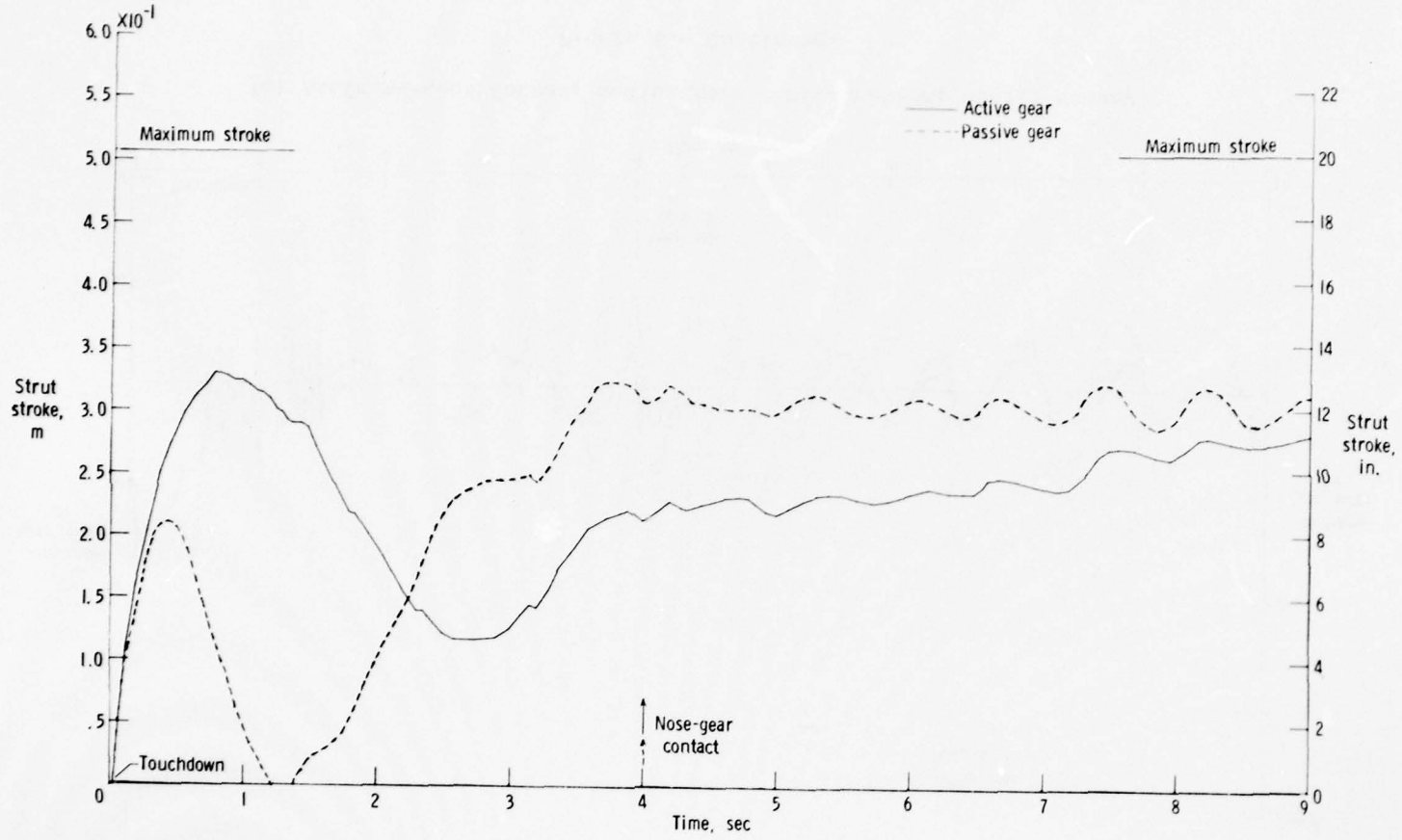

(f) Shock-strut strokes; medium mass configuration; uphill runway.

Figure 6.- Continued.

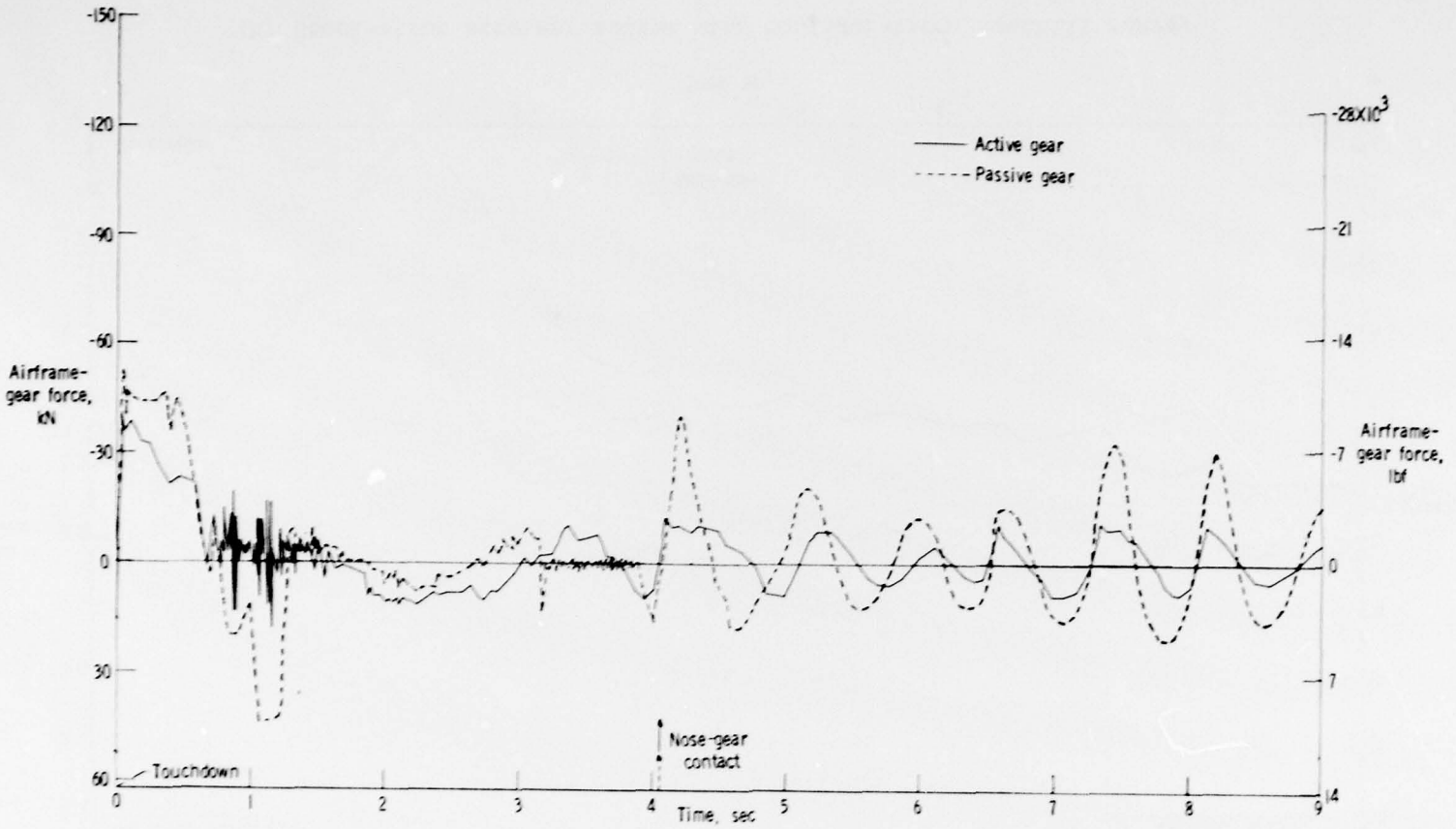

(g) Airframe-gear forces; medium mass configuration; downhill runway.

Figure 6.- Continued.

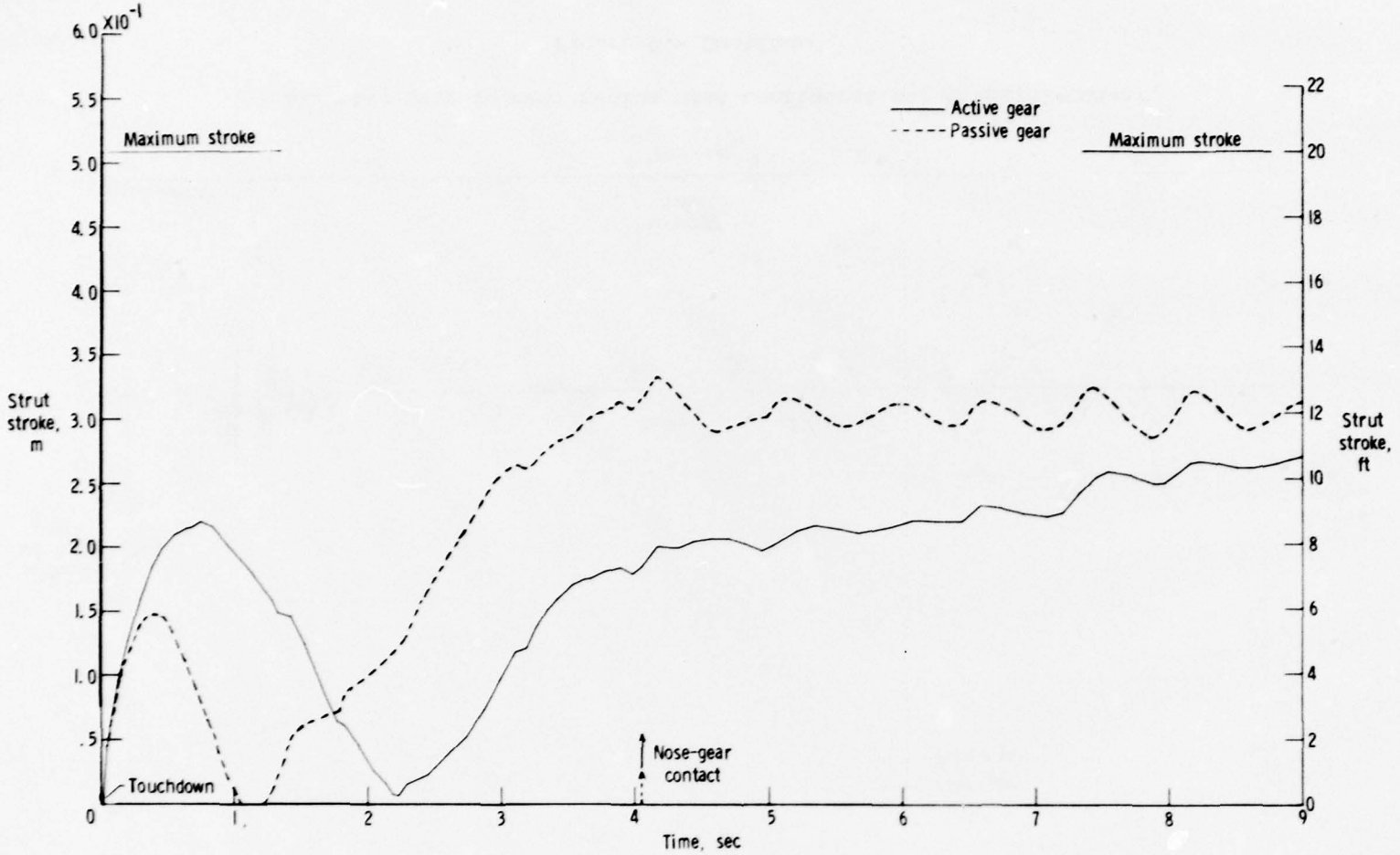

(h) Shock-strut strokes; medium mass configuration; downhill runway.

Figure 6.- Continued.

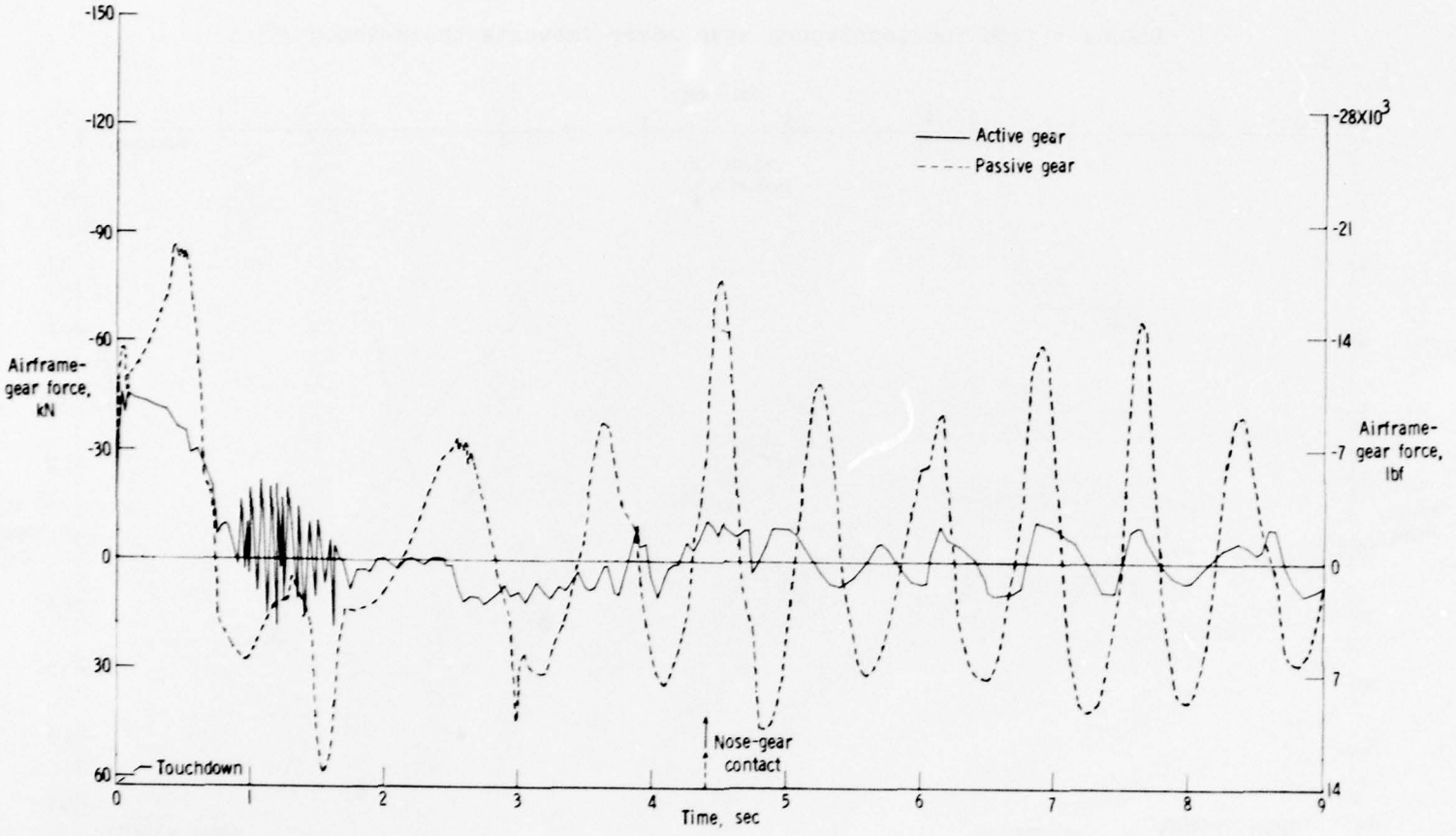

(i) Airframe-gear forces; large mass configuration; uphill runway.

Figure 6.- Continued.

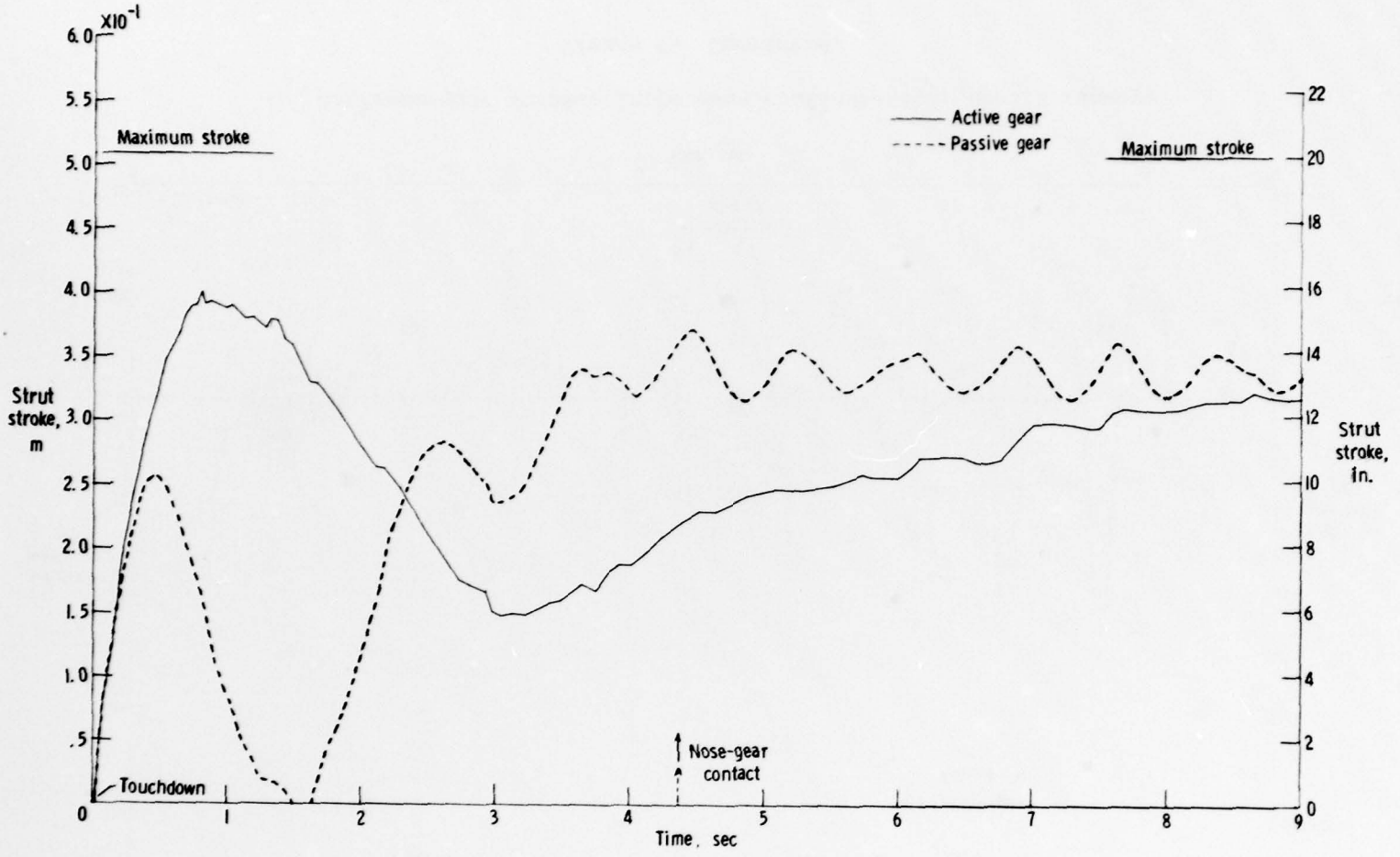

(j) Shock-strut strokes; large mass configuration; uphill runway.

Figure 6.- Continued.

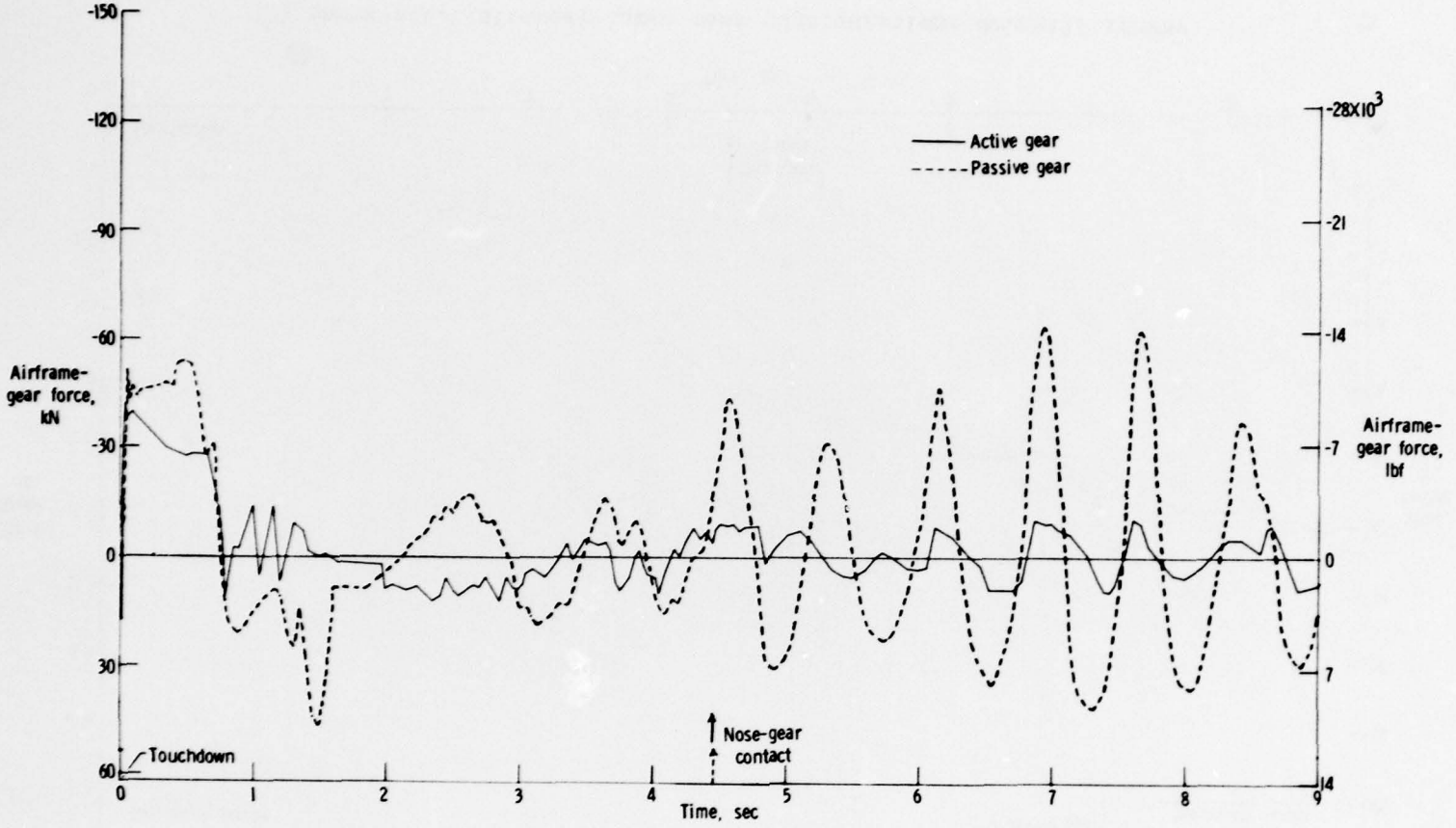

(k) Airframe-gear forces; large mass configuration; downhill runway.

Figure 6.- Continued.

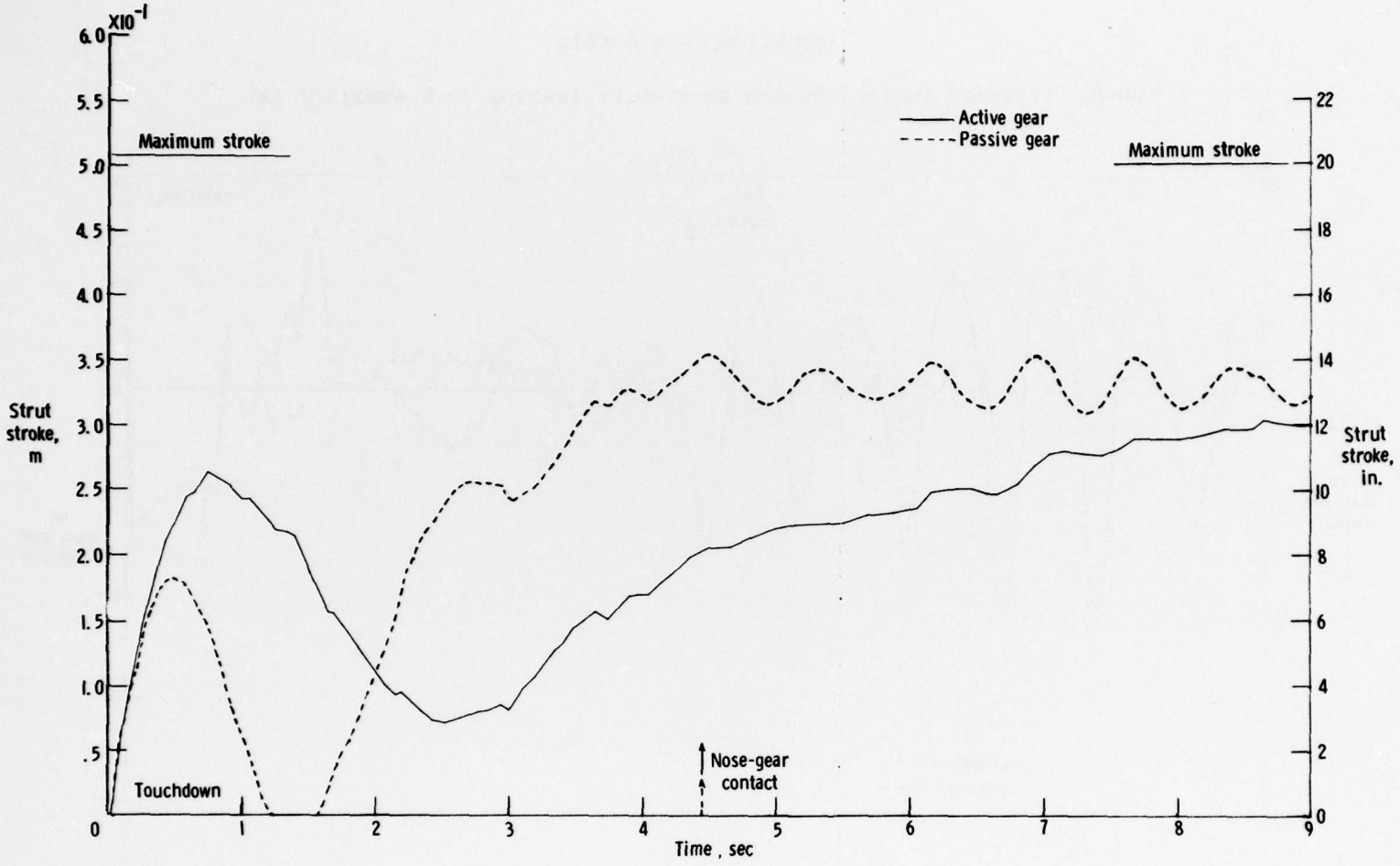

(1) Shock-strut strokes; large mass configuration; downhill runway.

Figure 6.- Concluded.

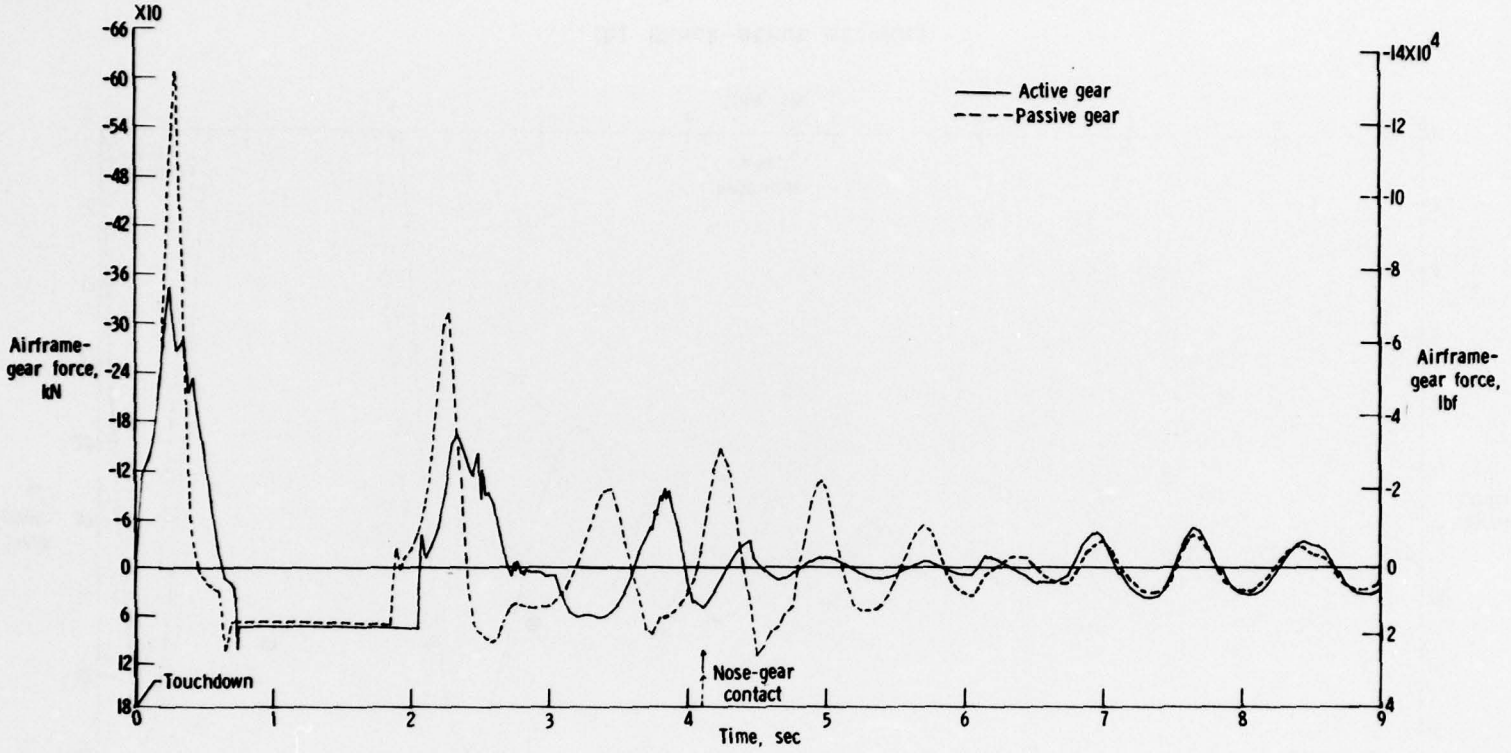

(a) Airframe-gear forces.

Figure 7.- Airframe-gear-force and shock-strut-stroke time histories for landing simulations with passive and active gears at above design touchdown sink rate. Large mass configuration; uphill slope of runway A; sink rate, 2.4 m/sec (8.0 ft/sec).

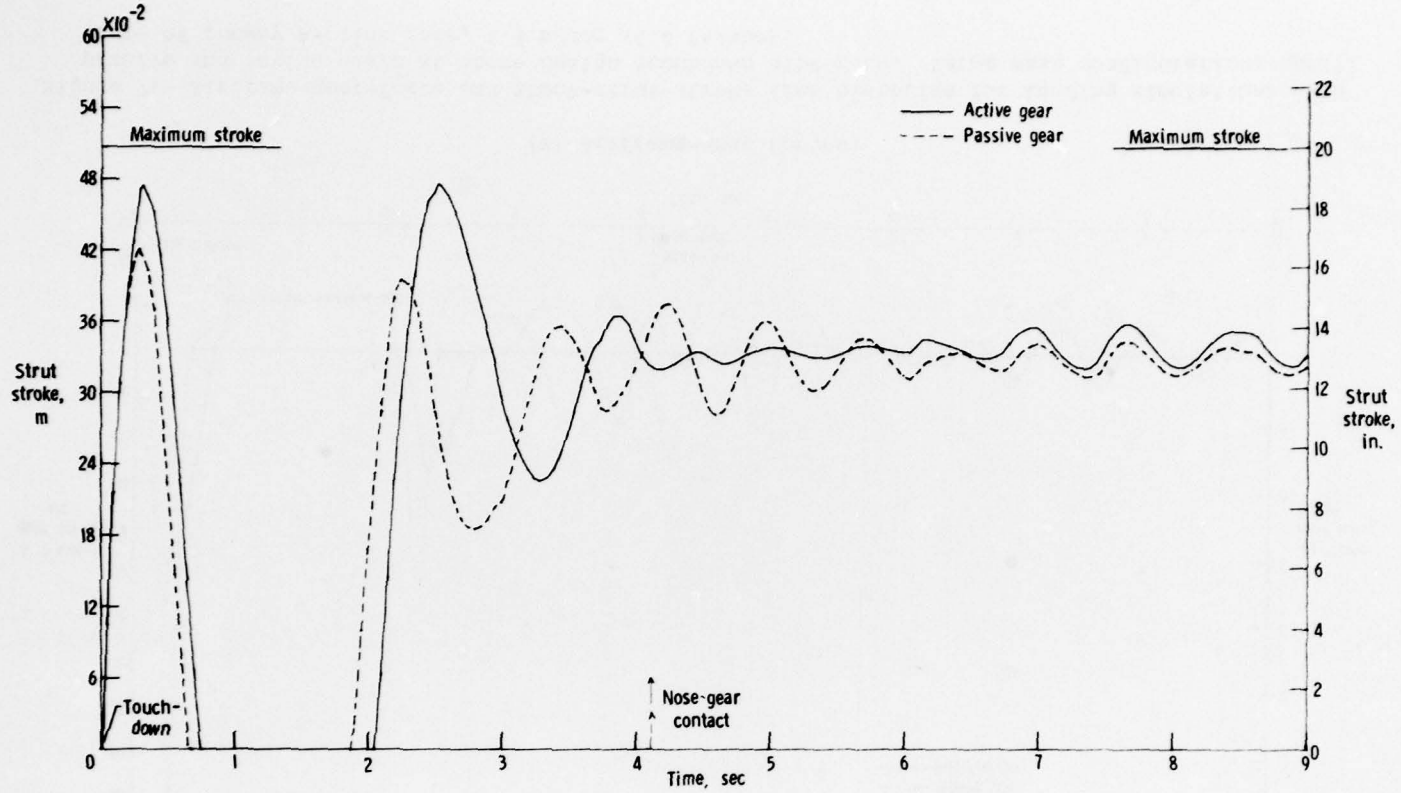

(b) Shock-strut strokes.

Figure 7.- Concluded.

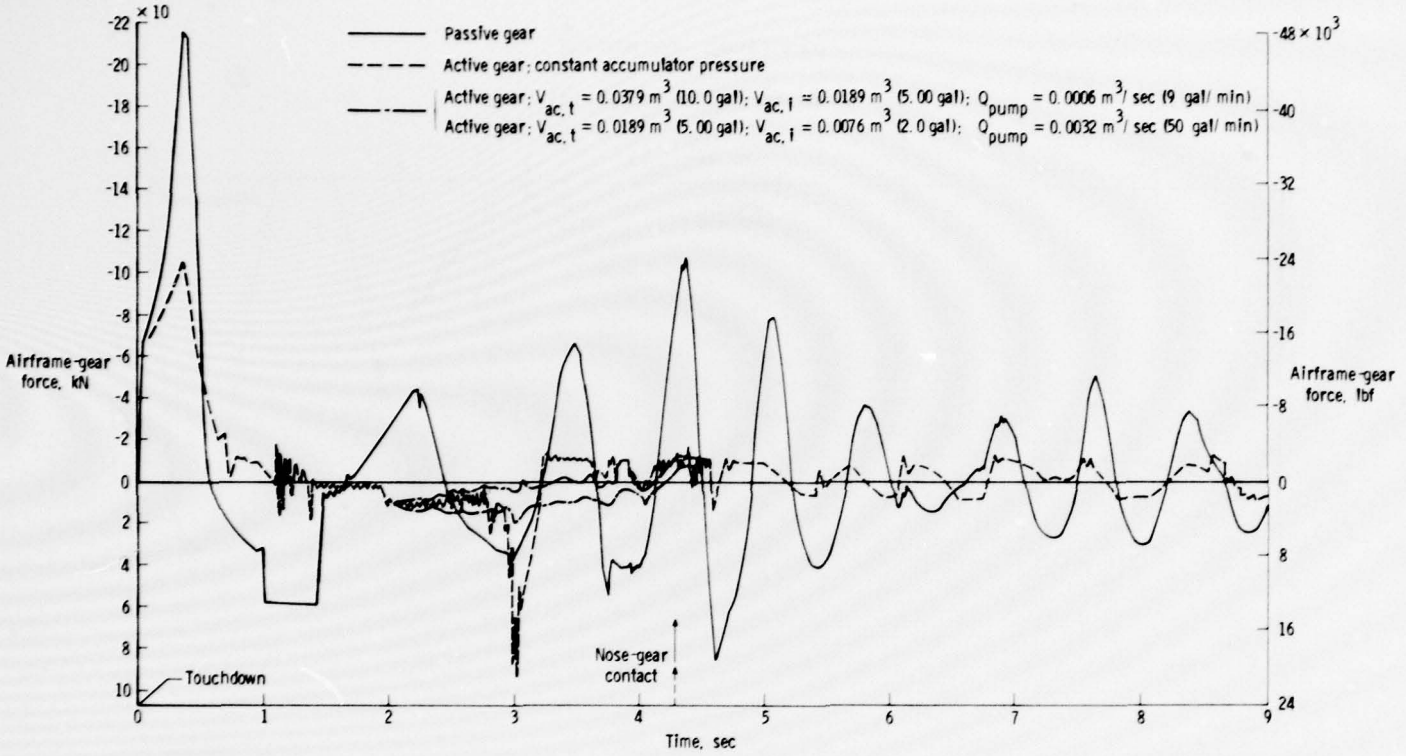

(a) Airframe-gear forces.

Figure 8.- Effect of high-pressure accumulator design on airframe-gear forces and shock-strut strokes for landing simulations with active gear. Large mass configuration; runway A with uphill slope; sink rate, 1.5 m/sec (5.0 ft/sec).

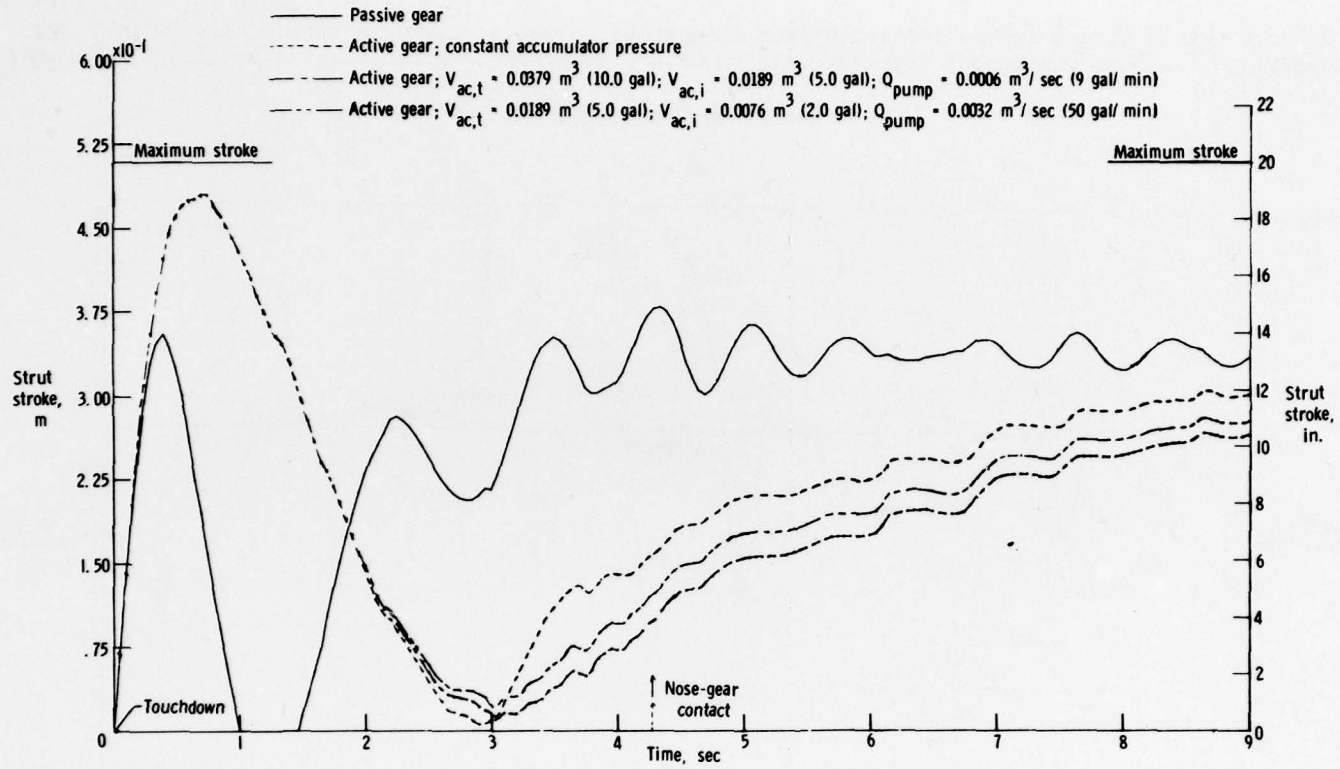

(b) Shock-strut strokes.

Figure 8.- Concluded.

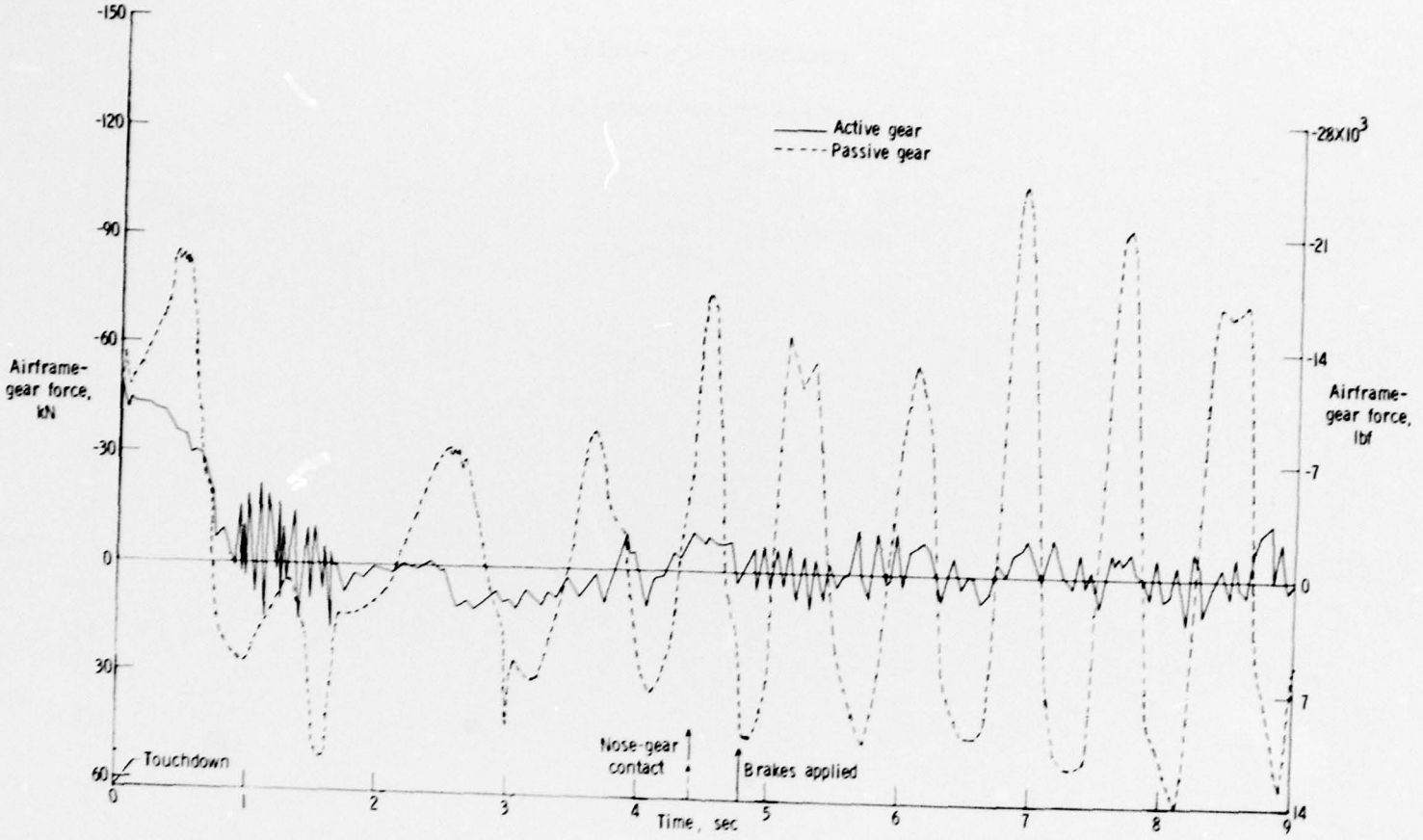

(a) Airframe-gear forces.

Figure 9.- Airframe-gear-force and shock-strut-stroke time histories for landing simulations with antiskid braking. Large mass configuration; runway A with uphill slope; sink rate, 0.9 m/sec (3.0 ft/sec).

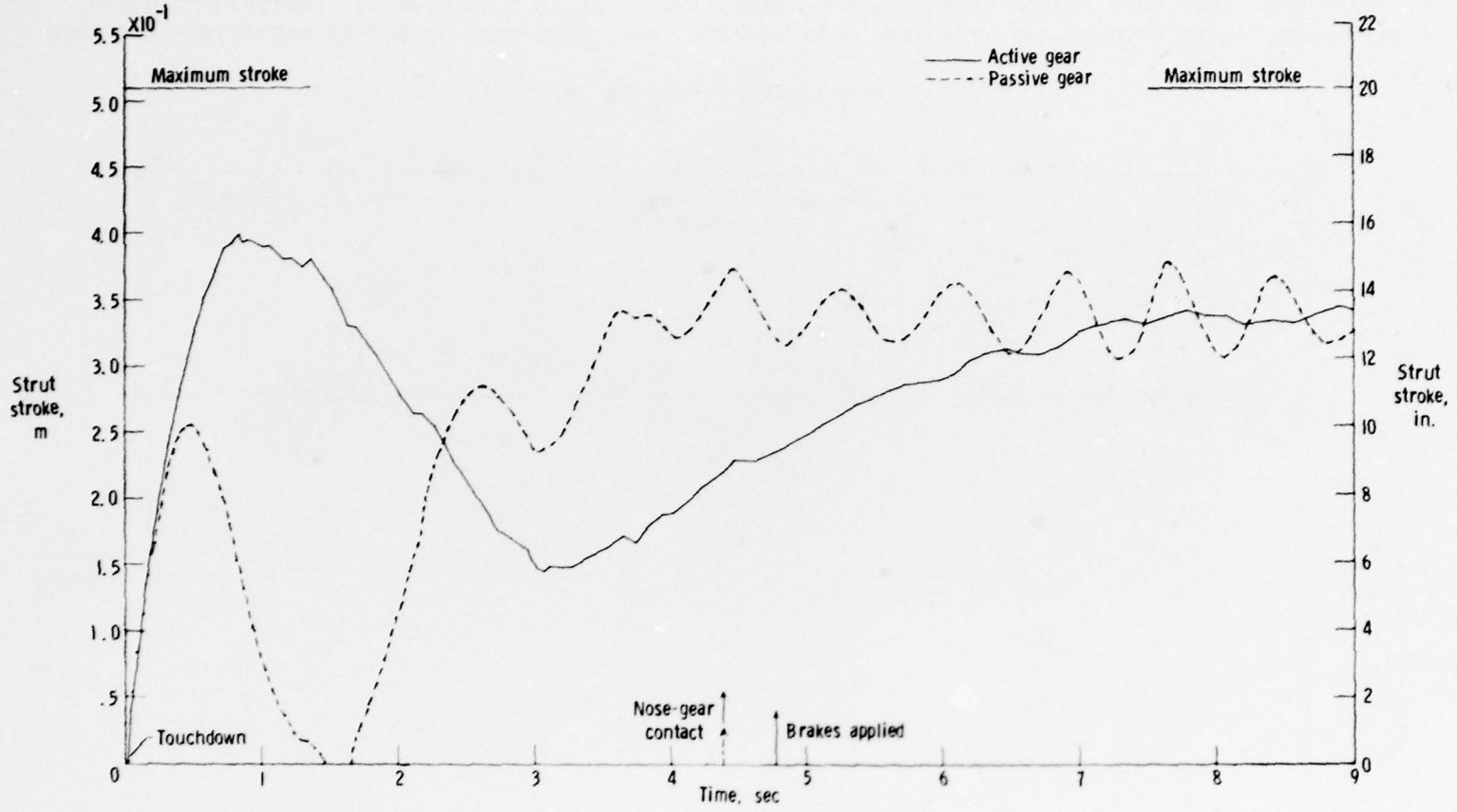

(b) Shock-strut strokes.

Figure 9.- Concluded.

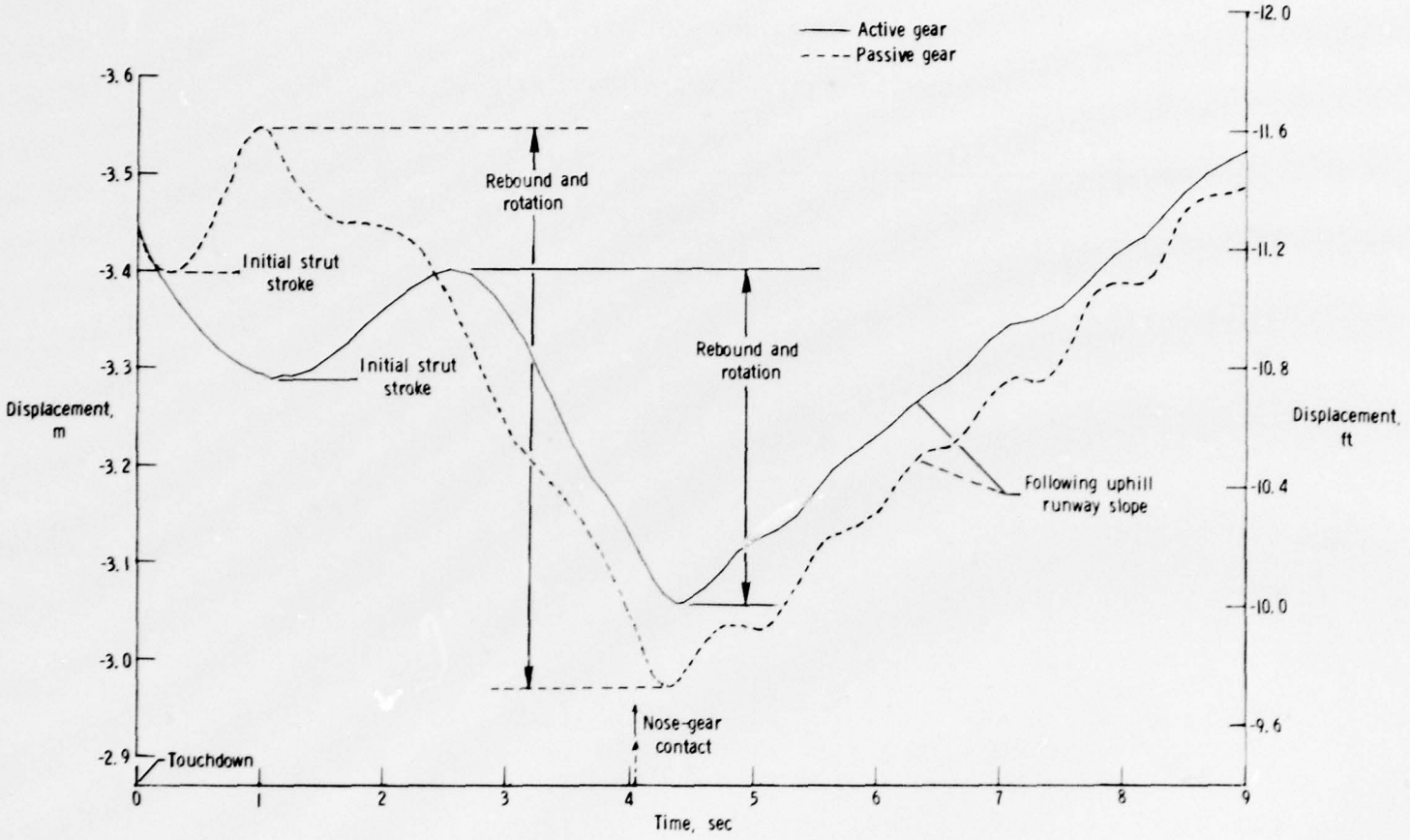

(a) Sink rate, 0.3 m/sec (1.0 ft/sec).

Figure 10.- Gravity Z-axis displacement time histories of fuselage mass center. Medium mass configuration; runway A with uphill slope.

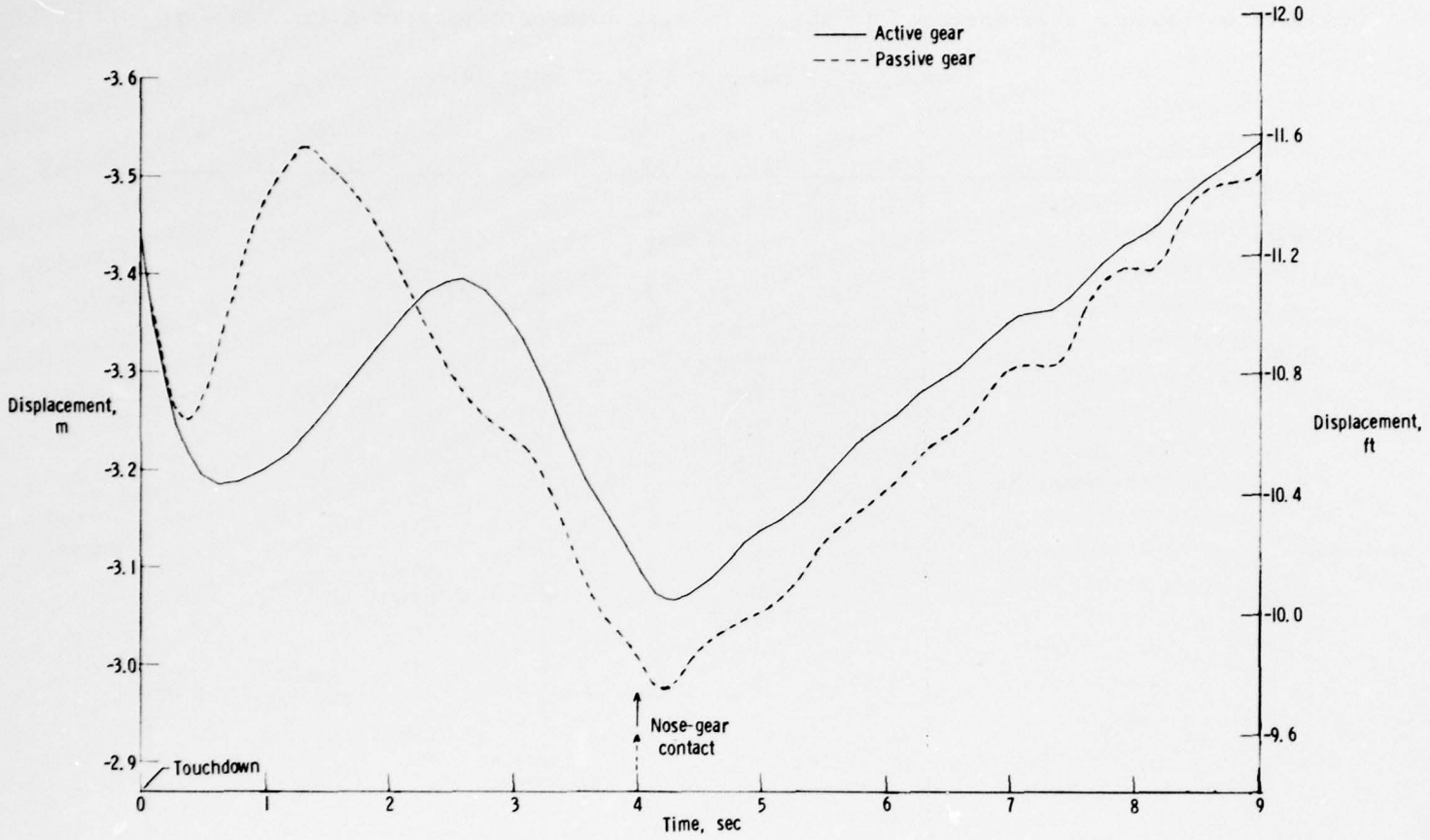

(b) Sink rate, 0.9 m/sec (3.0 ft/sec).

Figure 10.- Continued.

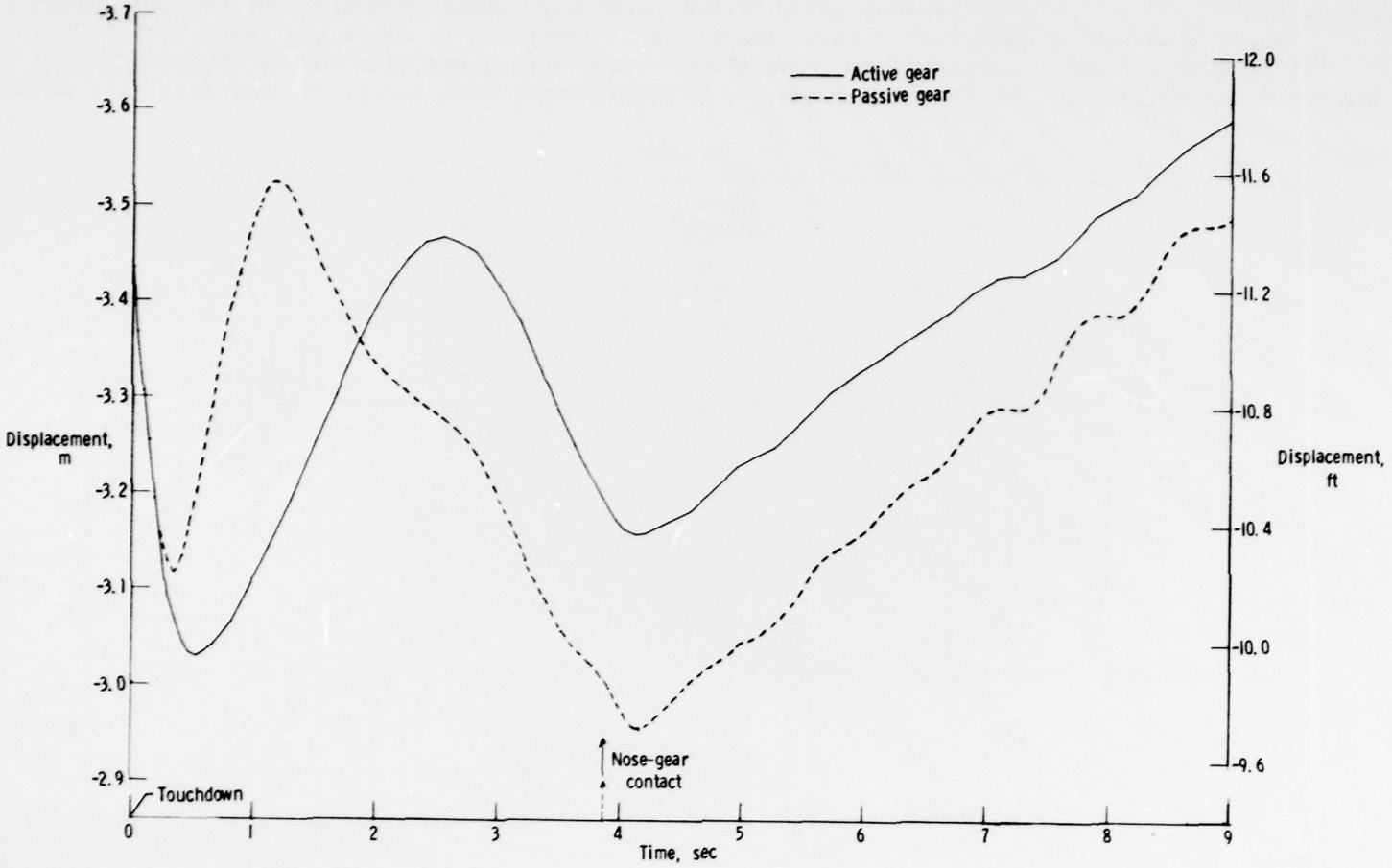

(c) Sink rate, 1.5 m/sec (5.0 ft/sec).

Figure 10.- Concluded.

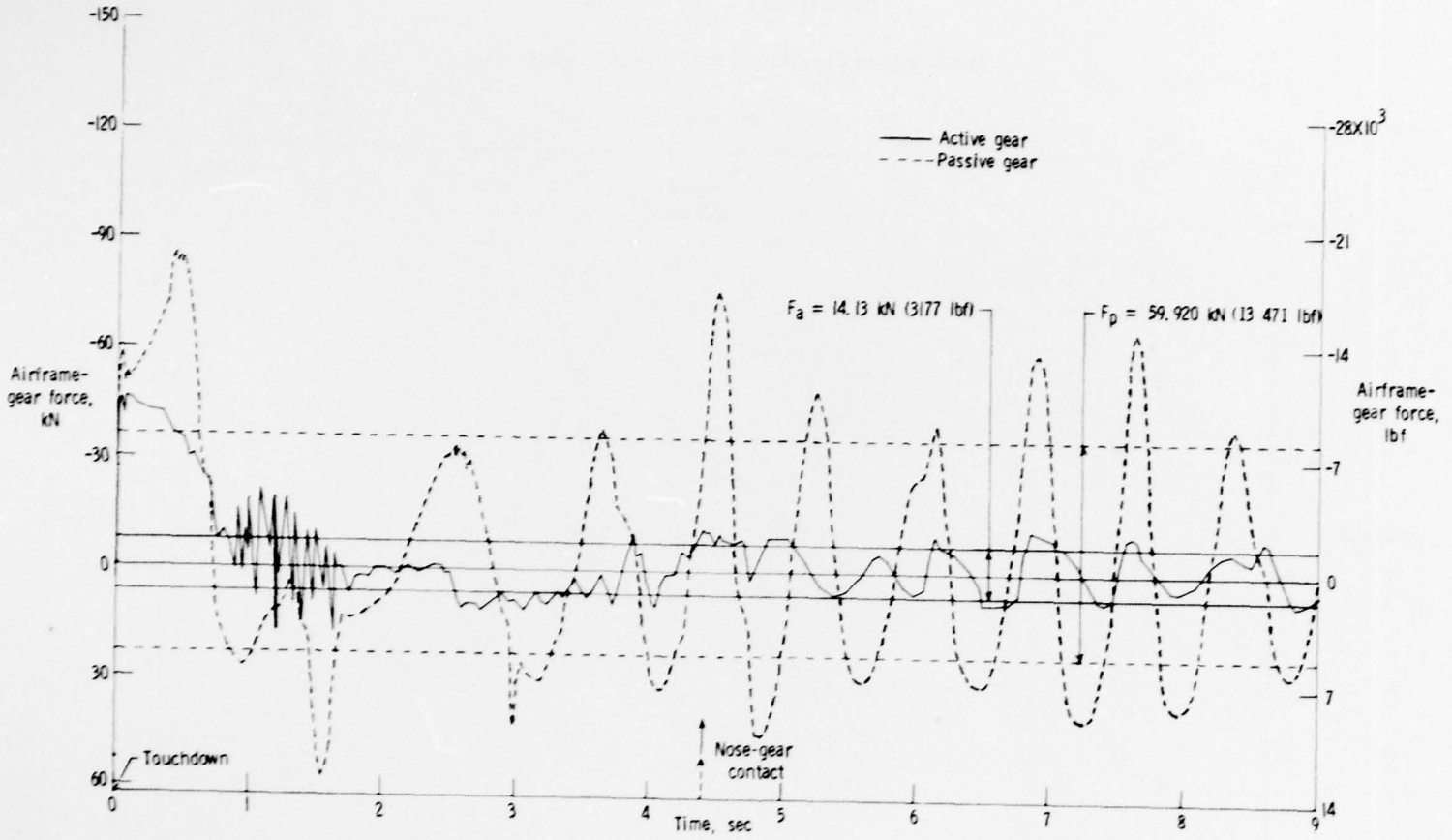

Figure 11.- Airframe-gear-force time histories with rms bounded forces for indicating potential for reduced fatigue damage with the active gear. Large mass configuration; runway A with uphill slope; sink rate, 0.9 m/sec (3.0 ft/sec). (Solid horizontal lines show active-gear force bounds and dashed horizontal lines show passive-gear force bounds.)

1. Report No.	2. Government Accession No.	3. Recipient's Catalog No.
NASA TP-1555		

4. Title and Subtitle
ANALYTICAL INVESTIGATION OF THE LANDING DYNAMICS OF A LARGE AIRPLANE WITH A LOAD-CONTROL SYSTEM IN THE MAIN LANDING GEAR

5. Report Date
December 1979

6. Performing Organization Code

7. Author(s)
John R. McGehee and Huey D. Carden

8. Performing Organization Report No.
NASA - L-13250

10. Work Unit No.
505-44-33-01

9. Performing Organization Name and Address
NASA Langley Research Center
Hampton, VA 23665

11. Contract or Grant No.

12. Sponsoring Agency Name and Address
National Aeronautics and Space Administration
Washington, DC 20546

13. Type of Report and Period Covered
Technical Paper

14. Sponsoring Agency Code

15. Supplementary Notes

16. Abstract

This paper presents the results of an evaluation of an active load-control landing gear computer program (ACOLAG) for predicting the landing dynamics of airplanes with passive and active main gears. ACOLAG was used in an analytical investigation of the landing dynamics of a large airplane with both passive and active main gears. The results of the evaluation of ACOLAG indicate that the program is valid for predicting the landing dynamics of airplanes with both passive and active main gears. The results of the analytical investigation of the landing dynamics of the large airplane show that the active gear reduces airframe-gear forces and airplane motions following initial impact and has the potential for significant reductions in structural fatigue damage relative to that which occurs with the passive gear.

83

17. Key Words (Suggested by Author(s))	18. Distribution Statement
Aircraft landing gear Active controls Landing loads	Unclassified - Unlimited Subject Category 05

19. Security Classif. (of this report)	20. Security Classif. (of this page)	21. No. of Pages	22. Price*
Unclassified	Unclassified	82	$6.00

*For sale by the National Technical Information Service, Springfield, Virginia 22161

NASA-Langley, 1979

387 543